MEMORY FUNCTION
FOR COLLECTIVE DIFFUSION
OF INTERACTING
BROWNIAN PARTICLES

Piotr Szymczak

A thesis submitted to the University of Warsaw
in accordance with the requirements
for the degree of Doctor of Philosophy

under the supervision of Prof. Bogdan Cichocki

Faculty of Physics
Warsaw University
Warszawa 2001
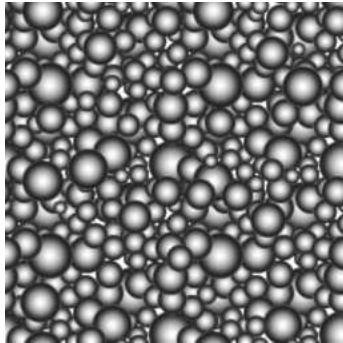
"The Brownian motion provides us with one
of the most beautiful and direct experimental
demonstrations of the fundamental principles
of the mechanical theory of heat"

G. Cantoni, 1867

Contents

Chapter 1

Introduction

In 1827 one of the greatest English botanists Robert Brown discovered that sufficiently small particles immersed in a fluid display an irregular motion. The understanding of physical processes which cause the minute particles to dance under the microscope's eye came only in the beginning of the XXth century with the works of Einstein [1, 2] and Smoluchowski [3], who have shown that the Brownian movement is caused by the thermal motion of fluid particles and their collisions with suspended bodies. They stated that on the macroscopic timescale the motion of a solitary Brownian particle is of a diffusive character with the diffusion coefficient D_o given by

$$D_o = \frac{k_B T}{\zeta_o},$$ (1.1)

where ζ_o is the friction coefficient, which for a spherical particle of radius a moving in a fluid of viscosity η is given by the Stokes formula [4]

$$\zeta_o = 6\pi\eta a.$$ (1.2)

The relation (1.1) shows that the two ways in which fluid affects the motion of the particle: the deterministic friction and the stochastic fluctuations are closely connected. In fact (1.1) is one of the manifestations of the fluctuation-dissipation theorem [5].

The renewed interest towards the Brownian motion came with the advent of the dynamic light scattering (DLS) techniques [6,7] as the mean to study the colloidal suspensions. It has namely turned out that on the timescale characteristic of the DLS experiments the best physical model of the broad class of suspensions is the system of Brownian particles. Everyday examples of colloids include a broad variety of substances from milk to inks and paints. Their technical applications are innumerable: from ceramic precursors, optical filters, porous sieves to liposome technology, not to mention rapidly growing biotechnology applications. Colloidal suspensions show a multitude of fascinating physico-chemical phenomena such as the crystallization into variety of structures, glass transition, electrokinetic phenomena, self and collective diffusion, shear melting, sedimentation and many others [8–11].

1.1   General characteristics of colloidal suspensions

Colloidal suspensions, commonly referred to simply as colloids are composed of small particles that are 10-1000 nm in diameter and dispersed in a solvent. The lower limit in the particle size comes from the requirement that they should be much larger than the fluid molecules, whereas the upper limit ensures that the Brownian motion would play a significant role in the dynamics in comparison with other processes such as sedimentation or convection.

Save for the case of extremely diluted suspensions, colloidal particles always interact with each other. These interactions may arise from direct interparticle forces (e.g. Coulomb) or - in a more indirect way - from the motion of the fluid disturbed by the particles. In the latter case we talk about hydrodynamic interactions, which are present in any suspension, even if direct interparticle forces vanish.

As in the present work we are going to concentrate on the effects of hydrodynamic interactions on the diffusion of colloidal suspension, it is no wonder that of the special interest for us here would be colloidal particles which behave effectively as hard spheres (as they interact with hydrodynamic interactions only). Although a century ago a suspension of hard spheres could be considered only as the physicist's dream, today the development of technology made it possible to produce such systems. Examples of these include the neutral suspensions like polymethylmethacrylate (PMMA) spheres and silica spheres in organic solvents, aqueous suspensions of polystyrene spheres as well as charged suspensions in which added electrolyte concentration is so high that the Debye-sphere of counter-ions is collapsed to a very thin layer.

1.2   Time scales involved in the dynamics of interacting Brownian particles

The system of mesoscopic particles suspended in a fluid, however simple it may seem, has a very rich dynamics revealing a myriad of interesting phenomena. Moreover, the character of dynamics is changing dramatically depending on the timescales and associated lengthscales of interest. Let us therefore start with specifying the timescales characterizing the motion of spherical particles of radius a and density ρ suspended in a solvent of density ρ_s. These include:

$$\tau_c = \frac{a}{c} \qquad \qquad \text{sound propagation time} \qquad \qquad (1.3)$$

(the time in which a sound wave propagates on a distance equal to the radius of a particle)

$$\tau_\eta = a^2 \frac{\rho_s}{\eta} \qquad \qquad \text{the viscous relaxation time} \qquad \qquad (1.4)$$

(characteristic lifetime of a viscous shear wave created by the unsteady motion of a particle)

$$\tau_B = \frac{M}{\zeta_o} = \frac{2a^2\rho_p}{9\eta} = \frac{2}{9}\frac{\rho}{\rho_s}\tau_\eta \quad \text{the momentum relaxation time} \tag{1.5}$$

(relaxation time of the particle velocity due to the solvent friction)

$$\tau_R = \frac{a^2}{D_o} \qquad\qquad \text{the structural relaxation time} \tag{1.6}$$

(time needed by the Brownian particle to diffuse over a distance equal to the radius)

In the above equations $M = 4\pi\rho a^3/3$ stands for the mass of the particle. Numerical values of characteristic times of typical suspensions are given in Table 1.1. Additionally the characteristic velocity of such a particle calculated from the equipartition law

$$\frac{MU^2}{2} = \frac{3}{2}k_B T, \tag{1.7}$$

and the values of the Reynolds number Re

$$\text{Re} = \frac{aU\rho}{\eta}, \tag{1.8}$$

which measures the ratio of inertial to viscous forces in the motion of the fluid around the suspended spheres. We see that for a typical suspension Re is very small, so that one can neglect the fluid inertia term $\rho\boldsymbol{v}\cdot\nabla\boldsymbol{v}$ in the Navier-Stokes equations.

In this work we would be interested in such domains in the suspension dynamics in which the Brownian motion plays a central role. In order to assure it not only the timescale of interest t should fulfil the condition $t \geq \tau_R$, but also the displacements of the particles associated with the Brownian motion should be larger than the displacements caused by other phenomena, such as the external force or the nonzero shear flow in which the suspension is immersed. The quantities that measure the relative importance of these effects are the Peclet numbers Pe. For example the convective Peclet number

$$\text{Pe}_{conv} = \gamma\tau_R = \frac{a^2\gamma}{D_o} \tag{1.9}$$

measures the relative strength of the Brownian effects in comparison to those induced by the shear flow, while

$$\text{Pe}_F = \frac{\dfrac{F}{\zeta_o}}{\dfrac{a}{\tau_R}} = \frac{Fa}{k_B T} \tag{1.10}$$

compares Brownian motion with the effects of the external force F. If all the Peclet numbers are small, then we may say that we are in the "Brownian" domain of system dynamics.

	a [nm]		
	10	100	1000
$\tau_c \; [s]$	$6.76 \cdot 10^{-12}$	$6.76 \cdot 10^{-11}$	$6.76 \cdot 10^{-10}$
$\tau_B \; [s]$	$2.2 \cdot 10^{-11}$	$2.2 \cdot 10^{-9}$	$2.2 \cdot 10^{-7}$
$U \; [cm/s]$	170	5.4	0.17
Re	$1.7 \cdot 10^{-4}$	$5.4 \cdot 10^{-5}$	$1.7 \cdot 10^{-5}$
$\tau_R [s]$	$4.7 \cdot 10^{-6}$	$4.7 \cdot 10^{-3}$	4.7
$\tau_\eta \; [s]$	$1 \cdot 10^{-10}$	$2.2 \cdot 10^{-8}$	$2.2 \cdot 10^{-6}$

Table 1.1: Various parameters as a function of the Brownian particle radius a: the momentum relaxation time τ_B, the characteristic velocity of the particles U, the Reynolds number Re, the structural relaxation time τ_R, viscous relaxation time τ_η and the sound propagation time τ_c. The following values were used in the calculations: particle and fluid density $\rho_p \approx \rho_s = 1 g/cm^3$; viscosity $\eta = 10^{-2}$poise; temperature $T = 293$K, fluid sound velocity $c = 1.5 \cdot 10^5 cm/s$. These parameters are typical for the aqueous suspension of polystyrene spheres. The table is partially reproduced from Pusey [8] and Nägele [9] (the latter contains many errors which were corrected in the present one)

Moreover from Table 1.1 one concludes that the larger the particles the longer τ_R is and, what follows, less important the Brownian motion is in their dynamics. For the large particles ($a > 10\mu m$) it gets more difficult to prepare a suspension with small Pe, as even for such a small shear rate as $1s^{-1}$ the Peclet number (in water) is of the order of 300.

Now we turn to the analysis of the time scales associated with the motion of the fluid. From inspecting Table 1.1 one can draw a conclusion that for the typical suspensions the timescales corresponding to τ_c, τ_η and τ_R are widely separated in a sense that

$$\tau_c \ll \tau_\eta \ll \tau_R. \tag{1.11}$$

Therefore if we are interested in processes with characteristic timescale $t \geq \tau_R$ then the description of the suspending medium (fluid) can be simplified by assuming that

1. the fluid can be treated as effectively incompressible (as $t \gg \tau_c$)

2. the flow can be treated as stationary: $\dfrac{\partial \boldsymbol{v}}{\partial t} = 0$ (a consequence of the fact that $t \gg \tau_\eta$)

This, together with the assumption that the Reynolds number Re $\ll 1$, allows us to describe the fluid by means of the steady Stokes equations

$$\eta \nabla^2 \boldsymbol{v} - \nabla p + \boldsymbol{f}(\boldsymbol{r}) = 0, \qquad \nabla \cdot \boldsymbol{v} = 0, \tag{1.12}$$

where $\boldsymbol{f}(\boldsymbol{r})$ is the force density exerted on the fluid.

It is important to note that the absence of the term $\partial \boldsymbol{v}/\partial t$ in the Stokes equations does not mean that velocity is independent of time - it only means that we assume the terms related to time dependence to be negligible. Nevertheless the geometric configuration of the fluid boundaries (including the surfaces of the spheres) or the force $\boldsymbol{f}$ acting on the fluid may change in time, which causes $\boldsymbol{v}$ to change as well. However, due to the separation of the timescales the flow follows instantaneously the motion of the particles. Therefore time remains in Eq. (2.3) as an implicit parameter.

From the observation that the flow follows instantaneously the motion of the particles we conclude that the communication between the particles via the "hydrodynamic interactions" can be also treated as effectively instantaneous: the motion of each particle creates the flow pattern, which instantaneously affects the motion of other particles.

1.3   Hydrodynamic interactions

If a fluid is sufficiently viscous, a particle - sufficiently small and its motion - not too fast - then under the influence of an external force the particle would almost immediately (in comparison with the structural relaxation time) attain a terminal velocity. The reason for it is the appearance of the viscous drag force proportional to the velocity of a particle. This drag force is dependent on the shape of the particle, presence of other particles etc: for an isolated small sphere of radius a moving with velocity $\boldsymbol{U}$ through the fluid it is given by the Stokes law [4]

$$\boldsymbol{F} = 6\pi\eta a\boldsymbol{U} = \zeta_o\boldsymbol{U}, \tag{1.13}$$

where ζ_o is called the translational friction coefficient.

In the terminal state the hydrodynamic drag force exactly balances the external force so that the Stokes formula can be used to calculate the particle velocity induced by the external force.

In the general case when there are many particles in a suspension subject to given forces as well as torques, the relation (1.13) should be replaced by [12, 13]

$$\tilde{\boldsymbol{\mathcal{F}}} = \boldsymbol{\zeta} \cdot \tilde{\boldsymbol{\mathcal{U}}}. \tag{1.14}$$

Here $\tilde{\boldsymbol{\mathcal{F}}} = (\boldsymbol{\mathcal{F}}, \boldsymbol{\mathcal{T}})$ is the 6N-dimensional vector comprising the forces and torques acting on the each of N particles: $(\boldsymbol{\mathcal{F}}, \boldsymbol{\mathcal{T}}) = (\boldsymbol{F}_1, \boldsymbol{F}_2, ..., \boldsymbol{F}_N, \boldsymbol{T}_1, ..., \boldsymbol{T}_N)$ whereas $\tilde{\boldsymbol{\mathcal{U}}} = (\boldsymbol{\mathcal{U}}, \boldsymbol{\Omega})$ is the vector built from the translational and rotational velocities of the particles $\tilde{\boldsymbol{\mathcal{U}}} = (\boldsymbol{U}_1, ..., \boldsymbol{U}_N, \boldsymbol{\Omega}_1, ..., \boldsymbol{\Omega}_N)$.

The tensor $\boldsymbol{\zeta}$ defined above, which has replaced the friction coefficient in (1.13) is called **the friction matrix**.

The relation reciprocal to (1.14)

$$\tilde{\boldsymbol{\mathcal{U}}} = \boldsymbol{\mu} \cdot \tilde{\boldsymbol{\mathcal{F}}}, \tag{1.15}$$

gives the velocities of the particles in terms of the applied forces and torques. The mobility matrix defined here is the inverse of the friction matrix $\boldsymbol{\zeta}$

$$\boldsymbol{\mu} = \boldsymbol{\zeta}^{-1}. \tag{1.16}$$

Strictly speaking (1.14) and (1.15) hold only if the fluid is quiescent, i.e. such that if we remove the particles from the fluid it would come to rest. Otherwise there should appear in (1.14) and (1.15) terms connected with $\boldsymbol{v}_o$ - the flow in the absence of the particles. The general expressions for this case will be given in Chapter 2.

1.4   Generalized Smoluchowski Equation

The separation of timescales between the structural relaxation time τ_R and the momentum relaxation time τ_B allows us to adopt the description of the dynamic of the system in terms of equilibration of the particle configurations only. For non- interacting Brownian particles the evolution of the probability density $P(\boldsymbol{R}, t)$ of finding at time t a particle at position R is given by the diffusion equation

$$\frac{\partial P(\boldsymbol{R}, t)}{\partial t} = D_o \sum_{i=1}^{N} \frac{\partial}{\partial \boldsymbol{R}_i} \cdot \frac{\partial}{\partial \boldsymbol{R}_i} P(\boldsymbol{R}, t). \tag{1.17}$$

A generalization of this equation to the case of N interacting particles is the Generalized Smoluchowski Equation [14], given by

$$\frac{\partial}{\partial t}P(\boldsymbol{X},t) = \sum_{i,j=1}^{N} \frac{\partial}{\partial \boldsymbol{R}_i} \cdot \boldsymbol{D}_{ij}(\boldsymbol{X}) \cdot \left[\frac{\partial}{\partial \boldsymbol{R}_j} - \beta \boldsymbol{F}_j\right] P(\boldsymbol{X},t), \tag{1.18}$$

where $\boldsymbol{X} = (\boldsymbol{R}_1, \boldsymbol{R}_2 \ldots, \boldsymbol{R}_N)$ and the absence of torques is assumed. The tensor $\boldsymbol{D}_{ij}$ is the diffusion matrix connected with the mobility matrix by relation

$$\boldsymbol{D}_{ij} = k_B T \boldsymbol{\mu}_{ij}^{tt}, \tag{1.19}$$

where $\boldsymbol{\mu}^{tt}$ is the part of μ linking the forces $\boldsymbol{\mathcal{F}}$ to the translational velocities $\boldsymbol{\mathcal{U}}$.

The relation (1.19) is a generalization of the Einstein relation (1.1) to the case of N interacting particles. The phenomenological derivation of the Smoluchowski equation together with its generalization to the case of hard sphere systems is presented in Chapter 3.

1.5 Static and dynamic properties of the suspended particles

The Brownian domain of the system's dynamics, corresponding to timescales $t \geq \tau_R$ can be assessed by means of light scattering experiments. Light scattering gives us direct information on spatial and temporal correlations between fluctuations of local concentration of the Brownian particles such as the static structure factor describing the average distribution of the interparticle separations in a suspension

$$S(k) = \lim_{\infty} \frac{1}{N} < \sum_{i=1}^{N} \sum_{j=1}^{N} e^{i\boldsymbol{k}\cdot(\boldsymbol{R}_i - \boldsymbol{R}_j)} >, \tag{1.20}$$

which can be assessed by static scattering experiments and its dynamic analogue, the dynamic structure factor (known also as intermediate scattering function)

$$F(k,t) = \lim_{\infty} \frac{1}{N} < \sum_{i=1}^{N} \sum_{j=1}^{N} e^{i\boldsymbol{k}\cdot(\boldsymbol{R}_i(0) - \boldsymbol{R}_j(t))} >, \tag{1.21}$$

for the determination of which the dynamic light scattering (DLS) is needed. In the above formulae $\boldsymbol{R}_i(t)$ is the position of i-th particle, brackets denote an ensemble average and $\boldsymbol{k}$ is the wavevector. Finally $\lim_{\infty}$ stands for the **thermodynamic limit** in which one lets the size of the sample go to infinity while keeping the densities of the extensive parameters constant. Moreover, it should be assumed that the system as a whole does not move, i.e we keep the walls in which the system is contained immobile.

The light scattering experiments probe a broad range of wave vectors, starting from $k \ll \frac{2\pi}{a}$ up to $k \geq \frac{2\pi}{a}$. The large k vectors probe the density fluctuations on scale of the order of the radius of the particle a, determined by the single-particle dynamics, whereas the

small k vectors correspond to the hydrodynamic domain, when one observes the collective motion of the particles.

It is convenient to work with the Laplace transform of the intermediate scattering function defined as

$$F(k, z) = \int_0^\infty e^{-zt} F(k, t) \mathrm{d}t. \tag{1.22}$$

In frames of the Zwanzig-Mori projection operator formalism [15,16] (which is described in Chapter 4 of the Thesis) one writes $F(k, z)$ in the following form

$$F(k, z) = \frac{S(k)}{z + D(k, z)k^2}, \tag{1.23}$$

which defines the generalized diffusion function $D(k, z)$.

The hydrodynamic (small z and small k) limit of $D(k, z)$ is called the **collective diffusion coefficient** D_c

$$\lim_{k \to 0} \lim_{z \to 0} D(k, z) = D_c. \tag{1.24}$$

In the Zwanzig-Mori formalism one gets the following expression for the generalized diffusion function

$$D(k, z) = \frac{1}{k^2} \Omega(k)(1 - M(k, z)), \tag{1.25}$$

where the z-dependent term $M(k, z)$ is called the **memory function**, whereas the z-independent term - **frequency function**

The reason for such a name of $M(k, t)$ can be understood by looking at the expression (1.23) with (1.25) inserted in the time domain

$$\frac{\partial}{\partial t} F(k, t) = -\Omega(k) F(k, t) + \Omega(k) \int_0^t d\tau M(k, \tau) F(k, t - \tau), \tag{1.26}$$

which shows that the decay rate of F depends on its values at earlier times and the details of this dependence are described by $M(k, t)$. On the other hand $\Omega(k)$ gives the contribution of the instantaneous value of $F(k, t)$ to the decay rate. One of the important characteristics of the memory effects is the mean memory time τ_M

$$\tau_M(k) = M(k, t = 0)^{-1} \int_0^\infty M(k, \tau) \mathrm{d}\tau, \tag{1.27}$$

which gives the timescale over which the memory in the system is lost.

If one is interested in the evolution of $F(k, t)$ on the timescale much longer than τ_M then only the overall memory effect given by the integral of the memory function is important and the Eq. (1.26) may be replaced by

$$\frac{\partial}{\partial t} F(k, t) = -\Omega(k) \left[1 - \int_0^\infty d\tau M(k, \tau) \right] F(k, t), \tag{1.28}$$

Therefore one sees that the collective diffusion coefficient (1.24) describes the decay of the dynamic structure factor on the timescale $t \gg \tau_M$ for small wavevectors. Note that D_c can be also written as

$$D_c = \lim_{k \to 0} \frac{\Omega(k)}{k^2} \left[1 - \Delta(k) \right], \tag{1.29}$$

with [17]

$$\Delta(k) = \int_0^\infty d\tau M(k, \tau). \tag{1.30}$$

On the other hand, if one neglects the memory effects in (1.28) and considers only the instantaneous response described by the function $\Omega(k)$ then one gets

$$F(k, t) = S(k) e^{-k^2 D_c^s t}, \tag{1.31}$$

with

$$D_c^s = \lim_{k \to 0} \frac{\Omega(k)}{k^2} \tag{1.32}$$

standing for the **short-time diffusion coefficient** in contradistinction to D_c which is sometimes called the **long-time diffusion coefficient** and to avoid confusion from here on will be denoted by D_c^l. From (1.29) and (1.32) one obtains

$$D_c^l = D_c^s (1 - \Delta). \tag{1.33}$$

where

$$\Delta = \lim_{k \to 0} \Delta(k) \tag{1.34}$$

is the small k and small z limit of the memory function.

One may ask, however, why D_c^l defined above by means of the dynamic structure factor is called the diffusion coefficient? Usually, when talking about diffusion phenomena, one thinks about the Fick's law, which gives the macroscopic current induced in the system by the small density gradient

$$\boldsymbol{J}_d = -D \nabla n. \tag{1.35}$$

Here n is the macroscopic number density of the particles given by

$$n(\boldsymbol{r}, t) = < \sum_{i=1}^N \delta(\boldsymbol{r} - \boldsymbol{R}_i(t)) >, \tag{1.36}$$

and the diffusion current $\boldsymbol{J}_d$ is defined as the particle current with respect to the velocity of a suspension as a whole. Finally D is the gradient diffusion coefficient. The thorough derivation of the diffusion law (1.35) from the nonequilibrium thermodynamics formalism

applied to the suspension treated as the two-phase (particles + fluid) system together with the exact definition of the diffusion current is presented in Chapter 5.

The Fourier transform of the diffusion law (1.35) together with the continuity equation

$$\frac{\partial n(\boldsymbol{r}, t)}{\partial t} + \nabla \cdot \boldsymbol{J}_d(\boldsymbol{r}, t) = 0 \tag{1.37}$$

leads to the diffusion equation for the particle density of the form

$$\frac{\partial n(\boldsymbol{r}, t)}{\partial t} - D\nabla^2 n(\boldsymbol{r}, t) = 0. \tag{1.38}$$

The gradient diffusion coefficient D can be linked with the D_c^l defined above if one assumes that the equations (1.35) and (1.38) hold also for the fluctuations of the density of the particles. This line of reasoning is due to Onsager [18, 19] (see also Forster [20]). Then one gets for the dynamic structure factor

$$F(k, z) = \frac{S(k)}{z + Dk^2}, \tag{1.39}$$

which is exactly of the form (1.23).

Then, when one remembers that the hydrodynamic equations like (1.35) hold only if the fields vary sufficiently slowly in space and time (which corresponds to the limit of small k and z), by comparing (1.23) with (1.39) one can identify D with D_c^l.

Calculation of the collective diffusion coefficients D_c^s and D_c^l from Eqs. (1.32) and (1.24) is cumbersome because of the limit $k \to 0$ involved. Even for the simplest approximations of hydrodynamic interactions, when only two- and three- body contributions to the diffusion matrix are taken into account, the calculations involving small k limit are quite elaborate (cf the calculations in [21–24]). The problem would be much more easy to tackle if, instead of performing the limit $k \to 0$, one could simply calculate the value of $D(k, 0)$ at $k = 0$. However, if there are long-range interactions in the system (and such is the case for colloidal suspensions because of the presence of hydrodynamic interactions) then generally $\lim_{k \to 0} A(k) \neq A(k = 0)$ [20].

In order to overcome this problem we are going to study yet another way of calculating the collective diffusion coefficient. We start with the relation (1.35) and then, after Einstein [1, 25, 26] note that the mean particle current down a small fluctuation gradient due to the diffusion is the same as if each of the particles is acted by a force of the magnitude

$$\boldsymbol{F} = -\frac{1}{1 - \phi} \left(\frac{\partial \mu}{\partial n} \right)_{p,T} \nabla n, \tag{1.40}$$

with the additional assumption that the suspending fluid is force-free. Therefore the diffusion coefficient can be found by studying the current induced in the system by the external force applied to the particles, which can be done with use of the linear reaction theory. It turns out that if it is done carefully, then one is able to obtain a well-defined, explicit expression for D_c which does not contain the cumbersome $\boldsymbol{k} \to 0$ limit. To clarify

what we mean by "carefully" in this case, let us look more closely at the response problems for heterogeneous media.

1.6   Response properties of the heterogeneous media

The suspension of Brownian particles is an example of **heterogeneous** system, as it consists of two phases of different physical nature: the solvent and the particles. Naturally we mean the microscopic heterogeneity here (in contradistinction to macroscopically heterogeneous materials such as cement enveloping gravel). Another example of the microscopically heterogeneous system is the extensively studied Kirkwood-Yvon model of nonpolar dielectric [27, 28], in which one considers polarizable inclusions dispersed in nonpolarizable medium. For the excellent review of heterogeneous media theory including a historical outline we refer to the paper by R. Landauer [29].

One of the main goals of a scientist studying such a system is to derive the effective macroscopic properties from the information on its structure and dynamics on the microscale. The above-mentioned macroscopic properties may include such quantities as dielectric constant or polarizability in case of dielectrics, elastic properties of solid composites or - in our case - the diffusion coefficients, viscosity or thermal conductivity of colloidal suspension.

By the microstructure of a nonhomogeneous material we understand the information on the boundaries of all the phases building up the material. For a suspension of identical spheres of a given radius, this information is reduced just to the set of positions of the spheres' centers. Usually the information that we have on the microstructure is of statistical character only: i.e. instead of the exact positions of all the spheres in a suspension at time t we are given the distribution function $P(\boldsymbol{R}_1, \dots, \boldsymbol{R}_N; t)$.

Such a statistical information is nevertheless sufficient to determine the properties of a macroscopic sample of a material, because for such a sample one can identify the macroscopic value of a given quantity a with the average

$$a^{mac}(\boldsymbol{r}, t) = \int a(\boldsymbol{r}, t, \Gamma) P(\Gamma, t) \mathrm{d}t, \tag{1.41}$$

where Γ is the set of variables determining the microstructure and $a(\boldsymbol{r}, t, \Gamma)$ stands for the value of a for the given microstructure Γ.

A very important class of macroscopic properties of a given material are these which describe the response of the material to the external or internal disturbances like the electric or gravitational field or temperature gradient. The response of the system is usually described by the equations of the form

$$\boldsymbol{\mathcal{J}}(\boldsymbol{r}) = \int \boldsymbol{L}(\boldsymbol{r}, \boldsymbol{r}') \boldsymbol{\mathcal{F}}(\boldsymbol{r}') \mathrm{d}\boldsymbol{r}', \tag{1.42}$$

where $\boldsymbol{\mathcal{F}}$ is the disturbance whereas $\boldsymbol{\mathcal{J}}$ describes system's response (heat flux, diffusion current, polarization and so on). The function $\boldsymbol{L}(\boldsymbol{r}, \boldsymbol{r}')$ is the response kernel determining the

way the system responds to the perturbations. One can divide $\boldsymbol{L}$ in two big classes: these describing the static response, called **susceptibilites** such as the polarizability, dielectric constant etc. and those describing the dynamic response called **transport coefficients**, The latter include all kinds of diffusion coefficients, conductivities, resistivities and others. In general $\boldsymbol{J}$ and $\boldsymbol{F}$ may be multidimensional vectors comprising many different quantities. In this case $\boldsymbol{L}(\boldsymbol{r}, \boldsymbol{r}')$ becomes multidimensional matrix. Moreover, both sides of (1.42) can be the functions of time as well.

In the bulk of macroscopically homogeneous suspension the kernel $\boldsymbol{L}(\boldsymbol{r}, \boldsymbol{r}')$ becomes translationally invariant, i.e.

$$\boldsymbol{L}(\boldsymbol{r}, \boldsymbol{r}') = \boldsymbol{L}(\boldsymbol{r} - \boldsymbol{r}'). \tag{1.43}$$

This means that the Fourier transform of the kernels, defined as

$$\boldsymbol{L}(\boldsymbol{k}, \boldsymbol{k}') = \int \int e^{-i\boldsymbol{k}\cdot\boldsymbol{r}} \, \boldsymbol{L}(\boldsymbol{r}, \boldsymbol{r}') \, e^{i\boldsymbol{k}'\cdot\boldsymbol{r}'} \mathrm{d}\boldsymbol{r}\mathrm{d}\boldsymbol{r}' \tag{1.44}$$

in the homogeneous bulk would simplify to

$$\boldsymbol{L}(\boldsymbol{k}, \boldsymbol{k}') = 8\pi^3 \boldsymbol{L}(\boldsymbol{k})\delta(\boldsymbol{k} - \boldsymbol{k}'), \tag{1.45}$$

with

$$\boldsymbol{L}(\boldsymbol{k}) = \int \boldsymbol{L}(\boldsymbol{r})e^{-i\boldsymbol{k}\cdot\boldsymbol{r}}\mathrm{d}\boldsymbol{r}. \tag{1.46}$$

When one introduces also the Fourier transform of $\boldsymbol{J}$

$$\boldsymbol{J}(\boldsymbol{k}) = \frac{1}{8\pi^3} \int \boldsymbol{J}(\boldsymbol{r})e^{-i\boldsymbol{k}\cdot\boldsymbol{r}}\mathrm{d}\boldsymbol{r} \tag{1.47}$$

and similarly for $\boldsymbol{F}(\boldsymbol{k})$, one can write the response equation (1.42) as

$$\boldsymbol{J}(\boldsymbol{k}) = \boldsymbol{L}(\boldsymbol{k})\boldsymbol{F}(\boldsymbol{k}). \tag{1.48}$$

The limit $\boldsymbol{k} \to 0$ of the above equation describes the system's response to a homogeneous disturbance, with the long wavelength limit of the response kernel

$$\lim_{\boldsymbol{k}\to 0} \boldsymbol{L}(\boldsymbol{k}) = \boldsymbol{L} \tag{1.49}$$

which for the isotropic system can be usually written as $\boldsymbol{L} = L\mathbf{1}$ (with $\mathbf{1}$ standing for the identity operator), giving the respective macroscopic response coefficient L.

The most interesting from the physical point of view are those kernels $\boldsymbol{L}(\boldsymbol{r}, \boldsymbol{r}')$ which describe the local properties of the material itself and are independent of the global properties like the size and the shape of the sample (provided that it is of macroscopic dimensions). The local kernels $\boldsymbol{L}(\boldsymbol{r}, \boldsymbol{r}')$ have finite range, i.e. they decay faster than $|\boldsymbol{r}' - \boldsymbol{r}|^3$ as $|\boldsymbol{r}' - \boldsymbol{r}| \to \infty$. Therefore such kernels do not cause any trouble when the limit $\boldsymbol{k} \to 0$ of their Fourier transform is calculated, as in this case

$$\lim_{\boldsymbol{k} \to 0} \boldsymbol{L}(\boldsymbol{k}) = \boldsymbol{L}(\boldsymbol{k} = 0) = \int \boldsymbol{L}(\boldsymbol{r}) \mathrm{d}\boldsymbol{r}, \tag{1.50}$$

is a perfectly well defined quantity. Therefore in order to get the response coefficients one does not have to change to Fourier space and perform $\boldsymbol{k} \to 0$ limit. Instead, one just calculates the integral (1.50) in the real space. Moreover, as the local kernels are not sensitive to the conditions on the boundaries of the system, while calculating them we are free to choose any shape and size of the sample we want (provided it stays macroscopic). In particular in such a case there are no problems with applying the usual thermodynamic limit, in which one lets the size of the sample go to infinity while keeping the densities of the extensive parameters constant. Therefore in this case one avoids a whole lot of problems encountered usually while trying to apply the statistical mechanics concepts to the systems with long-range forces [30–38].

It is important to note that the possibility of applying thermodynamic limit holds only for the kernels $\boldsymbol{L}$ (provided that $\boldsymbol{L}$ is short-ranged) and not for the response $\boldsymbol{J}$, as it would generally depend on the size and shape of the sample, which stems from the long range of the forces. To quote Tsallis [37]: "The amount of calories to be provided to a table in order to increase its temperature in one degree *only* depends on its weight and material (iron, wood), whereas the amount of Coulombs we must provide to a capacitor to generate a one Volt potential difference at its ends *also* depends on its *shape*!"

The crucial thing is that the locality or non-locality of the kernels depends in a fundamental way on the choice of the forces $\boldsymbol{\mathcal{F}}$ and response $\boldsymbol{\mathcal{J}}$ in the equation (1.42). The strategy to adopt here is to try to embed all the information about the macroscopic boundary conditions, shape and size of the sample into the force $\boldsymbol{\mathcal{F}}$. The exact tactics however depends on the specific problem.

Let us illustrate these ideas with the example of the Kirkwood-Yvon dielectric, in which the kernel connecting the polarization $\boldsymbol{P}$ with the externally imposed electric field turns out to be non-local in contradistinction to the kernel connecting $\boldsymbol{P}$ with the local electric field in the sample.

From a molecular point of view, the sample of Kirkwood-Yvon dielectric consists of N molecules - identical polarizable dipoles. Such system is immersed in the external field $\boldsymbol{E}_o$.

The dipole moment $\boldsymbol{p}_i$ of molecule i is given by

$$\boldsymbol{p}_i = \alpha \left(\boldsymbol{E}_o(\boldsymbol{R}_i) + \sum_{j \neq i} \hat{\boldsymbol{T}}_{ij} \cdot \boldsymbol{p}_j \right), \tag{1.51}$$

where α is the molecular polarizability and $\hat{\boldsymbol{T}}$ stands for the dipole-dipole interaction tensor given by

$$\hat{\boldsymbol{T}}_{ij} = \hat{\boldsymbol{T}}(\boldsymbol{R}_i - \boldsymbol{R}_j),$$
$$\hat{\boldsymbol{T}}(\boldsymbol{r}) = \nabla\nabla \frac{1}{r} = -\frac{\mathbf{1}}{r^3} + \frac{3\hat{\boldsymbol{r}}\hat{\boldsymbol{r}}}{r^3}. \tag{1.52}$$

The above equation can be solved by iteration to yield $\boldsymbol{p}_i$ in form of the following series

$$
\begin{aligned}
\boldsymbol{p}_i &= \alpha(\boldsymbol{E}_o(\boldsymbol{R}_i) + \sum_{j \neq i} \hat{\boldsymbol{T}}_{ij} \cdot \boldsymbol{p}_j) = \\
&= \alpha \boldsymbol{E}_o(\boldsymbol{R}_i) + \alpha^2 \sum_{j \neq i} \hat{\boldsymbol{T}}_{ij} \cdot \boldsymbol{E}_o(\boldsymbol{R}_j) + \alpha^3 \sum_{j \neq i} \sum_{k \neq j} \hat{\boldsymbol{T}}_{ij} \hat{\boldsymbol{T}}_{jk} \cdot \boldsymbol{E}_o(\boldsymbol{R}_k) + \ldots
\end{aligned}
\tag{1.53}
$$

From here on we are going to consider only the first two terms (up to the second power of polarizability) in the above series, as they are enough to show the above-mentioned problems with the long-range kernels which diverge in thermodynamic limit.

The macroscopic polarization is given by

$$
\begin{aligned}
\boldsymbol{P}(\boldsymbol{r}) =& < \sum_i \boldsymbol{p}_i \delta(\boldsymbol{r} - \boldsymbol{R}_i) >= \alpha n_1(\boldsymbol{r}) \boldsymbol{E}_o(\boldsymbol{r}) + \\
&+ \alpha^2 \int n_2(\boldsymbol{r}, \boldsymbol{r}') \hat{\boldsymbol{T}}(\boldsymbol{r} - \boldsymbol{r}') \cdot \boldsymbol{E}_o(\boldsymbol{r}') \mathrm{d}\boldsymbol{r}' + \ldots,
\end{aligned}
\tag{1.54}
$$

where $n_1(\boldsymbol{r})$ and $n_2(\boldsymbol{r}, \boldsymbol{r}')$ are 1- and 2-particle distribution functions respectively. For a homogeneous system

$$
n_1(\boldsymbol{r}) = n
\tag{1.55}
$$

and

$$
n_2(\boldsymbol{r}, \boldsymbol{r}') = n_2(|\boldsymbol{r} - \boldsymbol{r}'|).
\tag{1.56}
$$

Therefore we obtain the response equation of the form (1.42)

$$
\boldsymbol{P}(\boldsymbol{r}) = \int \boldsymbol{L}(\boldsymbol{r} - \boldsymbol{r}') \cdot \boldsymbol{E}_o(\boldsymbol{r}') \mathrm{d}\boldsymbol{r}',
\tag{1.57}
$$

with the response kernel $\boldsymbol{L}$ given by

$$
\boldsymbol{L}(\boldsymbol{r}) = \alpha n \delta(\boldsymbol{r}) + \alpha^2 n_2(\boldsymbol{r}) \hat{\boldsymbol{T}}(\boldsymbol{r}),
\tag{1.58}
$$

which, due to (1.52) is clearly of a long range. The integral of the second term of the above equation over $\boldsymbol{r}$

$$
\alpha^2 \int n_2(\boldsymbol{r}) \left(-\frac{1}{r^3} + \frac{3 \hat{\boldsymbol{r}} \hat{\boldsymbol{r}}}{r^3} \right) \mathrm{d}\boldsymbol{r},
\tag{1.59}
$$

is conditionally convergent, its value of depending on the way the integration is done. For example if the integration over polar angles (θ, ϕ) is performed first, then the integral vanishes, whereas the integration over r for given θ and ϕ leads to divergences.

The reason for such a behavior of $\boldsymbol{P}$ is connected with the fact that the polarization is not a local quantity in a sense elucidated above. The value of $\boldsymbol{P}$ in a given place $\boldsymbol{r}$ inside

the dielectric depends not only on the local properties of the material such as the density of inclusions $n(\boldsymbol{r})$ but also on the conditions imposed on the boundaries of the sample no matter how far from $\boldsymbol{r}$ they are. To see it, consider a macroscopically homogeneous and isotropic dielectric slab cut from our dielectric and inserted between two parallel plates of a condenser. It is therefore subjected to a constant and homogeneous electric field $\boldsymbol{E}_o$ produced by the surface charge density σ on the condenser plates (Fig. 1.1). The field induces the nonzero charge density σ' on the dielectric surface, which gives rise to the additional field $\boldsymbol{E}'$, so that the total field $\boldsymbol{E}$ inside a dielectric is given by $\boldsymbol{E}_o + \boldsymbol{E}'$. The polarization of the dielectric is given by

$$\boldsymbol{P} = \chi \boldsymbol{E}, \tag{1.60}$$

where χ stands for the polarizability, whereas the dielectric displacement $\boldsymbol{D} = \boldsymbol{E} + 4\pi \boldsymbol{P}$ can be written as

$$\boldsymbol{D} = \epsilon \boldsymbol{E}, \tag{1.61}$$

which defines the dielectric constant ϵ. (In general ϵ and χ are the tensor functions of $\boldsymbol{r}$ but in the case under consideration they are just scalar constants).
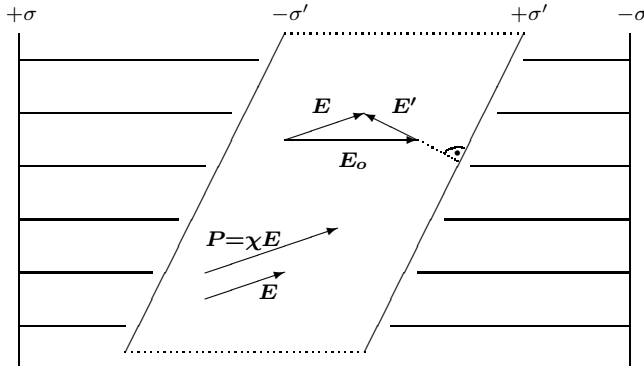
Figure 1.1: The dielectric slab immersed into an external electric field $\boldsymbol{E}_o$. The field of the induced dipoles inside the slab is denoted by $\boldsymbol{E}'$, whereas $\boldsymbol{E}$ denotes the total field inside the sample. While changing the orientation of the slab the direction and value of $\boldsymbol{E}$ and $\boldsymbol{P}$ would change, but the relation between them remains the same.

If we now rotate the slab, the value and the orientation of $\boldsymbol{E}'$, $\boldsymbol{E}$, $\boldsymbol{P}$ and $\boldsymbol{D}$ will change, as $\boldsymbol{E}'$ must be always perpendicular to the surface of the slab. Polarization therefore is not a local function of $\boldsymbol{E}_o$, as the value of $\boldsymbol{P}$ depends not only on $\boldsymbol{E}_o$ but also on the shape and the orientation of the sample. And so it is no wonder that the coefficient of proportionality between $\boldsymbol{P}$ and $\boldsymbol{E}_o$ calculated in (1.54) is given by a conditionally convergent integral -

to get the right value of $\boldsymbol{P}$ one needs additional information concerning the shape and orientation of the sample as a whole no matter how large it is.

However the situation would change dramatically if on studies the polarization as the function of the internal field $\boldsymbol{E}$ instead of $\boldsymbol{E}_o$. The functional dependence is now given by (1.60) in which a coefficient of proportionality χ is a local quantity, as all the boundary effects are already taken into account in $\boldsymbol{E}$.

To see it, let us calculate the polarization as a function of $\boldsymbol{E}$ following the algorithm presented in the paper by Felderhof, Ford and Cohen [39] based on the ideas of Finkel'berg [40].

First one expresses the internal field $\boldsymbol{E}$ by means of the external field $\boldsymbol{E}_o$

$$\boldsymbol{E}(\boldsymbol{r}) = \boldsymbol{E}_o(\boldsymbol{r}) + \alpha \int \hat{\boldsymbol{T}}(\boldsymbol{r} - \boldsymbol{r}') n_1(\boldsymbol{r}') \boldsymbol{E}_o(\boldsymbol{r}') \mathrm{d}\boldsymbol{r}' + ... \tag{1.62}$$

Then this relation is inverted to yield $\boldsymbol{E}_o$ as a function of $\boldsymbol{E}$

$$\boldsymbol{E}_o(\boldsymbol{r}) = \boldsymbol{E}(\boldsymbol{r}) - \alpha \int \hat{\boldsymbol{T}}(\boldsymbol{r} - \boldsymbol{r}') n_1(\boldsymbol{r}') \boldsymbol{E}(\boldsymbol{r}') \mathrm{d}\boldsymbol{r}' + \ldots \tag{1.63}$$

Finally the above results is inserted in (1.54) yielding to the second order in α

$$\begin{aligned} \boldsymbol{P}(\boldsymbol{r}) = {} & \alpha n_1(\boldsymbol{r}) \boldsymbol{E}(\boldsymbol{r}) + \\ & + \alpha^2 \int \hat{\boldsymbol{T}}(\boldsymbol{r} - \boldsymbol{r}') [n_2(\boldsymbol{r}, \boldsymbol{r}') - n_1(\boldsymbol{r}) n_1(\boldsymbol{r}')] \boldsymbol{E}(\boldsymbol{r}') \mathrm{d}\boldsymbol{r}' + ... \end{aligned} \tag{1.64}$$

The main difference between expressions (1.64) and (1.54) is that the two body distribution function $n_2(\boldsymbol{r}, \boldsymbol{r}')$ in (1.54) is replaced by the correlation function $h_2(\boldsymbol{r}, \boldsymbol{r}') = n_2(\boldsymbol{r}, \boldsymbol{r}') - n(\boldsymbol{r}) n(\boldsymbol{r}')$ which decays rapidly on the lengthscale of mean distance between the inclusions, which makes the integral in (1.64) convergent.

Naturally the above considerations could not serve as a proof that χ is a local quantity, as we have restricted ourselves only to the first two terms in expansion in α. The general proof where the whole series is taken into account has been obtained by Felderhof, Ford and Cohen in [39]. It is amazing that the statement that polarizability (and similarly the dielectric constant) are well-defined and independent of the shape of the sample in the limit of a large system has waited so long to be proved.

1.7   Long-range interactions and divergence problems for colloidal suspensions

The mesoscopic particles suspended in a fluid must be regarded as a system with long-range interactions even if the potential of direct interparticle forces is hard-sphere like. The source of this behavior is the long range of the hydrodynamic interactions, what can be seen even in the simplest problem of a sphere sedimenting in a quiescent fluid under the

influence of a constant force $\boldsymbol{F}$. As it was already mentioned the velocity of such a sphere is given by the Stokes law

$$\boldsymbol{U}_o = \frac{\boldsymbol{F}}{6\pi\eta a}. \tag{1.65}$$

The flow disturbance caused by the presence of a sphere, first derived also by Stokes [4], reads

$$\boldsymbol{v}(\boldsymbol{R}_1 + \boldsymbol{r}) = \boldsymbol{U}_o(\frac{3a}{4r} + \frac{a^3}{4r^3}) + \boldsymbol{r}\frac{\boldsymbol{r} \cdot \boldsymbol{U}_o}{r^2}(\frac{3a}{4r} - \frac{3a^3}{4r^3}), \tag{1.66}$$

where $\boldsymbol{r}$ measures the distance from the center of a sphere located at $\boldsymbol{R}_1$. Note that this disturbance is of a very long range: it decays as r^{-1}. Let us now add one more sphere at the position $\boldsymbol{R}_2$ sufficiently distant from $\boldsymbol{R}_1$ so that $|\boldsymbol{R}_1 - \boldsymbol{R}_2| = R_{12} \gg a$. Then from (1.66) to the first order in a/R_{12} sphere 1 feels the flow caused by sphere 2 of the following strength

$$\boldsymbol{U}_{12} = \frac{3a}{4R_{12}}(\mathbf{1} + \hat{\boldsymbol{R}}_{12}\hat{\boldsymbol{R}}_{12}) \cdot \frac{\boldsymbol{F}}{6\pi\eta a} + \dots \tag{1.67}$$

Therefore the velocity of the sphere 2 is now diminished with respect to the single-sphere sedimentation velocity and reads

$$\boldsymbol{U}_1 = \frac{\boldsymbol{F}}{6\pi\eta a} - \frac{3a}{4R_{12}}(\mathbf{1} + \hat{\boldsymbol{R}}_{12}\hat{\boldsymbol{R}}_{12}) \cdot \frac{\boldsymbol{F}}{6\pi\eta a} + \dots \tag{1.68}$$

Now if the same reasoning is applied to the sedimentation of the dilute cloud of N identical spheres then, to the first order in the inverse of interparticle distance one gets

$$\boldsymbol{U}_i = \frac{\boldsymbol{F}}{6\pi\eta a} - \sum_j \frac{3a}{4R_{ij}}(\mathbf{1} + \hat{\boldsymbol{R}}_{ij}\hat{\boldsymbol{R}}_{ij}) \cdot \frac{\boldsymbol{F}}{6\pi\eta a} + \dots \tag{1.69}$$

The macroscopic particle current, given in terms of $\boldsymbol{U}_i$ by

$$\boldsymbol{J}(\boldsymbol{r}) = < \sum_i \boldsymbol{U}_i \delta(\boldsymbol{r} - \boldsymbol{R}_i) >, \tag{1.70}$$

reads therefore (for the bit more general case of the space-dependent field $\boldsymbol{F}(\boldsymbol{r})$)

$$\boldsymbol{J}(\boldsymbol{r}) = \frac{\boldsymbol{F}(\boldsymbol{r})}{6\pi\eta a}n_1(\boldsymbol{r}) - \int_V \frac{3a}{4|\boldsymbol{r} - \boldsymbol{r}'|}(\mathbf{1} + \widehat{(\boldsymbol{r} - \boldsymbol{r}')}\widehat{(\boldsymbol{r} - \boldsymbol{r}')}) \cdot \frac{\boldsymbol{F}(\boldsymbol{r}')}{6\pi\eta a}n_2(\boldsymbol{r}, \boldsymbol{r}')\mathrm{d}\boldsymbol{r}' + \dots, \tag{1.71}$$

where $n_1(\boldsymbol{r})$ and $n_2(\boldsymbol{r}, \boldsymbol{r}')$ are 1- and 2-particle distribution functions respectively. We again recognize the structure of the response equation (1.42) this time with

$$\boldsymbol{L}(\boldsymbol{r}) = \frac{n\mathbf{1}}{6\pi\eta a}\delta(\boldsymbol{r}) - \frac{3a}{4r}(\mathbf{1} + \hat{r}\hat{r})\frac{1}{6\pi\eta a}n_2(\boldsymbol{r}) + \dots, \tag{1.72}$$

where the homogeneity of the system was assumed. We see here the problem analogous to that encountered previously while studying the polarization as a function of an external field (1.54): the integral of the kernel $\boldsymbol{L}$ over the volume V

$$\int_V \boldsymbol{L}(\boldsymbol{r})\mathrm{d}\boldsymbol{r} \tag{1.73}$$

is divergent as $V \to \infty$. This fact was noticed for the first time by Smoluchowski in 1912 [41]. As it was already remarked, such a behavior of the response kernels is a manifestation of the fact that the relation between $\boldsymbol{J}(\boldsymbol{r})$ and $\boldsymbol{F}$ is not local: depends not only on the microstructure of the material in vicinity of $\boldsymbol{r}$ but also on the global properties like the shape or size of the sample. In case of the dielectric the problem was resolved by studying the response of the system to the internal field $\boldsymbol{E}$ rather than the external $\boldsymbol{E}_o$. For the internal field $\boldsymbol{E}$ one gets the macroscopic equations in which the shape and size of the sample enter through the boundary conditions. We are going to show in Chapters 6 and 7 that the appropriate local equations for the response of the suspension to the external force acting on particles are given by

$$\boldsymbol{J}(\boldsymbol{r}) = \int \boldsymbol{L}_1(\boldsymbol{r} - \boldsymbol{r}') \cdot \boldsymbol{F}(\boldsymbol{r}')\mathrm{d}\boldsymbol{r}' + \int \boldsymbol{L}_2(\boldsymbol{r} - \boldsymbol{r}') \cdot < \boldsymbol{v}(\boldsymbol{r}') > \mathrm{d}\boldsymbol{r}', \tag{1.74}$$

where $\boldsymbol{v}(\boldsymbol{r})$ is the velocity field of the suspension as a whole (equal to the fluid velocity, if the point $\boldsymbol{r}$ belongs to the fluid domain or to the particle velocity whenever $\boldsymbol{r}$ is inside one of the particles). This time the kernels $\boldsymbol{L}_1$ and $\boldsymbol{L}_2$ are short ranged. In the case considered above these kernels reduce to

$$\boldsymbol{L}_1(\boldsymbol{r}) = \frac{n\mathbf{1}}{6\pi\eta a}\delta(\boldsymbol{r}) - \frac{3a}{4r}(\mathbf{1} + \hat{\boldsymbol{r}}\hat{\boldsymbol{r}})\frac{1}{6\pi\eta a}h_2(\boldsymbol{r}) + \ldots, \tag{1.75}$$

$$\boldsymbol{L}_2(\boldsymbol{r}) = n\delta(\boldsymbol{r})\mathbf{1} + \ldots, \tag{1.76}$$

where again as in (1.64) the two-particle correlation function $h_2(\boldsymbol{r})$ appeared instead of the distribution function $n_2(\boldsymbol{r})$ in (1.72). The presence of $h(\boldsymbol{r})$ makes the integral (1.76) convergent with the well-defined limit as $V \to \infty$. Again, the kernels $\boldsymbol{L}_1$ and $\boldsymbol{L}_2$ are much more complicated when all the hydrodynamic interactions are taken into account and not only the two-body, asymptotic terms like in Eq. (1.71). Nevertheless one can prove that always

$$\lim_{k \to 0} \boldsymbol{L}_2(k) = \boldsymbol{L}_2(k = 0) = n\mathbf{1}. \tag{1.77}$$

Therefore one sees that there appears in the natural way in our equations the diffusion current $\boldsymbol{J}_d = \boldsymbol{J} - n < \boldsymbol{v} >$, as in the limit $k \to 0$ the response equation (1.74) takes form

$$\boldsymbol{J}_d(k) = \boldsymbol{L}_1(k)\boldsymbol{F}(k) \tag{1.78}$$

The realization of the fact that one should look for the response equations in form (1.74) rather than (1.71) came surprisingly late: it was presented in papers by Nozières [42],

Felderhof [43] and Noetinger [23] in late eighties. Earlier, the calculations of D_c were performed by means of integrating the long-range response kernel and the problems with divergences encountered there were coped with by a number of "tips and tricks". The first who performed this kind of calculations was Burgers [44–47]. As Batchelor [48] comments: "Burgers tried a variety of ways of overcoming the difficulty presented by the lack of absolute convergence of the sum of the separate effects of an indefinitely large number of falling spheres on a given sphere (...) and his sequence of papers is remarkable for the number of different answers provided". Batchelor himself dealt with the divergent integrals in a very clever way. First he subtracted from the long-range diffusion kernel the quantities the value of which could be found exactly and which share the same long-range behaviour as the kernel. Then the remaining part could be expressed in terms of an absolutely convergent integral. In this way Batchelor succeeded in estimating the result for the collective diffusion coefficient to the first order in the volume fraction ϕ [48,49]

$$D_c^s = D_o(1 + 1.45\phi + \dots). \tag{1.79}$$

1.8 Goal of the Thesis and the means of reaching it

The goal of this work is to determine whether the memory contribution to the long time diffusion coefficient Δ vanishes or not. Ackerson [50, 51] in his paper from 1978 proved that the memory term vanishes in the suspensions in which the hydrodynamic interactions can be neglected. He shows also that the above statement remains true for the hydrodynamically interacting suspensions which are so dilute that only two-body hydrodynamic interactions are important. Finally Ackerson conjectures that for concentrated suspensions Δ should be different from zero. In the Thesis we would give this statement a more firm basis. First we are bound to cope with the long-range character of the kernels which describe the part of the system's response connected with the memory effects. Finding the short-range kernels in this case is quite formidable, as the operator $\boldsymbol{D}_{ij}$ governing the evolution of the system is long- ranged itself! When the correct short-range kernels are found, the next step is to estimate Δ and then the last step is the comparison of the results with the experimental data. It is surprising that since the Ackerson papers in late seventies, there was practically no progress in assessing the memory contribution to the collective diffusion in the small wavevector limit (corresponding to the $\lim_{k\to 0}\Delta(k)$). Much more attention was devoted to the problem of calculating $\Delta(k)$ for finite k, mainly in frames of the mode-mode coupling theory. The papers of Nägele and co-workers [9, 52–54], Verberg, de Schepper and Cohen [55, 56] and Felderhof and Vogel [57] should be mentioned in this connection. However in all these papers the hydrodynamic interactions are either neglected or assumed to be pairwise additive which, as it was shown by Ackerson leads to $\lim_{k\to 0}\Delta(k) = 0$.

1.9 The outline of the Thesis

The Thesis is organized as follows. Chapter 2 is devoted to the hydrodynamic formalism, which allows one to obtain the velocities of the suspended particles and the velocity field of the suspending fluid, once the positions of the particles and the forces acting on the suspension are known. Chapter 3 deals with the question of statistical description of suspended particles; here the Smoluchowski equation is presented. Then, in Chapter 4 the dynamic structure factor is analyzed by means of the Zwanzig-Mori formalism and the key concepts for this work, such as the memory function and collective diffusion coefficient, are introduced. Finally, the expression for the long-time collective diffusion coefficient for the system of interacting Brownian particles is obtained. In the next Chapter the problem of collective diffusion is approached in a different way. By use of the nonequilibrium thermodynamics formalism the phenomenological equation for D_c is obtained and it is shown that instead of considering the system response to the density gradient one can obtain D_c by studying response of the suspension to the external force applied to each particle. This is the ground for the derivation of the expression for D_c for interacting Brownian particles in frame of linear response theory, which is presented in the second part of the Chapter. Unfortunately, this way of calculating the collective diffusion coefficient requires performing the small k limit of long-ranged kernels, which, although correct, is not entirely satisfying, as one would like to have the local equations describing system's response, independent of the boundary conditions. The derivation of such equations is presented in Chapters 6 and 7. Chapter 6 deals with the instantaneous response described by the short-time diffusion coefficient. This is really a re-derivation of the results obtained by Nozières [42], Felderhof [43] and Noetinger [23] but our point here is to introduce the novel, diagrammatic representation of the kernels which greatly facilitates all the derivations. This method is used in Chapter 7 to cope with the part of system's response connected with the memory effects. This is the main theoretical part of the Thesis and the results obtained here are original. Next two Chapters are devoted to numerical estimation of Δ with use of both the equilibrium Monte Carlo averaging and Brownian Dynamics simulations. Finally, in the last Chapter, the comparison of obtained results with the experimental data is performed.

Chapter 2

Hydrodynamics of suspensions

In this Chapter a general formalism is presented by means of which the problem of finding the friction and mobility matrices defined by (1.14) and (1.15) for a given configuration of particles in a suspension can be solved. This formalism was developed by Bedeaux, Mazur and van Saarlos [58, 59] and Cichocki, Felderhof and Schmitz [60–70]. Here we follow the notation of the latter group.

2.1 Hydrodynamic equations

We model the colloidal suspension as a system of N identical spherical particles with radius a and position vectors $\boldsymbol{R}_i$ immersed in a suspending fluid of shear viscosity η contained in the volume V. It is argued in the Introduction that, in the timescales of interest, the velocity and pressure of the suspending fluid can be described by the stationary Stokes equations of the form

$$\eta \nabla^2 \boldsymbol{v} - \nabla p + \boldsymbol{f}_o(\boldsymbol{r}) = 0, \qquad \nabla \cdot \boldsymbol{v} = 0. \qquad (2.1)$$

In the above equation $\boldsymbol{f}_o(\boldsymbol{r})$ represents the external force density exerted on the fluid (for example gravity or the centrifugal force).

The equation should be supplemented with appropriate boundary conditions on the fluid boundaries - i.e. on the surfaces of the spheres and the external boundary ∂V. For the stick boundary conditions on the surface of each sphere we have

$$\boldsymbol{v}(\boldsymbol{r}) = \boldsymbol{u}_i(\boldsymbol{r}) \equiv \boldsymbol{U}_i + \boldsymbol{\Omega}_i \times (\boldsymbol{r} - \boldsymbol{R}_i) \qquad \text{for } |\boldsymbol{r} - \boldsymbol{R}_i| = a, \qquad (2.2)$$

where $\boldsymbol{U}_i(t)$ and $\boldsymbol{\Omega}_i(t)$ are the translational and rotational velocities of the i-th sphere situated at $\boldsymbol{R}_i(t)$. The field $\boldsymbol{u}_i$ describes therefore the rigid motion of the particle i.

It was shown by Mazur and Bedeaux [58] that if the particles are impenetrable to the flow and the stick boundary conditions at their surfaces are assumed, then the validity of Eq. (2.1) may be formally extended inside the particles:

$$\eta \nabla^2 \boldsymbol{v} - \nabla p + \boldsymbol{f}_o(\boldsymbol{r}) + \boldsymbol{f}(\boldsymbol{r}) = 0,$$
$$\nabla \cdot \boldsymbol{v} = 0,$$
$$\boldsymbol{v}(\boldsymbol{r}) = \boldsymbol{u}_i(\boldsymbol{r}) = \boldsymbol{U}_i + \boldsymbol{\Omega}_i \times (\boldsymbol{r} - \boldsymbol{R}_i) \qquad \text{for} \quad |\boldsymbol{r} - \boldsymbol{R}_i| \le a,$$
$$p(\boldsymbol{r}) = 0 \qquad \qquad \text{for} \quad |\boldsymbol{r} - \boldsymbol{R}_i| \le a, \qquad (2.3)$$

with the additional force density $\boldsymbol{f}(\boldsymbol{r})$ localized on the surfaces of the spheres

$$\boldsymbol{f}(\boldsymbol{r}) = \sum_i \boldsymbol{f}(\boldsymbol{r}; i) \qquad \qquad (2.4)$$

$$\boldsymbol{f}(\boldsymbol{r}; i) \neq 0 \qquad \qquad \text{only if} \quad |\boldsymbol{r} - \boldsymbol{R}_i| = a. \qquad (2.5)$$

From now on we restrict ourselves to the particles impenetrable to the flow, although the generalization to the case of the particles permeable to the flow is possible.

We introduce also the notion of the **ambient flow** $\tilde{\boldsymbol{v}}_o$ - i.e. the flow which would satisfy Eqs. (2.1) in the absence of the particles and the external forces (the boundary conditions on the external boundary ∂V remain the same). Therefore $\tilde{\boldsymbol{v}}_o$ satisfies

$$\eta \nabla^2 \tilde{\boldsymbol{v}}_o - \nabla p_o = 0, \qquad \nabla \cdot \tilde{\boldsymbol{v}}_o = 0. \qquad (2.6)$$

together with the boundary conditions on the outer boundary ∂V, which remain the same as in the case when spheres are present.

2.2   Hydrodynamic Green function

To introduce the hydrodynamic Green function we seek the solution $\big(\boldsymbol{v}(\boldsymbol{r}), p(\boldsymbol{r})\big)$ of Eq. (2.1) with the delta point force

$$\eta \nabla^2 \boldsymbol{v} - \nabla p + \boldsymbol{f} \delta(\boldsymbol{r} - \boldsymbol{r}_o) = 0, \qquad \nabla \cdot \boldsymbol{v} = 0. \qquad (2.7)$$

We write the solution in the form

$$\boldsymbol{v}(\boldsymbol{r}) = \boldsymbol{G}(\boldsymbol{r}, \boldsymbol{r}_o) \cdot \boldsymbol{f} \qquad p(\boldsymbol{r}) = \boldsymbol{P}(\boldsymbol{r}, \boldsymbol{r}_o) \cdot \boldsymbol{f} \qquad (2.8)$$

and hereby define the Green tensor $\boldsymbol{G}(\boldsymbol{r}, \boldsymbol{r}_o)$ and its associated pressure vector $\boldsymbol{P}(\boldsymbol{r}, \boldsymbol{r_o})$.

In case when the fluid fills the whole space (i.e. $\partial V \to \infty$) the hydrodynamic Green function is given by the Oseen tensor $\boldsymbol{G_o}$

$$\boldsymbol{G}(\boldsymbol{r}, \boldsymbol{r}') = \boldsymbol{G}_o(\boldsymbol{r} - \boldsymbol{r}'),$$
$$\boldsymbol{G}_o(\boldsymbol{r}) \equiv \frac{1}{8\pi\eta} \frac{\boldsymbol{1} + \hat{\boldsymbol{r}}\hat{\boldsymbol{r}}}{r}, \qquad (2.9)$$

whereas its pressure field reads

$$\boldsymbol{P}(\boldsymbol{r}, \boldsymbol{r}') = \boldsymbol{P}_o(\boldsymbol{r} - \boldsymbol{r}'),$$
$$\boldsymbol{P}_o(\boldsymbol{r}) = \frac{\boldsymbol{r}}{4\pi r^2}. \tag{2.10}$$

The Green function can be used to write the solution of (2.3) as

$$\boldsymbol{v}(\boldsymbol{r}) = \boldsymbol{v}_o(\boldsymbol{r}) + \int \boldsymbol{G}(\boldsymbol{r}, \boldsymbol{r}') \cdot \boldsymbol{f}(\boldsymbol{r}') d\boldsymbol{r}', \tag{2.11}$$

where $\boldsymbol{v}_o(\boldsymbol{r})$ is the flow in the absence of the particles given by

$$\boldsymbol{v}_o(\boldsymbol{r}) = \tilde{\boldsymbol{v}}_o(\boldsymbol{r}) + \int \boldsymbol{G}(\boldsymbol{r}, \boldsymbol{r}') \cdot \boldsymbol{f}_o(\boldsymbol{r}') d\boldsymbol{r}'. \tag{2.12}$$

From the linearity of equations (2.3) we infer that the relation between $\boldsymbol{f}$ and $\boldsymbol{v} - \boldsymbol{v}_o$ should also be linear, i.e. there exists an operator $\boldsymbol{\mathcal{Z}}(\boldsymbol{r}, \boldsymbol{r}')$ called "friction kernel", such that

$$\boldsymbol{f}(\boldsymbol{r}) = \int \boldsymbol{\mathcal{Z}}(\boldsymbol{r}, \boldsymbol{r}') \cdot (\boldsymbol{v}(\boldsymbol{r}') - \boldsymbol{v}_o(\boldsymbol{r}')) d\boldsymbol{r}', \tag{2.13}$$

where the operator $\boldsymbol{\mathcal{Z}}$ is localized on the surfaces of the spheres.

To keep the formulae as simple as possible we are going to use sometimes the compact notation, in which the dependence of the quantities on the space variables as well as integration over these variables is suppressed. According to this notation Eq. (2.13) is written as

$$\boldsymbol{f} = \boldsymbol{\mathcal{Z}}(\boldsymbol{v} - \boldsymbol{v}_o). \tag{2.14}$$

Let us consider now some point on the surface of i-th sphere $\boldsymbol{r} \in S_i$. The expression (2.11) for the flow velocity $\boldsymbol{v}(\boldsymbol{r})$, which in this case must be equal to $\boldsymbol{u}_i(\boldsymbol{r})$, can be written as a sum of the following terms

$$\boldsymbol{v}(\boldsymbol{r}) = \boldsymbol{u}_i(\boldsymbol{r}) = \boldsymbol{v}_o(\boldsymbol{r}) + \int \boldsymbol{G}(\boldsymbol{r}, \boldsymbol{r}') \cdot \boldsymbol{f}(\boldsymbol{r}'; i) \mathrm{d}\boldsymbol{r}' +$$
$$+ \sum_{j \neq i} \int \boldsymbol{G}(\boldsymbol{r}, \boldsymbol{r}') \cdot \boldsymbol{f}(\boldsymbol{r}'; j) \mathrm{d}\boldsymbol{r}' \qquad \boldsymbol{r} \in S_i, \quad i = 1, \ldots, N, \tag{2.15}$$

where the contributions to $\boldsymbol{u}_i(\boldsymbol{r})$ from the force density on the particle i and on the particles $j \neq i$ have been singled out. The first of these terms can be written using the **one-particle friction operator** $\boldsymbol{Z}_o(i)$ (defined by (2.13) for a single sphere) as

$$[\boldsymbol{Z}_o^{-1}(i)\boldsymbol{f}(i)](\boldsymbol{r}) = \int \boldsymbol{G}(\boldsymbol{r}, \boldsymbol{r}') \cdot \boldsymbol{f}(\boldsymbol{r}'; i) \mathrm{d}\boldsymbol{r}' \qquad \boldsymbol{r} \in S_i. \tag{2.16}$$

whereas the second one is used to define the **Green operator** $\boldsymbol{G}(ij)$ [71]

$$[\boldsymbol{G}(ij)\boldsymbol{f}(j)](\boldsymbol{r}) \equiv \int \boldsymbol{G}(\boldsymbol{r},\boldsymbol{r}') \cdot \boldsymbol{f}(\boldsymbol{r}';j)d\boldsymbol{r}' \quad i \neq j \quad \boldsymbol{r} \in S_i. \tag{2.17}$$

The operator $\boldsymbol{Z}_o$ can be derived by solving the relatively simple problem of one sphere moving in a given flow field. The important thing is that changing of the boundary conditions in our problem (for example choosing slip instead of stick boundary conditions at the surfaces of the spheres in (2.2)) results only in change of $\boldsymbol{Z}_o$ - the form of all the other operators remain the same. For the explicit form of $\boldsymbol{Z}_o$ for variety of boundary conditions we refer the reader to the paper [67].

The equation (2.15) can be rewritten in a compact way as

$$\boldsymbol{u}_i - \boldsymbol{v}_o = (\boldsymbol{\mathcal{G}} + \boldsymbol{\mathcal{Z}}_o^{-1})_{ij}\boldsymbol{f}_j \tag{2.18}$$

where

$$\boldsymbol{\mathcal{Z}}_{oij} = \boldsymbol{Z}_o(i)\delta_{ij} \qquad \boldsymbol{\mathcal{G}}_{ij} = \boldsymbol{G}(ij)(1 - \delta_{ij}) \tag{2.19}$$

are the NxN operator matrices in the particle indexes. We adopt here (as well as further on in the Thesis) the following convention with regard to the notation: the script letters $(\boldsymbol{\mathcal{G}}, \boldsymbol{\mathcal{Z}}, \tilde{\boldsymbol{\mathcal{F}}}, ...)$ would denote multidimensional (to be exact: more than three dimensional) vectors and matrices. On the other hand usual block letters $(\boldsymbol{E}, \boldsymbol{F}, \boldsymbol{U}...)$ stand for the three dimensional objects.

By comparison of the relation (2.13) with the equation (2.18) we get

$$\boldsymbol{\mathcal{Z}} = \frac{1}{\boldsymbol{\mathcal{G}} + \boldsymbol{\mathcal{Z}}_o^{-1}} = \boldsymbol{\mathcal{Z}}_o(1 + \boldsymbol{\mathcal{G}}\boldsymbol{\mathcal{Z}}_o)^{-1}, \tag{2.20}$$

2.3 Construction of the hydrodynamic matrices

Now that we have the friction kernel $\boldsymbol{\mathcal{Z}}$ we can construct the friction matrix $\boldsymbol{\zeta}$ (1.14) which relates the forces and torques acting on the particles to their translational and rotational velocities in absence of the ambient flow

$$\tilde{\boldsymbol{\mathcal{F}}} = \boldsymbol{\zeta} \cdot \tilde{\boldsymbol{\mathcal{U}}}, \tag{2.21}$$

with $\tilde{\boldsymbol{\mathcal{F}}} = (\boldsymbol{\mathcal{F}}, \boldsymbol{\mathcal{T}})$ and $\tilde{\boldsymbol{\mathcal{U}}} = (\boldsymbol{\mathcal{U}}, \boldsymbol{\Omega})$.

Sometimes instead of one big 6Nx6N matrix $\boldsymbol{\zeta}$ the four smaller matrices $\boldsymbol{\zeta}^{tt}, \boldsymbol{\zeta}^{tr}, \boldsymbol{\zeta}^{rt}, \boldsymbol{\zeta}^{rr}$ are used:

$$\begin{pmatrix} \boldsymbol{\mathcal{F}} \\ \boldsymbol{\mathcal{T}} \end{pmatrix} = \begin{bmatrix} \boldsymbol{\zeta}^{tt} & \boldsymbol{\zeta}^{tr} \\ \boldsymbol{\zeta}^{rt} & \boldsymbol{\zeta}^{rr} \end{bmatrix} \begin{pmatrix} \boldsymbol{\mathcal{U}} \\ \boldsymbol{\Omega} \end{pmatrix}. \tag{2.22}$$

So the matrix $\boldsymbol{\zeta}^{tr}$ connects the translational (t) part of the velocities $(\boldsymbol{\mathcal{U}})$ with the rotational (r) part of forces $(\boldsymbol{\mathcal{T}})$ etc.

The force $\boldsymbol{F}_i$ and the torque $\boldsymbol{T}_i$ acting on i-th particle can be obtained from the force density $\boldsymbol{f}$ by the following operations

$$\boldsymbol{F}_i = \int \boldsymbol{f}(\boldsymbol{r})\theta_i(\boldsymbol{r})\mathrm{d}\boldsymbol{r} \tag{2.23}$$

$$\boldsymbol{T}_i = \int (\boldsymbol{r} - \boldsymbol{R}_i) \times \boldsymbol{f}(r)\theta_i(\boldsymbol{r})\mathrm{d}\boldsymbol{r},$$

where

$$\theta_i(\boldsymbol{r}) = \theta(a - |\boldsymbol{r} - \boldsymbol{R}_i|) \tag{2.24}$$

is the characteristic function for the particle.

The above relations can be written in the operator language as

$$\tilde{\boldsymbol{\mathcal{F}}} = \boldsymbol{\mathcal{P}}\boldsymbol{f}, \tag{2.25}$$

where the tensor projection operator $\boldsymbol{\mathcal{P}} = (\boldsymbol{\mathcal{P}}^t, \boldsymbol{\mathcal{P}}^r)$ is given by

$$\boldsymbol{\mathcal{P}}^t(\boldsymbol{r}; i) = \theta_i(\boldsymbol{r})\boldsymbol{1}$$
$$\boldsymbol{\mathcal{P}}^r(\boldsymbol{r}; i) = \theta_i(\boldsymbol{r})\epsilon_{\alpha\beta\gamma}(\boldsymbol{r} - \boldsymbol{R}_i)_\gamma. \tag{2.26}$$

With the use of $\boldsymbol{\mathcal{P}}$ the relation between the friction matrix and the friction kernel can be written as

$$\boldsymbol{\zeta} = \boldsymbol{\mathcal{P}}\boldsymbol{\mathcal{Z}}\boldsymbol{\mathcal{P}}. \tag{2.27}$$

For example $\boldsymbol{\zeta}_{12}^{tt}$ is given by

$$\boldsymbol{\zeta}_{12}^{tt} = \int\int \mathrm{d}\boldsymbol{r}\mathrm{d}\boldsymbol{r}'\theta_1(\boldsymbol{r})\boldsymbol{\mathcal{Z}}(\boldsymbol{r}, \boldsymbol{r}')\theta_2(\boldsymbol{r}') = \boldsymbol{\mathcal{P}}^t\boldsymbol{\mathcal{Z}}\boldsymbol{\mathcal{P}}^t. \tag{2.28}$$

When the ambient flow is present, from (2.14) together with (2.21) one gets for the forces $\tilde{\boldsymbol{\mathcal{F}}}$ as functions of $\tilde{\boldsymbol{\mathcal{U}}}$ and $\boldsymbol{v}_o$

$$\tilde{\boldsymbol{\mathcal{F}}} = \boldsymbol{\zeta} \cdot \tilde{\boldsymbol{\mathcal{U}}} - \boldsymbol{\mathcal{P}}\boldsymbol{\mathcal{Z}}\boldsymbol{v}_o. \tag{2.29}$$

Let us now consider a task of finding $\tilde{\boldsymbol{\mathcal{U}}}$ for given $\tilde{\boldsymbol{\mathcal{F}}}$ and $\boldsymbol{v}_o$. Such a problem is quite common in experiments, when we can control the forces acting on the particles (for example by putting them into a gravitational field) as well as the ambient flow (for example by putting the suspension into a shear flow) and seek the velocities that the suspended particles acquire.

From the relation (2.29) together with (2.14) one gets

$$\tilde{\mathcal{U}} = \zeta^{-1}\tilde{\mathcal{F}} + \zeta^{-1}\mathcal{P}\mathcal{Z}v_o \equiv \mu\tilde{\mathcal{F}} + \mathcal{C}v_o, \tag{2.30}$$

which defines the **mobility matrix μ**

$$\mu = \zeta^{-1} \tag{2.31}$$

together with the convection kernel $\mathcal{C}$

$$\mathcal{C} = \mu\mathcal{P}\mathcal{Z}. \tag{2.32}$$

In the analogous way as it was done for the friction matrix (2.22) one can introduce the 3Nx3N matrices $\mu^{tt}, \mu^{tr}, \mu^{rt}$ and μ^{rr}.

It is worth to note that the transpose of the $\mathcal{C}$ operator

$$\tilde{\mathcal{C}} = \mathcal{Z}\mathcal{P}\mu \tag{2.33}$$

can be used to solve the problem of finding the force density f when $\tilde{\mathcal{F}} \neq 0$ is given and the ambient flow vanishes. From (2.29) and (2.14) we get in this case

$$f = \mathcal{Z}\mathcal{P}\mu\tilde{\mathcal{F}}. \tag{2.34}$$

2.4   Scattering expansion

When we expand the operator $(1 + \mathcal{G}\mathcal{Z}_o)^{-1}$ in (2.20) in a series we get the following expression for the friction matrix

$$\zeta(1..N)_{ij} = \mathcal{P}\mathbf{Z}_o(i)\mathcal{P}\delta_{ij} - \mathcal{P}\mathbf{Z}_o(i)\mathbf{G}(ij)\mathbf{Z}_o(j)\mathcal{P} +$$
$$(-1)^{l+1}\sum_{l=1}^{\infty}\mathcal{P}\mathbf{Z}_o(i)\sum{}'[\prod_{k=1}^{l}\mathbf{G}(m_{k-1}m_k)\mathbf{Z}_o(m_k)]\mathbf{G}(m_l j)\mathbf{Z}_o(j)\mathcal{P}, \tag{2.35}$$

where $m_0 = i$ and the sum $\sum'$ is over all sequences $(m_1, m_2, \ldots, m_l)$ of l labels with the condition that no label should be repeated in succession and moreover $m_1 \neq i$ as well as $m_l \neq j$. Such a series is called a multiple scattering expansion: the flow velocity around the particle j gives rise to the force density on this particle $f(j) = \mathbf{Z}_o(j)v$, which in turn generates flow patterns around the particle m_l: $v = \mathbf{G}(m_l, j)f(j)$ which contributes to $f(m_l)$ etc.

The similar multiple scattering expansion can be derived for the mobility operator μ. In the Appendix A we show that

$$\mu = \mu_o + \mu_o\mathcal{P}\mathcal{Z}_o\frac{1}{1 + \mathcal{G}\hat{\mathcal{Z}}_o}\mathcal{G}\mathcal{Z}_o\mathcal{P}\mu_o = \mu_o + \sum_{k=0}^{\infty}\mu_o\mathcal{P}\mathcal{Z}_o(-\mathcal{G}\hat{\mathcal{Z}}_o)^k\mathcal{G}\mathcal{Z}_o\mathcal{P}\mu_o, \tag{2.36}$$

where

$$\boldsymbol{\mu}_o = \boldsymbol{\zeta}_o^{-1} \tag{2.37}$$

is the one particle mobility matrix, and $\hat{\boldsymbol{\mathcal{Z}}}_{\boldsymbol{o}}$ - the convective extended friction matrix [64] defined as

$$\hat{\boldsymbol{\mathcal{Z}}}_{\boldsymbol{o}} = \boldsymbol{\mathcal{Z}}_o - \boldsymbol{\mathcal{Z}}_o \boldsymbol{\mathcal{P}} \boldsymbol{\mu}_o \boldsymbol{\mathcal{P}} \boldsymbol{\mathcal{Z}}_o. \tag{2.38}$$

Note that

$$\hat{\boldsymbol{\mathcal{Z}}}_{\boldsymbol{o}} \boldsymbol{\mathcal{P}} = \boldsymbol{\mathcal{Z}}_o \boldsymbol{\mathcal{P}} - \boldsymbol{\mathcal{Z}}_o \boldsymbol{\mathcal{P}} \boldsymbol{\mu}_o \boldsymbol{\mathcal{P}} \boldsymbol{\mathcal{Z}}_o \boldsymbol{\mathcal{P}} = 0, \tag{2.39}$$

where we have used the relation (2.37) and (2.14).

In order to simplify the notation we introduce after Felderhof the convective friction kernel

$$\hat{\boldsymbol{\mathcal{Z}}} = \hat{\boldsymbol{\mathcal{Z}}}_{\boldsymbol{o}}(1 + \boldsymbol{\mathcal{G}} \hat{\boldsymbol{\mathcal{Z}}}_{\boldsymbol{o}})^{-1} = \sum_{k=0}^{\infty} \hat{\boldsymbol{\mathcal{Z}}}_{\boldsymbol{o}}(-\boldsymbol{\mathcal{G}} \hat{\boldsymbol{\mathcal{Z}}}_{\boldsymbol{o}})^k. \tag{2.40}$$

Now (2.36) takes form

$$\boldsymbol{\mu} = \boldsymbol{\mu}_o + \boldsymbol{\mu}_o \boldsymbol{\mathcal{P}} \boldsymbol{\mathcal{Z}}_o \boldsymbol{\mathcal{G}} \boldsymbol{\mathcal{Z}}_o \boldsymbol{\mathcal{P}} \boldsymbol{\mu}_o - \boldsymbol{\mu}_o \boldsymbol{\mathcal{P}} \boldsymbol{\mathcal{Z}}_o \boldsymbol{\mathcal{G}} \hat{\boldsymbol{\mathcal{Z}}} \boldsymbol{\mathcal{G}} \boldsymbol{\mathcal{Z}}_o \boldsymbol{\mathcal{P}} \boldsymbol{\mu}_o. \tag{2.41}$$

The similar scattering expansions can be also found for the kernels $\boldsymbol{\mathcal{C}}$ and $\tilde{\boldsymbol{\mathcal{C}}}$ introduced in the preceding Chapter. In Appendix A we show that

$$\tilde{\boldsymbol{\mathcal{C}}} = \boldsymbol{\mathcal{Z}}_o \boldsymbol{\mathcal{P}} \boldsymbol{\mu}_o - \hat{\boldsymbol{\mathcal{Z}}} \boldsymbol{\mathcal{G}} \boldsymbol{\mathcal{Z}}_o \boldsymbol{\mathcal{P}} \boldsymbol{\mu}_o = \sum_{k=0}^{\infty} (-\hat{\boldsymbol{\mathcal{Z}}}_{\boldsymbol{o}} \boldsymbol{\mathcal{G}})^k \boldsymbol{\mathcal{Z}}_o \boldsymbol{\mathcal{P}} \boldsymbol{\mu}_o. \tag{2.42}$$

The respective expansion of $\tilde{\boldsymbol{\mathcal{C}}}$ is the transpose of the above, i.e.

$$\boldsymbol{\mathcal{C}} = \boldsymbol{\mu}_o \boldsymbol{\mathcal{P}} \boldsymbol{\mathcal{Z}}_o - \boldsymbol{\mu}_o \boldsymbol{\mathcal{P}} \boldsymbol{\mathcal{Z}}_o \boldsymbol{\mathcal{G}} \hat{\boldsymbol{\mathcal{Z}}} = \sum_{k=0}^{\infty} \boldsymbol{\mu}_o \boldsymbol{\mathcal{P}} \boldsymbol{\mathcal{Z}}_o (-\boldsymbol{\mathcal{G}} \hat{\boldsymbol{\mathcal{Z}}}_{\boldsymbol{o}})^k. \tag{2.43}$$

The most efficient way to calculate $\boldsymbol{\mathcal{Z}}$, $\boldsymbol{\zeta}$ and $\boldsymbol{\mu}$ in practice is to use the multipole expansion. This method is presented in the next section.

2.5 Multipole expansion

To find the friction kernel $\boldsymbol{\mathcal{Z}} = \dfrac{1}{\boldsymbol{\mathcal{G}} + \boldsymbol{\mathcal{Z}}_o^{-1}}$ one must solve the integral equation (2.18). The most efficient way of doing it is to decompose $[\boldsymbol{u}_i(\boldsymbol{r}) - \boldsymbol{v}_o(\boldsymbol{r})]_{\boldsymbol{r} \in S_i}$ on the multipoles. In this way $\boldsymbol{\mathcal{G}}$ and $\boldsymbol{\mathcal{Z}}_o$ become (infinite-dimensional) matrices and the problem of finding $\boldsymbol{\mathcal{Z}}$ reduces to inverting the appropriate matrix. To be more precise, the velocity on the surface of i-th sphere can be written as

$$[\boldsymbol{u}_i(\boldsymbol{r}) - \boldsymbol{v}_o(\boldsymbol{r})]_{\boldsymbol{r} \in S_i} = \sum_{l=1}^{\infty} \boldsymbol{c}^l(i)(\boldsymbol{r} - \boldsymbol{R}_i)^l, \qquad (2.44)$$

where the multipole tensors $\boldsymbol{c}^l(i)$ are given by

$$\boldsymbol{c}^{(l+1)}(i) = \frac{1}{l!} \nabla^l [\boldsymbol{u}_i(\boldsymbol{r}) - \boldsymbol{v}_o(\boldsymbol{r})]_{\boldsymbol{r}=\boldsymbol{R}_i}. \qquad (2.45)$$

Here ∇^l is the l fold direct product of ∇. We construct also the force multipole tensors $\boldsymbol{f}^{(l+1)}(l = 0, 1, 2...)$ for the sphere i

$$\boldsymbol{f}^{(l+1)}(i) = \frac{1}{l!} \int \boldsymbol{f}(\boldsymbol{r}; i)(\boldsymbol{r} - \boldsymbol{R}_i)^l d\boldsymbol{r}. \qquad (2.46)$$

It is convenient to express the multipole moments as a sum of their irreducible parts with respect to the group $O(3)$. Such sets of irreducible multipoles $\{\boldsymbol{f}_{\sigma l}\}$ and $\{\boldsymbol{c}_{\sigma l}\}$ [72] are given explicitly in Appendix B. Here the subscript l takes integer values $l = 1, 2 \ldots$, whereas σ takes the three values $0, 1, 2$. For given l and σ both $\{\boldsymbol{f}_{\sigma l}\}$ and $\{\boldsymbol{c}_{\sigma l}\}$ have $2l + 1$ independent components.

The first irreducible force multipole

$$\boldsymbol{f}_{0,1}(i) = \int \boldsymbol{f}(\boldsymbol{r}, i) d\boldsymbol{r} = \boldsymbol{F}_i \qquad (2.47)$$

is just the total force acting i-th particle whereas the multipole $\boldsymbol{f}_{1,1}$ is equal to the half of the total torque $\boldsymbol{T}_i$. For the velocity field the vector

$$\boldsymbol{c}_{0,1} = \boldsymbol{U}_i - \boldsymbol{v}_o(\boldsymbol{R}_i) \qquad (2.48)$$

gives the difference between the translational velocity of a sphere and the value of $\boldsymbol{v}_o$ in the center of the sphere while $\boldsymbol{c}_{1,1}$ gives the analogous difference of rotational velocities.

In the multipole notation, the operators $\boldsymbol{\mathcal{Z}}$, $\boldsymbol{\mathcal{Z}}_o$ and $\boldsymbol{\mathcal{G}}$ become matrices, which are given explicitly in [71] and in Appendix C of this work. Here we only mention the fact that the matrix element $\boldsymbol{G}_{\sigma,l;\sigma',l'}(\boldsymbol{R}_i - \boldsymbol{R}_j)$ describing the influence of the force multipole (σ', l') on the i-th sphere on the velocity multipole (σ, l) on the j-th sphere for the case of infinite space decays with $\boldsymbol{R} = \boldsymbol{R}_i - \boldsymbol{R}_j$ as $R^{-(l+l'+\sigma+\sigma'-1)}$. One concludes that the interactions between low multipoles are of infinite range, as they decay as R^{-1}, R^{-2} or R^{-3}.

The friction matrix relates the two lowest velocity multipoles $\boldsymbol{c}_{0,1}$ and $\boldsymbol{c}_{1,1}$ to the two lowest force multipoles $\boldsymbol{f}_{0,1}$ and $\boldsymbol{f}_{1,1}$. Therefore it can be obtained from the multipole matrix $\boldsymbol{\mathcal{Z}}$ by the projection on subspace $\sigma = (0, 1); l = 1$. So in the multipole language the projection operator defined in (2.26) corresponds to the projection on subspace $\sigma = (0, 1); l = 1$. In the multipole notation the operator $\hat{\boldsymbol{\mathcal{Z}}}_o$ defined by (2.38)

$$\hat{\boldsymbol{\mathcal{Z}}}_o = \boldsymbol{\mathcal{Z}}_o - \boldsymbol{\mathcal{Z}}_o \boldsymbol{\mathcal{P}} \boldsymbol{\mu}_o \boldsymbol{\mathcal{P}} \boldsymbol{\mathcal{Z}}_o \qquad (2.49)$$

differs from $\boldsymbol{\mathcal{Z}}_o$ only in the $l = 1$ subspace. Moreover, from the fact that

$$\hat{\mathcal{Z}}_o \mathcal{P} = 0 \tag{2.50}$$

we infer that all the components of $\hat{\mathcal{Z}}_o(l = 1, \sigma; l' = 1, \sigma')$ except for the $\hat{\mathcal{Z}}_o(l = 1, \sigma = 2; l' = 1, \sigma' = 2)$ vanish.

2.6 The numerical calculations of the friction and mobility matrices

The above-described multipole expansion is a good starting for numerical calculations of the hydrodynamic matrices $\boldsymbol{\mu}$ and $\boldsymbol{\zeta}$. In the numerical implementation the infinite matrices $\mathcal{G}$, $\mathcal{Z}$ and $\mathcal{Z}_o$ are truncated to the finite ones in such a way that only the elements with $l \leq L$ are taken into account (this corresponds to working with $n_L = 3L(L+2)$ multipoles per particle). In this way one obtains the truncated matrices $\boldsymbol{\mu}_L$ and $\boldsymbol{\zeta}_L$. Cichocki et al. have shown in [70] that in order to obtain the accurate approximation for the hydrodynamic matrices, the scheme with $L \geq 3$ must be applied. The discrepancy between $\boldsymbol{\zeta}_3$ and the real $\boldsymbol{\zeta}$ was estimated to be less than 1% [70]. The further increase of L is not reasonable from the numerical point of view, as the computational time grows rapidly with L. On the other hand taking $L < 3$ leads to incorrect results, as then some of the contributions to $\mathcal{G}$ with infinite range (i.e. decaying as $1/R^\gamma$ with $\gamma \leq 3$) are not taken into account.

There is one more problem with which every numerical package calculating the hydrodynamic matrixes have to cope with. Namely, when the distance between two given particles becomes small, the force required to push them together diverges as the inverse of the spacing between the particles [13, 73]. To describe accurately these so-called lubrication forces one would have to use a very large number of multipoles, which is extremely expensive numerically. Here we present the way of dealing with this problem developed by Durlofsky et al. [74] and then improved by Cichocki et al. [75]. It is based on the observation that the lubrication effects are well described by the following two-body object

$$\boldsymbol{s} = \sum_{i<j} \boldsymbol{s}(i,j) \equiv \sum_{i<j} \boldsymbol{q}^T \cdot \boldsymbol{\zeta}(i,j) \cdot \boldsymbol{q}, \tag{2.51}$$

where $\boldsymbol{q}$ is a 12x12 matrix, which projects the collective motion of a given pair of particles, leaving only the relative motion. The explicit form of $\boldsymbol{q}$ can be found in [75]. The two-body friction matrices $\boldsymbol{\zeta}(i,j)$ are known with a very high accuracy [13, 73]. Then, the results of the multipole expansion and the lubrication contributions are combined and the friction matrix corrected for the lubrication effects is given by

$$\boldsymbol{\zeta}_L^{corrected} = \boldsymbol{\zeta}_L + \boldsymbol{s} - \boldsymbol{s}_L, \tag{2.52}$$

with

$$\boldsymbol{s}_L = \sum_{i<j} \boldsymbol{s}_L(i,j), \tag{2.53}$$

where in turn $\boldsymbol{s}_L(i,j)$ is the $\boldsymbol{s}(i,j)$ matrix in which only the multipoles with $l \leq L$ are included.

It should be noted that such a throughout treatment of hydrodynamic interactions is not very common in the literature on the subject. In particular, in numerical computations of the mobility matrix $\boldsymbol{\mu}$, which is the crucial object for the problem considered in this paper, quite severe approximations are frequently made. The most crude of them is the so-called Oseen tensor approximation, which in the multipole language corresponds to taking into account only the multipole $(l = 1, \sigma = 0)$ and neglecting all the other multipoles. The mobility matrix reads in this case

$$\boldsymbol{\mu}_{ij} = \delta_{ij}\boldsymbol{\mu}_o + (1 - \delta_{ij})\frac{1}{8\pi\eta}\frac{\mathbf{1} + \hat{\boldsymbol{R}}_{ij}\hat{\boldsymbol{R}}_{ij}}{R_{ij}}. \tag{2.54}$$

In another approximation $\boldsymbol{\mu}_{ij}$ is approximated by the so called Rote-Pragner tensor that reads

$$\boldsymbol{\mu}_{ij} = \delta_{ij}\boldsymbol{\mu}_o + (1 - \delta_{ij})\frac{1}{8\pi\eta R_{ij}}\big(\mathbf{1} + \hat{\boldsymbol{R}}_{ij}\hat{\boldsymbol{R}}_{ij} + \frac{2a^2}{5R_{ij}^2}(\mathbf{1} - \hat{\boldsymbol{R}}_{ij}\hat{\boldsymbol{R}}_{ij})\big). \tag{2.55}$$

This corresponds to truncating the mobility matrix scattering expansion (2.41) to

$$\boldsymbol{\mu}_o + \boldsymbol{\mu}_o\boldsymbol{\mathcal{Z}}_o\boldsymbol{\mathcal{G}}\boldsymbol{\mathcal{Z}}_o\boldsymbol{\mu}_o \tag{2.56}$$

and taking only those multipoles in $\boldsymbol{\mathcal{G}}$, which have a long range-behavior in the sense elucidated above (i.e. decay as $R^{-\gamma}$ with $\gamma \leq 3$).

Therefore the advantage of the Rote-Pragner tensor over the Oseen tensor is that it takes into account all the infinite range terms in the two-body hydrodynamic interactions. Nevertheless it is still a very crude approximation, as the many-body terms (some of them of long range) are completely neglected. In particular, as it is shown in Chapter 7.9, in the Rote- Pragner approximation $\Delta = 0$.

The general many-body treatment of the hydrodynamic interactions similar to the one presented above is used in the numerical calculations of Ladd [76–78] and Brady and co-workers [74, 79–81]. Ladd's approach is generally analogous to the one presented above, the main difference is that he uses only partially reduced multipole moments. Therefore in his truncation schemes more multipoles must be included if one wants to take into account all the long-range terms. Brady, on the other hand, does not take into account all the long-range multipoles contributing to $\boldsymbol{G}$. It was shown by Cichocki et al. [70, 71] that the discrepancy between the result obtained with such a scheme and the real one can be quite considerable (in some cases even up to 30% of the value) The above-cited paper should be referred for the more information on various truncation schemes and comparison of different algorithms.

Based on the above scheme for calculating the mobility and friction matrices in the L multipole approximation the numerical algorithm was developed by Cichocki et. al. [70]. The algorithm was implemented numerically by E. Wajnryb in form of a package in FORTRAN capable of calculating $\boldsymbol{\mu}$ and $\boldsymbol{\zeta}$ for a given configuration of spheres both in

infinite space and in periodic boundary conditions. This package will be used extensively in various numerical calculations in this Thesis. We are going to refer to it subsequently as CFW (**C**ichocki-**F**elderhof-**W**ajnryb) package.

Chapter 3

Interacting Brownian particles: Evolution of the distribution function

In this Chapter the statistical description of a system of interacting Brownian particles is presented. The Generalized Smoluchowski Equation, which governs the evolution of the probability distribution of the particles on timescales $(t \geq \tau_R \gg \tau_B)$ is derived. Finally the particular case of hard sphere systems is considered and the problems arising from the singular nature of the interparticle potential in that case are discussed.

3.1 Generalized Smoluchowski Equation

The statistics of a suspension is described by a distribution function $P(\boldsymbol{R}_1, ..., \boldsymbol{R}_N)$, such that $P(\boldsymbol{R}_1, ..., \boldsymbol{R}_N)\mathrm{d}\boldsymbol{R}_1...\mathrm{d}\boldsymbol{R}_N$ is the probability of finding a configuration in which the particle i is centered in volume $\mathrm{d}\boldsymbol{R}_i$ about $\boldsymbol{R}_i$. We omit the velocity dependence in P as on the timescales of interest $(t \geq \tau_R \gg \tau_B)$ the relaxation of particle velocities can be taken as instantaneous (see Introduction).

Provided the particles are sufficiently small, the significant role in the evolution of $P(\boldsymbol{R}_1, ..., \boldsymbol{R}_N)$ is played by the Brownian motion caused by the thermal agitation of the suspension medium. The appropriate description of such a stochastic process can be obtained by means of the N-particle Fokker-Planck equation [5], the general form of which reads

$$\frac{\partial}{\partial t}P(\boldsymbol{X}, t) = \left[-\frac{\partial}{\partial \boldsymbol{X}} \cdot \boldsymbol{A}(\boldsymbol{X}) + \frac{\partial}{\partial \boldsymbol{X}}\frac{\partial}{\partial \boldsymbol{X}} : \boldsymbol{D}(\boldsymbol{X}) \right] P(\boldsymbol{X}, t), \qquad (3.1)$$

where $\frac{\partial}{\partial \boldsymbol{X}}$ is the 3N-dimensional vector

$$\frac{\partial}{\partial \boldsymbol{X}} = (\frac{\partial}{\partial R_{1x}}, \frac{\partial}{\partial R_{1y}}, ..., \frac{\partial}{\partial R_{Nz}}). \qquad (3.2)$$

The Fokker-Planck equation (3.1) has a form of the balance equation for the probability

37

$$\frac{\partial}{\partial t}P(\boldsymbol{X},t) = -\frac{\partial}{\partial \boldsymbol{X}}\boldsymbol{J}(\boldsymbol{X},t), \tag{3.3}$$

where the probability current $\boldsymbol{J}(\boldsymbol{X},t)$ is given by

$$\boldsymbol{J}(\boldsymbol{X},t) = [\boldsymbol{A}(\boldsymbol{X}) - \frac{\partial}{\partial \boldsymbol{X}} \cdot \boldsymbol{D}(\boldsymbol{X})]P(\boldsymbol{X},t). \tag{3.4}$$

First we consider a case of an isolated system of Brownian particles without external forces or imposed flow ($\boldsymbol{\mathcal{E}} = \boldsymbol{v}_o = 0$). The equilibrium distribution for such a system is given by

$$P_{eq}(\boldsymbol{X}) = \frac{e^{-\beta\Phi(\boldsymbol{X})}}{Q}, \tag{3.5}$$

where Q is the normalization constant and $\Phi(\boldsymbol{X})$ – the potential of particle interactions.

In the equilibrium the probability current vanishes, so

$$[\boldsymbol{A}(\boldsymbol{X}) - \frac{\partial}{\partial \boldsymbol{X}} \cdot \boldsymbol{D}(\boldsymbol{X})]P_{eq}(\boldsymbol{X},t) = 0. \tag{3.6}$$

After substituting (3.5) into (3.6) we get the following relation between $\boldsymbol{A}$ and $\boldsymbol{D}$

$$\boldsymbol{A}(\boldsymbol{X}) = \frac{\partial}{\partial \boldsymbol{X}} \cdot \boldsymbol{D}(\boldsymbol{X}) - \beta\boldsymbol{D}(\boldsymbol{X}) \cdot \frac{\partial\Phi(\boldsymbol{X})}{\partial \boldsymbol{X}} \tag{3.7}$$

and the current $\boldsymbol{J}(\boldsymbol{X},t)$ takes form

$$\boldsymbol{J}(\boldsymbol{X},t) = \boldsymbol{D}(\boldsymbol{X}) \cdot \left[\frac{\partial}{\partial \boldsymbol{X}} - \beta\boldsymbol{\mathcal{F}}(\boldsymbol{X})\right]P(\boldsymbol{X},t), \tag{3.8}$$

where the interparticle force $\boldsymbol{\mathcal{F}}$ is given by

$$\boldsymbol{\mathcal{F}} = -\frac{\partial\Phi(\boldsymbol{X})}{\partial \boldsymbol{X}}. \tag{3.9}$$

In this case the evolution equation (3.1) becomes

$$\frac{\partial}{\partial t}P(\boldsymbol{X},t) = \frac{\partial}{\partial \boldsymbol{X}} \cdot \boldsymbol{D}(\boldsymbol{X}) \cdot \left[\frac{\partial}{\partial \boldsymbol{X}} - \beta\boldsymbol{\mathcal{F}}(\boldsymbol{X})\right]P(\boldsymbol{X},t) \equiv \boldsymbol{\mathcal{D}}(\boldsymbol{X},t)P(\boldsymbol{X},t), \tag{3.10}$$

The evolution operator $\boldsymbol{\mathcal{D}}(\boldsymbol{X},t)$ in Eq. (3.10) is called the Smoluchowski operator whereas the equation (3.10) - the generalized N-body **Smoluchowski equation**. It is worthwhile to notice here that when one analyzes the dynamics on the timescale of the order of τ_B (1.5) (which is much shorter than the timescales of interest here) then the non-Markovian effects become important. This stems from the fact that there is no separation of timescales between the momentum relaxation time τ_B and the viscous relaxation time τ_η, so that the inertia of particles is linked to the solvent inertia and one should treat them both on the same level. Because of these effects the description of a system by a

Fokker-Planck equation (this time in full phase space, including momenta and positions) on this timescale is not correct. For the rigorous results concerning the dynamics on this timescale one should refer to the papers of Piasecki, Bocquet and Hansen [82–84].

Nevertheless, it turns out that when one studies the dynamics on the timescale of the order of the structural relaxation time τ_R, which is much longer than both τ_η and τ_B, the process of spatial relaxation is Markovian [85, 86] and therefore the description of dynamics in terms of the Fokker-Planck equation in configuration space (3.10), as presented here, is correct in this regime.

The $\boldsymbol{D}$ operator can be found by remembering that the macroscopic velocities of the particles $\boldsymbol{\mathcal{U}}$ are linearly related to the forces $\boldsymbol{\mathcal{F}}$ by the relation

$$\boldsymbol{\mathcal{U}} = \boldsymbol{\mu}^{tt} \cdot \boldsymbol{\mathcal{F}}. \tag{3.11}$$

This motion contributes to $\boldsymbol{\mathcal{J}}$, so that we expect to find the term

$$\boldsymbol{\mu}^{tt}(\boldsymbol{X}) \cdot \boldsymbol{\mathcal{F}} P(\boldsymbol{X}, t) \tag{3.12}$$

in the expression for $\boldsymbol{\mathcal{J}}$. By comparison with (3.8) one sees that the only possibility for this to hold is that

$$\boldsymbol{D} = \beta^{-1} \boldsymbol{\mu}^{tt} \tag{3.13}$$

From now on we are going to denote $\boldsymbol{\mu}^{tt}$ simply by $\boldsymbol{\mu}$, as only $\boldsymbol{\mu}^{tt}$ would appear in the subsequent considerations. Analogous convention is to be adopted when writing other hydrodynamic operators like $\boldsymbol{\mathcal{C}}$ and $\tilde{\boldsymbol{\mathcal{C}}}$. Here we would also be concerned only with their translational parts, but we are not going to denote them by $\tilde{\boldsymbol{\mathcal{C}}}^t$ and $\boldsymbol{\mathcal{C}}^t$ in order to keep the notation as simple as possible.

In case where an external force acting on the particles $\boldsymbol{\mathcal{E}}$ and an imposed flow $\boldsymbol{v}_o$ are different from zero, the deterministic contribution to the current reads

$$\boldsymbol{\mathcal{U}} P(\boldsymbol{X}, t) = (\boldsymbol{\mu}\boldsymbol{\mathcal{F}} + \boldsymbol{\mu}\boldsymbol{\mathcal{E}} + \boldsymbol{\mathcal{C}}\boldsymbol{v}_o) P(\boldsymbol{X}, t). \tag{3.14}$$

In order to satisfy it, one has to replace the relation (3.7) by

$$\boldsymbol{A}(\boldsymbol{X}) = \frac{\partial}{\partial \boldsymbol{X}} \cdot \boldsymbol{D}(\boldsymbol{X}) - \beta \boldsymbol{D}(\boldsymbol{X}) \cdot \frac{\partial \Phi(\boldsymbol{X})}{\partial \boldsymbol{X}} - \beta \boldsymbol{D}(\boldsymbol{X}) \cdot \boldsymbol{\mathcal{E}} - \boldsymbol{\mathcal{C}}\boldsymbol{v}_o. \tag{3.15}$$

So the general form of the Fokker-Planck equation which describes the evolution of the configuration space distribution $P(\boldsymbol{X}, t)$ is

$$\frac{\partial}{\partial t} P(\boldsymbol{X}, t) = \frac{\partial}{\partial \boldsymbol{X}} \cdot \left[\boldsymbol{D}(\boldsymbol{X}) \cdot (\frac{\partial}{\partial \boldsymbol{X}} - \beta \boldsymbol{\mathcal{F}} - \beta \boldsymbol{\mathcal{E}}) - \boldsymbol{\mathcal{C}}\boldsymbol{v}_o \right] P(\boldsymbol{X}, t). \tag{3.16}$$

Such an equation is called the extended Smoluchowski equation.

As the averaging over the probability distributions P will be used extensively in this work, it is the right place here to introduce some important notation

– the symbol $< >_t$ will stand for the average over the time dependent, nonequilibrium probability distribution $P(\boldsymbol{X}, t)$

– for the equilibrium average of the function y over $P_{eq}(\boldsymbol{X})$ we are going to use simply $< y >$

Moreover, as the expression under averaging may contain operators, one needs to adopt some convention as to where the distribution function P_{eq} is placed in $< >$. To this end it is convenient to adopt the following bra and ket notation

$$< A| = \int \mathrm{d}\boldsymbol{X} P_{eq}(\boldsymbol{X}) A(\boldsymbol{X}) \tag{3.17}$$

and

$$|B> = B^*(\boldsymbol{X}), \tag{3.18}$$

i.e. the distribution function is placed always on the left hand side of the integrand. The star * denotes here the complex conjugation. For example

$$< f \mid \frac{\partial}{\partial \boldsymbol{X}} \mid g > = \int \mathrm{d}\boldsymbol{X} P_{eq}(\boldsymbol{X}) f \frac{\partial g^*}{\partial \boldsymbol{X}}. \tag{3.19}$$

For the later use we also introduce the operator $\boldsymbol{\mathcal{L}}$

$$\boldsymbol{\mathcal{L}} = [\frac{\partial}{\partial \boldsymbol{X}} + \beta \boldsymbol{\mathcal{F}}] \cdot \boldsymbol{D}(\boldsymbol{X}) \cdot \frac{\partial}{\partial \boldsymbol{X}} = [\beta^{-1} \frac{\partial}{\partial \boldsymbol{X}} + \boldsymbol{\mathcal{F}}] \cdot \boldsymbol{\mu}(\boldsymbol{X}) \cdot \frac{\partial}{\partial \boldsymbol{X}}. \tag{3.20}$$

The operators $\boldsymbol{\mathcal{D}}$ and $\boldsymbol{\mathcal{L}}$ are adjoint in a sense that for any two operators A and B the following equality holds

$$\int A(\boldsymbol{X}) \boldsymbol{\mathcal{D}} B(\boldsymbol{X}) d\boldsymbol{X} = \int [\boldsymbol{\mathcal{L}} A(\boldsymbol{X})] B(\boldsymbol{X}) d\boldsymbol{X}. \tag{3.21}$$

In particular using $\boldsymbol{\mathcal{L}}$ we can write down the evolution equation for the mean value of a given quantity y in the absence of external perturbations ($\boldsymbol{\mathcal{E}} = \boldsymbol{v}_o = 0$) as

$$< \frac{dy}{dt} >_t = \int y \frac{\partial P(\boldsymbol{X}, t)}{\partial t} d\boldsymbol{X} = \int y \boldsymbol{\mathcal{D}} P(\boldsymbol{X}, t) d\boldsymbol{X} = \int [\boldsymbol{\mathcal{L}} y] P(\boldsymbol{X}, t) d\boldsymbol{X} = < \boldsymbol{\mathcal{L}} y >_t . \tag{3.22}$$

Moreover, as it can be checked, for arbitrary operator $A(\boldsymbol{X})$ the following holds

$$\boldsymbol{\mathcal{D}} P_{eq}(\boldsymbol{X}) A(\boldsymbol{X}) = P_{eq}(\boldsymbol{X}) \boldsymbol{\mathcal{L}} A(\boldsymbol{X}). \tag{3.23}$$

In the case where there is a nonzero external perturbation (either $\boldsymbol{\mathcal{E}}$ or $\boldsymbol{v}_o \neq 0$) instead of $\boldsymbol{\mathcal{L}}$ one should use in (3.22) the extended operator $\boldsymbol{\mathcal{L}}_{ext}$

$$\boldsymbol{\mathcal{L}}_{ext} = \left\{ [\frac{\partial}{\partial \boldsymbol{X}} + \beta \boldsymbol{\mathcal{F}} + \beta \boldsymbol{\mathcal{E}}] \cdot \boldsymbol{D}(\boldsymbol{X}) + \boldsymbol{\mathcal{C}} \boldsymbol{v}_o \right\} \cdot \frac{\partial}{\partial \boldsymbol{X}}. \tag{3.24}$$

3.2 Smoluchowski equation for hard spheres

In case of the hard sphere particles, the interparticle forces become singular and the above-derived Smoluchowski equation cannot be directly applied. One way of dealing with this problem is to supply (3.10) with the boundary conditions of the form [87]

$$\boldsymbol{R}_{ij} \cdot (\boldsymbol{\mathcal{J}}_i - \boldsymbol{\mathcal{J}}_j)|_{R_{ij}=d^+} = 0 \qquad i \neq j, \tag{3.25}$$

where

$$d^+ = d + \epsilon \qquad \epsilon \to 0. \tag{3.26}$$

Unfortunately working with the Smoluchowski equation supplied with the boundary conditions is very inconvenient. One would like to incorporate somehow the boundary conditions into the equation instead of treating them separately.

Such a program was fulfilled by Cichocki in [87], who has shown that the Smoluchowski equation for the hard spheres can be written as

$$\frac{\partial}{\partial t} P(\boldsymbol{X}, t) = \frac{\partial}{\partial \boldsymbol{X}} \cdot \boldsymbol{D}(\boldsymbol{X}) \cdot \left[\frac{\partial}{\partial \boldsymbol{X}} - \boldsymbol{\mathcal{T}} \right] P(\boldsymbol{X}, t) \equiv \mathcal{D}(\boldsymbol{X}, t) P(\boldsymbol{X}, t), \tag{3.27}$$

where $\boldsymbol{\mathcal{T}}$ is a $3N$ dimensional vector with components given by

$$\boldsymbol{\mathcal{T}}_i = \sum_{i \neq j} \boldsymbol{\mathcal{T}}_{ij}, \qquad \boldsymbol{\mathcal{T}}_{ij} = \hat{\boldsymbol{R}}_{ij} \delta(R_{ij} - d^+). \tag{3.28}$$

The sign $(+)$ in the above equation indicates that the product of the delta function $\delta(R_{ij}-d)$ with functions that have discontinuity at the surface $R_{ij} = d$ should be taken in the limit (3.26). It can be proved that if one takes as the initial condition in (3.27) the distribution with the property that $P(\boldsymbol{X}, t = 0) = 0$ for all overlapping configurations, then this property propagates in time and one would never end up with the nonzero probability of overlaps.

Chapter 4

The memory function

In this section the problem of collective diffusion coefficient for interacting Brownian parti-cle system will be approached by means of the powerful general theoretical scheme for the calculation of time-correlation functions known as Zwanzig-Mori formalism [15, 16]. The expressions for the memory function, generalized diffusion function as well as the diffusion coefficients are derived in frames of this formalism.

4.1 Projection operators and memory function

As we are going to study the evolution of the configuration of the Brownian particles the main object of interest for us is the microscopic number density

$$n^{mic}(\boldsymbol{r}, t) = \sum_{i=1}^{N} \delta(\boldsymbol{r} - \boldsymbol{R}_i), \tag{4.1}$$

with the following Fourier transform

$$C(\boldsymbol{k}, t) = \sum_i e^{i\boldsymbol{k}\cdot\boldsymbol{R}_i(t)}. \tag{4.2}$$

Let us denote the deviations of $C(k)$ from its equilibrium value by

$$c(\boldsymbol{k}, t) >= C(\boldsymbol{k}, t) > - < C(\boldsymbol{k}, t) > . \tag{4.3}$$

The dynamic structure factor (1.21) is the density correlation function in the Fourier space

$$F(k, t) = \lim_{\infty} \frac{1}{N} < c(\boldsymbol{k}, 0)c(-\boldsymbol{k}, t) >= \lim_{\infty} \frac{1}{N} < c(\boldsymbol{k}, 0)|e^{\mathcal{L}t}|c(\boldsymbol{k}, 0) >, \tag{4.4}$$

where the bra and ket notation introduced in Chapter 3 has been used.
From now on we denote $c(\boldsymbol{k}) = c(\boldsymbol{k}, 0)$. After the Laplace transform of Eq. (4.4) one gets

$$F(k, z) = \lim_{\infty} \frac{1}{N} < c(\boldsymbol{k})|\frac{1}{z - \mathcal{L}}|c(\boldsymbol{k}) > . \tag{4.5}$$

From here on we are going to omit the thermodynamic limit $\lim_\infty$ sign in the equations and assume it understood without being explicitly present.

We notice that in order to calculate $F(k, t)$ one does not have to know $c(\mathbf{k}, t)$ in full detail. All we really need is its projection on $c(\mathbf{k}, 0)$. Therefore let us introduce the projection operator:

$$P = \frac{|c(\mathbf{k}) >< c(\mathbf{k})|}{S(k)}. \tag{4.6}$$

In terms of P the dynamic structure factor can be written as

$$F(k, t) = \lim_\infty \frac{1}{N} < c(\mathbf{k})|P|c(\mathbf{k}, t) > . \tag{4.7}$$

We introduce also the operator Q

$$Q = 1 - P. \tag{4.8}$$

In further calculations we make use of the following operator identity

$$\frac{1}{X + Y} = \frac{1}{X} - \frac{1}{X} Y \frac{1}{X + Y}. \tag{4.9}$$

Using (4.9) in (4.5) one obtains

$$F(k, z) = \frac{1}{N} < c(\mathbf{k})| \frac{1}{z - \mathcal{L}} |c(\mathbf{k}) >= \frac{1}{N} < c(\mathbf{k})| \frac{1}{z - \mathcal{L}Q - \mathcal{L}P} |c(\mathbf{k}) >=$$

$$= \frac{1}{N} < c(\mathbf{k})| \frac{1}{z - \mathcal{L}Q} + \frac{1}{z - \mathcal{L}Q} \mathcal{L}P \frac{1}{z - \mathcal{L}} |c(\mathbf{k}) > . \tag{4.10}$$

But

$$P \frac{1}{z - \mathcal{L}Q} P = \frac{1}{z}, \tag{4.11}$$

which can be proved by expanding $\dfrac{1}{z - \mathcal{L}Q}$ in powers of $\mathcal{L}Q$. From Eqs. (4.6), (4.10) and (4.11) one gets

$$F(k, z) = \frac{S(k)}{z} + \frac{1}{N} < c(\mathbf{k})| \frac{1}{z - \mathcal{L}Q} \mathcal{L} |c(\mathbf{k}) > \frac{F(k, z)}{S(k)} \tag{4.12}$$

Using (4.9) the term in brackets can be rewritten in the form

$$< c(\mathbf{k})| \frac{1}{z - \mathcal{L}Q} \mathcal{L} |c(\mathbf{k}) >= \frac{1}{z} < c(\mathbf{k})|(1 + \mathcal{L}Q \frac{1}{z - \mathcal{L}Q}) \mathcal{L} |c(\mathbf{k}) > . \tag{4.13}$$

We arrive therefore at the following expression for $F(k, z)$

$$F(k, z) = \frac{S(k)}{z + \Omega(k)(1 - M(k, z))}, \tag{4.14}$$

where

$$\Omega(k) = -\frac{1}{NS(k)} < c(\boldsymbol{k})|\boldsymbol{\mathcal{L}}|c(\boldsymbol{k}) > \tag{4.15}$$

and the memory function $M(k, z)$ is given by:

$$M(k, z) = \frac{1}{NS(k)\Omega(k)} < c(\boldsymbol{k})|\boldsymbol{\mathcal{L}}Q\frac{1}{z - \boldsymbol{\mathcal{L}}Q}\boldsymbol{\mathcal{L}}|c(\boldsymbol{k}) > . \tag{4.16}$$

We can write the above formula in a slightly different manner if we use once more the identity (4.9). Namely:

$$\frac{1}{z - \boldsymbol{\mathcal{L}}Q} = \frac{1}{z - Q\boldsymbol{\mathcal{L}}Q - P\boldsymbol{\mathcal{L}}Q} = \frac{1}{z - \hat{\boldsymbol{\mathcal{L}}}} + \frac{1}{z - \hat{\boldsymbol{\mathcal{L}}}}P\boldsymbol{\mathcal{L}}Q\frac{1}{z - \boldsymbol{\mathcal{L}}Q}, \tag{4.17}$$

where $\hat{\boldsymbol{\mathcal{L}}}$ is the orthogonal part of the operator $\boldsymbol{\mathcal{L}}$:

$$\hat{\boldsymbol{\mathcal{L}}} = Q\boldsymbol{\mathcal{L}}Q. \tag{4.18}$$

But, similarly to (4.11)

$$Q\frac{1}{z - \boldsymbol{\mathcal{L}}Q}P = 0. \tag{4.19}$$

So finally one gets for the memory function

$$M(k, z) = \frac{1}{S(k)\Omega(k)} < c(\boldsymbol{k})|\boldsymbol{\mathcal{L}}Q\frac{1}{z - \hat{\boldsymbol{\mathcal{L}}}}Q\boldsymbol{\mathcal{L}}|c(\boldsymbol{k}) >= \frac{k^2}{S(k)\Omega(k)} < \hat{\boldsymbol{j}}(\boldsymbol{k})|\frac{1}{z - \hat{\boldsymbol{\mathcal{L}}}}|\hat{\boldsymbol{j}}(\boldsymbol{k}) >, \tag{4.20}$$

where the orthogonal microscopic current $\hat{\boldsymbol{j}}(\boldsymbol{k})$ is given by

$$\boldsymbol{k}|\hat{\boldsymbol{j}}(\boldsymbol{k}) >= Q\boldsymbol{\mathcal{L}}|c(\boldsymbol{k}) > . \tag{4.21}$$

We can also define the generalized diffusion function

$$D(k, z) = \frac{1}{k^2}\Omega(k)(1 - M(k, z)). \tag{4.22}$$

In the limit of small k and z the function $D(k, z)$ gives the long-time diffusion coefficient

$$D_c^l = \lim_{k \to 0}\lim_{z \to 0} D(k, z), \tag{4.23}$$

which describes the rate of exponential decay of the dynamic structure factor on the timescale long compared with the mean memory time τ_M (1.27)

$$F(k, t) = S(k)e^{-k^2 D_c^l t} \tag{4.24}$$

in the small wavevector limit.

On the other hand, one sees from (4.20) that the asymptotic behavior of $M(k,z)$ is

$$M(k,z) \sim \frac{<\hat{\boldsymbol{j}}(\boldsymbol{k})|\hat{\boldsymbol{j}}(\boldsymbol{k})>}{z}, \qquad z \to \infty \qquad (4.25)$$

so that in this limit the memory function vanishes. The respective limit of the generalized diffusion function defines the short time collective diffusion coefficient

$$\lim_{k \to 0} \lim_{z \to \infty} D(k,z) = \lim_{k \to 0} \frac{1}{k^2}\Omega(k) \equiv D_c^s, \qquad (4.26)$$

which gives the rate of decay of $F(k,t)$ for small k in the absence of memory effects.

All the formalism presented so far holds in principle for any operator $\boldsymbol{\mathcal{L}}$ governing the evolution of the phase-space variables. In the next section we obtain the explicit formulae for $\Omega(k)$ and $M(k,z)$ for the case of interacting Brownian particles.

4.2   Memory function for interacting Brownian particles

Let us turn to the specific case of interacting Brownian particles with the dynamics determined by the operator $\boldsymbol{\mathcal{L}}$ given by (3.20). To calculate the function $\Omega(k)$ in this case let us notice first that if f_1 and f_2 are arbitrary functions of the configuration variables, we get

$$< f_1 \boldsymbol{\mathcal{L}} f_2 >= \int d\boldsymbol{X} P_{eq} f_1 [\beta \boldsymbol{\mathcal{F}} + \frac{\partial}{\partial \boldsymbol{X}}] \cdot \boldsymbol{D} \cdot \frac{\partial}{\partial \boldsymbol{X}} f_2^* =$$
$$= - < \frac{\partial f_1}{\partial \boldsymbol{X}} \cdot |\boldsymbol{D}| \cdot \frac{\partial f_2}{\partial \boldsymbol{X}} >, \qquad (4.27)$$

where we used integration by parts together with the fact that

$$\frac{\partial P_{eq}}{\partial \boldsymbol{X}} = -\beta \boldsymbol{\mathcal{F}} P_{eq}. \qquad (4.28)$$

The above formula allows us to write $\Omega(k)$ as

$$\Omega(k) = \frac{1}{S(k)N} < \frac{\partial c(\boldsymbol{k})}{\partial \boldsymbol{X}} \cdot |\boldsymbol{D}| \cdot \frac{\partial c(\boldsymbol{k})}{\partial \boldsymbol{X}} >=$$
$$= k^2 \sum_{i,j=1}^{N} \frac{1}{S(k)N} < \hat{\boldsymbol{k}} \cdot \boldsymbol{D}_{ij} \cdot \hat{\boldsymbol{k}} e^{i\boldsymbol{k}(\boldsymbol{R}_i - \boldsymbol{R}_j)} > . \qquad (4.29)$$

So that the expression (4.26) for the short-time diffusion coefficient takes form

$$D_c^s = \lim_{k \to 0} \frac{1}{S(k)N} \sum_{i,j=1}^{N} < \hat{\boldsymbol{k}} \cdot \boldsymbol{D}_{ij} \cdot \hat{\boldsymbol{k}} e^{i\boldsymbol{k}(\boldsymbol{R}_i - \boldsymbol{R}_j)} > \equiv \lim_{k \to 0} \frac{D_o H(k)}{S(k)} \qquad (4.30)$$

where we have introduced the so-called **hydrodynamic factor** [8]

$$H(k) = \frac{1}{D_o N} \sum_{i,j=1}^{N} < \hat{\boldsymbol{k}} \cdot \boldsymbol{D}_{ij} \cdot \hat{\boldsymbol{k}} e^{i\boldsymbol{k}(\boldsymbol{R}_i - \boldsymbol{R}_j)} >, \tag{4.31}$$

which is the measure of the influence of hydrodynamic interactions on the system's dynamics. If hydrodynamic interactions are negligible, then $H(k) = 1$.

4.3 Small k limit of the memory function

Because of the presence of the reduced evolution operator $\hat{\boldsymbol{\mathcal{L}}}$ the expression (4.20) for the memory function is quite cumbersome for practical calculations. Fortunately in the limit $k \to 0$ the memory function can be related to the unreduced correlation function of the form

$$M^u(k, z) = \frac{1}{S(k)\Omega(k)} < c(\boldsymbol{k})|\mathcal{L}Q\frac{1}{z - \mathcal{L}}Q\mathcal{L}|c(\boldsymbol{k}) > . \tag{4.32}$$

We have namely [16]

$$M(k, z) = M^u(k, z)\left[1 + \frac{M^u(k, z)}{zS(k) + k^2\Omega(k)}\right]. \tag{4.33}$$

However

$$\mathcal{L}|c(\boldsymbol{k}) >= |\boldsymbol{k} \cdot \sum_{i,j,m=1}^{N} \left[\nabla_j + \beta \boldsymbol{F}_{mj}\right] \cdot \boldsymbol{D}_{ij} e^{i\boldsymbol{k}\boldsymbol{R}_i} - k^2 \sum_i \boldsymbol{D}_{ii} e^{i\boldsymbol{k}\boldsymbol{R}_i} >, \tag{4.34}$$

$$< c(\boldsymbol{k})|\mathcal{L} =< \boldsymbol{k} \cdot \sum_{i,j=1}^{N} \nabla_j \cdot \boldsymbol{D}_{ij} e^{i\boldsymbol{k}\boldsymbol{R}_i} - k^2 \sum_i \boldsymbol{D}_{ii} e^{i\boldsymbol{k}\boldsymbol{R}_i}|,$$

which behaves in the following way as $k \to 0$

$$\mathcal{L}|c(\boldsymbol{k}) >= |\boldsymbol{k} \cdot \sum_{i,j,m=1}^{N} \left[\nabla_j + \beta \boldsymbol{F}_{mj}\right] \cdot \boldsymbol{D}_{ij} > +\mathcal{O}(k^2), \tag{4.35}$$

$$< c(\boldsymbol{k})|\mathcal{L} =< \boldsymbol{k} \cdot \sum_{i,j=1}^{N} \nabla_j \cdot \boldsymbol{D}_{ij}| + \mathcal{O}(k^2). \tag{4.36}$$

At the same time

$$P\mathcal{L}|c(\boldsymbol{k}) >= \Omega(k)S(k)N|c(\boldsymbol{k}) >, \tag{4.37}$$

which due to (4.29) is at least of the order k^2. This means that in the limit $k \to 0$ both $\mathcal{L}|c(\boldsymbol{k}) >$ and $Q\mathcal{L}|c(\boldsymbol{k}) >$ share the same asymptotic form (4.35). Therefore memory

function is at least of the order k^2 as $k \to 0$ and the same holds for $\boldsymbol{M}^u(k)$. But then from (4.33) one concludes that $\boldsymbol{M}(k, z)$ approaches $\boldsymbol{M}^u(k, z)$ in the limit $k \to 0$. Note that we have actually proved more, namely that

$$\lim_{k \to 0} \boldsymbol{M}(k, z) = \lim_{k \to 0} \frac{1}{S(k)\Omega(k)} < c(\boldsymbol{k})|\mathcal{L}\frac{1}{z - \mathcal{L}}\mathcal{L}|c(\boldsymbol{k}) > . \tag{4.38}$$

Hence in the limit $k \to 0$ we can cross out all the projections operators Q from the expression for the memory function $\boldsymbol{M}(k, z)$.

Now we are ready to calculate small z and small k limit of the generalized diffusion function $D(k, z)$. From Eqs. (4.22), (4.29) and (4.38) we get

$$D_c^l = \lim_{k \to 0} \lim_{z \to 0} D(k, z) = \frac{1}{S(0)N} \lim_{k \to 0} \left(\sum_i \sum_j < \hat{\boldsymbol{k}} \cdot \boldsymbol{D}_{ij} \cdot \hat{\boldsymbol{k}} e^{i\boldsymbol{k}(\boldsymbol{R}_i - \boldsymbol{R}_j)} > \right.$$

$$- \int_0^\infty \mathrm{d}t < \hat{\boldsymbol{k}} \cdot c(\boldsymbol{k})|\mathcal{L}e^{\mathcal{L}t}\mathcal{L}|c(\boldsymbol{k}) \cdot \hat{\boldsymbol{k}} >), \tag{4.39}$$

In the next Chapter another approach to the diffusion phenomena is presented: first by means of the nonequilibrium thermodynamics and then - linear reaction theory. The reason for it is expounded in the Introduction - we are looking for an expression for D_c which would be well-defined at $k = 0$. The above expression is not defined at $k = 0$, because of the long-range terms present in $\boldsymbol{D}_{ij}$. On the other hand, using the linear reaction theory we have a freedom of choice of the thermodynamic forces and fluxes and we can manipulate them in an appropriate way to obtain the short-range kernels with well defined value in $k = 0$.

We end up this Chapter with a comment concerning the order of the limits in the expressions for the diffusion coefficient like (4.23) or (4.39). In fact for the Hamiltonian systems there is a problem here: the expressions are sensitive to whether one performs first $k \to 0$ limit and then $z \to 0$ or vice versa (see eg. [20] or [88]). However, the dynamics described by the Smoluchowski equation is not a Hamiltonian one (in fact one can prove the H-theorem for Smoluchowski dynamics [5]) and does not lead to this kind of problems: the z and k limits may be taken in any order with the same result.

Chapter 5

Collective diffusion coefficient

In this section the collective diffusion phenomenon is analyzed from the point of view of phenomenological theory of nonequilibrium thermodynamics. It is shown, in frames of this theory, that the diffusion coefficient can be assessed by studying the response of a system to an external force. To this end we adopt the linear reaction theory and end up with an expression for collective diffusion coefficient, which is shown to be equivalent with the previous expression for D_c derived in Chapter 4 from the memory function theory. Nevertheless, the reformulation of the problem in language of the linear response theory is important for us, because by manipulating of the response kernels we would be able to arrive at an explicit expression for D_c, which does not involve the troublesome limit $k \to 0$. This program will be fulfilled in the next two Chapters.

5.1 Diffusion constant: the phenomenological theory

A suspension is a two component system, in which one of the components is discrete (particles) whereas the other one is continuous (fluid). In frames of nonequilibrium thermodynamics [89] one shows that the entropy source strength for the two-component system reads

$$\sigma = \frac{1}{T} \sum_{i=1}^{2} \boldsymbol{J}_i^a (\boldsymbol{F}_i - (\operatorname{grad}\mu_i)_T), \tag{5.1}$$

where we have assumed that the temperature of the suspension remains constant. In the above formula $\boldsymbol{F}_i$ stands for the external force (per unit mass) acting on a component i, μ is its chemical potential and $\boldsymbol{J}_i^a$ - the diffusion flow

$$\boldsymbol{J}_i^a = \rho_i (\boldsymbol{v}_i - \boldsymbol{v}_a), \tag{5.2}$$

with respect to some reference velocity $\boldsymbol{v}_a$. In the above expression ρ_i stands for the density of the i-th component. In our case the natural choice for the reference velocity $\boldsymbol{v}_a$ is the velocity of a suspension as a whole

$$\boldsymbol{v}_s = \phi_1 \boldsymbol{v}_1 + \phi_2 \boldsymbol{v}_2, \tag{5.3}$$

which can be interpreted as the total flux of volume of a material (either fluid or solid). Here ϕ_i is the volume fraction of the component i, i.e. the fraction of the total volume occupied by the component i. Naturally

$$\phi_1 + \phi_2 = 1. \tag{5.4}$$

The diffusion currents $\boldsymbol{J}_1$ and $\boldsymbol{J}_2$ are not independent as

$$\frac{\phi_1}{\rho_1}\boldsymbol{J}_1 + \frac{\phi_2}{\rho_2}\boldsymbol{J}_2 = 0. \tag{5.5}$$

The Gibbs-Duhem relation allows us to connect the gradients of μ_1 and μ_2

$$\rho_1 \, \mathrm{grad}\mu_1 + \rho_2 \, \mathrm{grad}\mu_2 = 0. \tag{5.6}$$

Using (5.5) and (5.6) we in (5.1) we get

$$\sigma = \frac{1}{T}\boldsymbol{J}_1(\boldsymbol{F}_1 - \frac{\phi_1}{\phi_2}\frac{\rho_2}{\rho_1}\boldsymbol{F}_2 - \frac{1}{1-\phi_1} \, \mathrm{grad}\mu_1). \tag{5.7}$$

The above expression, like all the expressions for the entropy source strength, has the form of a product of the thermodynamic flux ($\boldsymbol{J}_1$) with the corresponding thermodynamic force

$$\frac{1}{T}(\boldsymbol{F}_1 - \frac{\phi_1}{\phi_2}\frac{\rho_2}{\rho_1}\boldsymbol{F}_2 - \frac{1}{1-\phi_1} \, \mathrm{grad}\mu_1).$$

If the thermodynamic forces are small, the nonequilibrium thermodynamics [89] gives us the linear relation between the fluxes and the forces, which in our case reads

$$\boldsymbol{J}_1 = L\frac{1}{T}(\boldsymbol{F}_1 - \frac{\phi_1}{\phi_2}\frac{\rho_2}{\rho_1}\boldsymbol{F}_2 - \frac{1}{1-\phi_1} \, \mathrm{grad}\mu_1), \tag{5.8}$$

where L is a phenomenological coefficient.

On the other hand, starting from the formula (5.7) in the absence of external forces ($\boldsymbol{F}_1 = \boldsymbol{F}_2 = 0$) and expressing the chemical potential gradient as

$$\mathrm{grad}\mu_1 = \left(\frac{\partial\mu_1}{\partial n_1}\right)_{p,T} \mathrm{grad}\rho_1 \tag{5.9}$$

we get

$$\sigma = \frac{1}{T}\boldsymbol{J}_1\frac{1}{1-\phi_1}\left(\frac{\partial\mu_1}{\partial n_1}\right)_{p,T} \mathrm{grad}\rho_1. \tag{5.10}$$

If we now treat $\mathrm{grad}\rho_1$ as a thermodynamic force and write down the linear relation between this force and the diffusion current $\boldsymbol{J}_1$ we get the Fick's law

$$J_1 = -D_c \, \mathrm{grad}\rho_1, \tag{5.11}$$

where the phenomenological constant is called the collective diffusion coefficient. Comparing (5.11) with (5.8) we get the following relation between L and D_c

$$D_c = -\frac{1}{T}\frac{1}{1-\phi_1}\left(\frac{\partial \mu_1}{\partial \rho_1}\right)_{p,T} L. \tag{5.12}$$

The chemical potential gradient $\left(\frac{\partial \mu_1}{\partial n_1}\right)_{p,T}$ is connected with the long-wavelength limit of the static structure factor 1.20 by [8, 90]

$$\left(\frac{\partial \mu_1}{\partial \rho_1}\right)_{p,T} = k_B T \frac{1-\phi_1}{\rho_1 S(0)}, \tag{5.13}$$

which stems from the fluctuation theorem. Using (5.13) one can rewrite the expression for D_c as

$$D_c = -\frac{L}{T\rho_1 S(0)}. \tag{5.14}$$

If we now consider the case when there is a nonzero external force acting on the particles ($\boldsymbol{F}_1 \neq 0$) in the absence of the concentration gradient ($\mathrm{grad}\rho_1 = 0$) we get from (5.8) and (5.14) the following expression for the diffusion current

$$\boldsymbol{J}_1 = \frac{\rho_1 S(0)}{k_B T} D_c \boldsymbol{F}_1. \tag{5.15}$$

Hence we see that the diffusion constant can be obtained by studying the flow induced by the external force acting on the particles. The classical example of such an experiment is **sedimentation** of a suspension, where the particles flow down under the influence of the gravitational force. The main characteristic of this process is so-called sedimentation coefficient K [48] defined by the relation between the force and the velocity of the particles

$$\boldsymbol{J}_1 = \rho_1 K \boldsymbol{F}_1. \tag{5.16}$$

From (5.15) we get immediately

$$D_c = \frac{k_B T}{S(0)} K, \tag{5.17}$$

which shows that the collective diffusion coefficient can be assessed by the sedimentation measurements.

Let us end this section with a few remarks concerning notation. First of all it would be a bit more convenient to work with the number density of particles n_1 instead of the mass density ρ_1. Therefore, instead of $\boldsymbol{J}_1$ we are going to use the current

$$\boldsymbol{J}_d = n_1(\boldsymbol{v}_1 - \boldsymbol{v}_s), \tag{5.18}$$

which we are going to call subsequently "diffusion current". We would use also the "naked" particle current, defined with respect to the laboratory frame ($\boldsymbol{v}_a = 0$ in (5.2)) denoted simply by $\boldsymbol{J}$

$$\boldsymbol{J} = n_1\boldsymbol{v}_1. \tag{5.19}$$

Finally we are going to drop the subscript "1" in the particle density n_1 and call it simply n, as the fluid density will not appear in the remaining part of the Thesis.

5.2   Microscopic expression for the diffusion current

Our goal now is to construct a microscopic theory which would give an explicit expression for the collective diffusion coefficient D_c. First step would be to find the microscopic counterpart of the diffusion current $\boldsymbol{J}$ introduced above. Next, we would relate this current to the external force acting on the particles and finally arrive again at Eq. (5.15), but this time with the explicit expression for D_c.

In frames of the Smoluchowski dynamics on timescale $t \geq \tau_R$ the particle "velocity" can be defined by the relation

$$< \frac{d\boldsymbol{R}_i}{dt} >_t = < \boldsymbol{U}_i^I >_t \tag{5.20}$$

with $< >_t$ defined as in Chapter 3. Using Eq. (3.22) and Eq. (3.24) one gets for $\boldsymbol{U}_i^I$

$$\boldsymbol{U}_i^I = \left\{ \left[\left(\beta^{-1}\frac{\partial}{\partial \boldsymbol{X}} + \boldsymbol{\mathcal{F}} + \boldsymbol{\mathcal{E}} \right) \cdot \boldsymbol{\mu}(\boldsymbol{X}) + \boldsymbol{\mathcal{C}}(\boldsymbol{X})\boldsymbol{v}_o \right] \cdot \frac{\partial}{\partial \boldsymbol{X}}\boldsymbol{X} \right\}_i =$$
$$= \left\{ \left(\beta^{-1}\frac{\partial}{\partial \boldsymbol{X}} + \boldsymbol{\mathcal{F}} + \boldsymbol{\mathcal{E}} \right) \cdot \boldsymbol{\mu}(\boldsymbol{X}) + \boldsymbol{\mathcal{C}}(\boldsymbol{X})\boldsymbol{v}_o \right\}_i . \tag{5.21}$$

This "Smoluchowski velocity" $\boldsymbol{U}^I$, however, should not be identified with the real velocity of the particle. The **average** of the former measures the mean displacement of the particle in the unit time on the structural relaxation time scale τ_R, in which the latter has undergone millions of fluctuations (see the discussion in Introduction). As it was already pointed out by Felderhof [91] $\boldsymbol{U}^I$ has only a statistical meaning and must be understood as a property of the ensemble.

The microscopic expression for the current corresponding to the Smoluchowski velocity reads

$$\boldsymbol{j}(\boldsymbol{r}, \boldsymbol{X}) = \sum_i \boldsymbol{U}_i^I \delta(\boldsymbol{r} - \boldsymbol{R}_i). \tag{5.22}$$

while its average gives the macroscopic particle current $\boldsymbol{J}$

$$\boldsymbol{J}(\boldsymbol{r}, t) = < \boldsymbol{j}(\boldsymbol{r}, \boldsymbol{X}) >_t, \tag{5.23}$$

In a similar way one can express the hydrodynamic velocity of a suspension as a whole $\boldsymbol{v}_s$ in terms of the microscopic velocity $\boldsymbol{v}(\boldsymbol{r}, \boldsymbol{X})$. The velocity $\boldsymbol{v}(\boldsymbol{r})$ is linked with the force density $\boldsymbol{f}(\boldsymbol{r})$ by the $\boldsymbol{G}$ operator

$$\boldsymbol{v} = \boldsymbol{G}(\boldsymbol{f}_o + \boldsymbol{f}) = \boldsymbol{v}_o + \boldsymbol{G}\boldsymbol{f}. \tag{5.24}$$

The force density in turn can be expressed as [92]

$$\boldsymbol{f}(\boldsymbol{r}, \boldsymbol{X}) = (\beta^{-1}\frac{\partial}{\partial \boldsymbol{X}} + \boldsymbol{\mathcal{E}} + \boldsymbol{\mathcal{F}}) \cdot \boldsymbol{\mathcal{C}}(\boldsymbol{X}) - \hat{\boldsymbol{\mathcal{Z}}}(\boldsymbol{X})\boldsymbol{v}_o. \tag{5.25}$$

So eventually for the suspension velocity we get

$$\boldsymbol{v}(\boldsymbol{r}, \boldsymbol{X}) = \boldsymbol{v}_o - \boldsymbol{G}\hat{\boldsymbol{\mathcal{Z}}}(\boldsymbol{X})\boldsymbol{v}_o + \boldsymbol{G}(\beta^{-1}\frac{\partial}{\partial \boldsymbol{X}} + \boldsymbol{\mathcal{E}} + \boldsymbol{\mathcal{F}}) \cdot \boldsymbol{\mathcal{C}}(\boldsymbol{X}) \tag{5.26}$$

and the microscopic counterpart of the diffusion current is given by

$$\boldsymbol{j}_d(\boldsymbol{r}, \boldsymbol{X}) = \boldsymbol{j}(\boldsymbol{r}, \boldsymbol{X}) - n\boldsymbol{v}(\boldsymbol{r}, \boldsymbol{X}). \tag{5.27}$$

Analogously to (5.23) the corresponding macroscopic quantities are connected with the microscopic ones by

$$\boldsymbol{v}_s(\boldsymbol{r}, t) = <\boldsymbol{v}(\boldsymbol{r}, \boldsymbol{X})>_t \tag{5.28}$$

$$\boldsymbol{J}_d(\boldsymbol{r}, t) = <\boldsymbol{j}_d(\boldsymbol{r}, \boldsymbol{X})>_t \tag{5.29}$$

5.3   The linear reaction for Smoluchowski dynamics

The goal of this section is to calculate the particle current $\boldsymbol{J}$ in a situation, when the system is disturbed out of the equilibrium by the external force $\boldsymbol{\mathcal{E}}$ and the imposed flow $\boldsymbol{v}_o = \tilde{\boldsymbol{v}}_o + \boldsymbol{G}\boldsymbol{f}_o$. The disturbances are assumed to be sufficiently small for the linear theory to hold. It must be stressed, though, that the linear reaction is only the mean for getting the explicit expression for the memory factor Δ which does not involve the cumbersome $\boldsymbol{k} \to 0$ limit. It turns out that the expression for Δ obtained in frames of the memory function formalism can be re-derived using the linear reaction theory. However, in the linear reaction we have a freedom of choice of the disturbances and quantities characterizing response. By means of such operations we would be able to arrive at the wanted expression for Δ which would not involve any limiting procedures. Therefore we are not concerned here with a whole lot of problems concerning the range of applicability of the linear reaction theory etc. - it would only serve us as the way to analyze the expression for Δ. In deriving the linear reaction formulae for the system of Brownian particles the line of reasoning due to Felderhof and Jones [92, 93] is adopted. We assume that the particles were at equilibrium in the infinite past, so that the distribution function $P(\boldsymbol{X}, t \to -\infty)$ is given by the equilibrium distribution

$$P_{eq}(\boldsymbol{X}) = e^{-\beta\phi(\boldsymbol{X})}/Q. \tag{5.30}$$

Then we turn on the fields $\boldsymbol{\mathcal{E}}$ and $\boldsymbol{v}_o$ and look what effect it would have on the distribution in linear approximation. We write

$$P(\boldsymbol{X}, t) = P_{eq}(\boldsymbol{X}) + \delta P(\boldsymbol{X}, t). \tag{5.31}$$

Inserting such a form of P into the extended Smoluchowski equation (3.16) one finds that to the linear order $\delta P(\boldsymbol{X}, t)$ satisfies the equation

$$\frac{\partial \delta P(\boldsymbol{X}, t)}{\partial t} - \boldsymbol{\mathcal{D}}\delta P = -\frac{\partial}{\partial \boldsymbol{X}} \cdot \left[(\boldsymbol{\mu}\boldsymbol{\mathcal{E}}(t) + \boldsymbol{\mathcal{C}}\boldsymbol{v}_o(t))P_{eq} \right]. \tag{5.32}$$

The solution with initial condition $\delta P = 0$ for $t = -\infty$ is given by

$$\delta P(\boldsymbol{X}, t) = -\int_{-\infty}^{t} e^{\boldsymbol{\mathcal{D}}(t-t')} \frac{\partial}{\partial \boldsymbol{X}} \cdot \left[(\boldsymbol{\mu}\boldsymbol{\mathcal{E}}(t') + \boldsymbol{\mathcal{C}}\boldsymbol{v}_o(t'))P_{eq} \right] dt'. \tag{5.33}$$

The equilibrium distribution can be dragged out of the divergence

$$\frac{\partial}{\partial \boldsymbol{X}} \cdot \left[(\boldsymbol{\mu}\boldsymbol{\mathcal{E}}(t') + \boldsymbol{\mathcal{C}}\boldsymbol{v}_o(t'))P_{eq} \right] = P_{eq}(\frac{\partial}{\partial \boldsymbol{X}} + \beta\boldsymbol{\mathcal{F}}) \cdot \left[\boldsymbol{\mu}\boldsymbol{\mathcal{E}}(t') + \boldsymbol{\mathcal{C}}\boldsymbol{v}_o(t') \right]. \tag{5.34}$$

Then, using the operator $\boldsymbol{\mathcal{L}}$ we can write δP as

$$\delta P(\boldsymbol{X}, t) = -P_{eq} \int_{-\infty}^{t} dt' e^{\boldsymbol{\mathcal{L}}(t-t')}(\frac{\partial}{\partial \boldsymbol{X}} + \beta\boldsymbol{\mathcal{F}}) \cdot \left[\boldsymbol{\mu}\boldsymbol{\mathcal{E}}(t') + \boldsymbol{\mathcal{C}}\boldsymbol{v}_o(t') \right]. \tag{5.35}$$

Hence the nonequilibrium average of a given observable $A(\boldsymbol{X})$ obeys

$$< A >_t = < A > - \int_{-\infty}^{t} dt' \int d\boldsymbol{X} A(\boldsymbol{X}) e^{\boldsymbol{\mathcal{L}}(t-t')}(\frac{\partial}{\partial \boldsymbol{X}} + \beta\boldsymbol{\mathcal{F}}) \cdot \left[\boldsymbol{\mu}\boldsymbol{\mathcal{E}}(t') + \boldsymbol{\mathcal{C}}\boldsymbol{v}_o(t') \right]. \tag{5.36}$$

Now we can write down such formulae for the particle flow $\boldsymbol{j}$ and the force density $\boldsymbol{f}$. They read

$$< \boldsymbol{j} >_t = < \boldsymbol{j} > - \int_{-\infty}^{t} dt' \int d\boldsymbol{X}\, \boldsymbol{j}(\boldsymbol{X})\, P_{eq} e^{\boldsymbol{\mathcal{L}}(t-t')}(\frac{\partial}{\partial \boldsymbol{X}} + \beta\boldsymbol{\mathcal{F}}) \cdot (\boldsymbol{\mu}\boldsymbol{\mathcal{E}}(t') + \boldsymbol{\mathcal{C}}\boldsymbol{v}_o(t')] \equiv \boldsymbol{J}_{ins} + \boldsymbol{J}_{ret},$$

$$< \boldsymbol{f} >_t = < \boldsymbol{f} > - \int_{-\infty}^{t} dt' \int d\boldsymbol{X}\, \boldsymbol{f}(\boldsymbol{X})\, P_{eq} e^{\boldsymbol{\mathcal{L}}(t-t')}(\frac{\partial}{\partial \boldsymbol{X}} + \beta\boldsymbol{\mathcal{F}}) \cdot (\boldsymbol{\mu}\boldsymbol{\mathcal{E}}(t') + \boldsymbol{\mathcal{C}}\boldsymbol{v}_o(t')] \equiv \boldsymbol{f}_{ins} + \boldsymbol{f}_{ret},$$

$$\tag{5.37}$$

where we have singled out the instantaneous and retarded parts of the system response. The former appears immediately after $\boldsymbol{\mathcal{E}}$ or $\boldsymbol{f}_o$ is turned on and "follows" the change of the external perturbation, while the latter describes memory effects due to the change of the distribution function induced by the external forces.

The instantaneous response terms are just the equilibrium averages of $\boldsymbol{j}$ and $\boldsymbol{f}$ respectively. But, using Eqs. (5.22) and (5.25)

$$\boldsymbol{J}_{ins}(\boldsymbol{r}) =< \sum_i [(\beta^{-1}\frac{\partial}{\partial \boldsymbol{X}} + \boldsymbol{\mathcal{F}} + \boldsymbol{\mathcal{E}}) \cdot \boldsymbol{\mu}(\boldsymbol{X}) + \boldsymbol{\mathcal{C}}\boldsymbol{v}_o]_i \delta(\boldsymbol{r} - \boldsymbol{R}_i) >,$$

$$\boldsymbol{f}_{ins} =< -\hat{\boldsymbol{\mathcal{Z}}}\boldsymbol{v}_o + (\beta^{-1}\frac{\partial}{\partial \boldsymbol{X}} + \boldsymbol{\mathcal{F}} + \boldsymbol{\mathcal{E}}) \cdot \boldsymbol{\mathcal{C}} > . \tag{5.38}$$

However, by integrating by parts and using the identity

$$\frac{\partial}{\partial \boldsymbol{X}} P_{eq}(\boldsymbol{X}) = \beta \boldsymbol{\mathcal{F}} P_{eq}(\boldsymbol{X}), \tag{5.39}$$

one proves that

$$< (\beta^{-1}\frac{\partial}{\partial \boldsymbol{X}} + \boldsymbol{\mathcal{F}}) \cdot \boldsymbol{\mu}(\boldsymbol{X})\delta(\boldsymbol{r} - \boldsymbol{R}_i) >= 0 \tag{5.40}$$

and similarly

$$< (\beta\frac{\partial}{\partial \boldsymbol{X}} + \boldsymbol{\mathcal{F}}) \cdot \boldsymbol{\mathcal{C}} >= 0, \tag{5.41}$$

so that

$$\boldsymbol{J}_{ins}(\boldsymbol{r}) =< \sum_i [(\boldsymbol{\mu}\boldsymbol{\mathcal{E}} + \boldsymbol{\mathcal{C}}\boldsymbol{v}_o)]_i \delta(\boldsymbol{r} - \boldsymbol{R}_i) >,$$

$$\boldsymbol{f}_{ins} =< -\hat{\boldsymbol{\mathcal{Z}}}\boldsymbol{v}_o + \tilde{\boldsymbol{\mathcal{C}}}\boldsymbol{\mathcal{E}} > . \tag{5.42}$$

Now we turn to the retarded response terms. Inserting (5.22) and (5.25) into the expressions for $\boldsymbol{J}_{ret}$ and $\boldsymbol{f}_{ret}$, dragging P_{eq} to the left side of the integrand with use of relation (5.39) and keeping only the linear terms in $\boldsymbol{\mathcal{E}}$ and $\boldsymbol{f}_o$ one gets

$$\boldsymbol{J}_{ret}(\boldsymbol{r}, t) = -\beta^{-1} < \int_{-\infty}^{t} dt' \sum_i [\boldsymbol{\mu} \cdot \overleftarrow{\nabla}]_i \delta(\boldsymbol{r} - \boldsymbol{R}_i) e^{\mathcal{L}(t-t')} (\overrightarrow{\nabla} + \beta \boldsymbol{\mathcal{F}}) \cdot [\boldsymbol{\mu}\boldsymbol{\mathcal{E}}(t') + \boldsymbol{\mathcal{C}}\boldsymbol{v}_o(t')] >,$$

$$\boldsymbol{f}_{ret}(t) = -\beta^{-1} < \int_{-\infty}^{t} dt' \tilde{\boldsymbol{\mathcal{C}}} \cdot \overleftarrow{\nabla} e^{\mathcal{L}(t-t')} (\overrightarrow{\nabla} + \beta \boldsymbol{\mathcal{F}}) \cdot [\boldsymbol{\mu}\boldsymbol{\mathcal{E}}(t') + \boldsymbol{\mathcal{C}}\boldsymbol{v}_o(t')] >, \tag{5.43}$$

where we have introduced the symbols $\overrightarrow{\nabla}$ and $\overleftarrow{\nabla}$ to show which part of the expression is under differentiation.

Finally the expression (5.37) for the current and force density induced in a system as a response to the external perturbations takes form

$$< \boldsymbol{j} >_t = \boldsymbol{J}_{ins} + \boldsymbol{J}_{ret} = \int (\boldsymbol{Y}_{jE}(\boldsymbol{r}, \boldsymbol{r}') \boldsymbol{E}(\boldsymbol{r}', t) + \boldsymbol{Y}_{jv}(\boldsymbol{r}, \boldsymbol{r}') \boldsymbol{v}_o(\boldsymbol{r}', t)) \mathrm{d}\boldsymbol{r}' +$$

$$+ \int \mathrm{d}\boldsymbol{r}' \int_{-\infty}^{t} \mathrm{d}t' (\boldsymbol{X}_{jE}(\boldsymbol{r}, \boldsymbol{r}', t - t') \boldsymbol{E}(\boldsymbol{r}', t') + \boldsymbol{X}_{jv}(\boldsymbol{r}, \boldsymbol{r}', t - t') \boldsymbol{v}_o(\boldsymbol{r}', t')),$$

$$(5.44)$$

$$< \boldsymbol{f} >_t = \boldsymbol{f}_{ins} + \boldsymbol{f}_{ret} = \int (\boldsymbol{Y}_{fE}(\boldsymbol{r}, \boldsymbol{r}') \boldsymbol{E}(\boldsymbol{r}', t) + \boldsymbol{Y}_{fv}(\boldsymbol{r}, \boldsymbol{r}') \boldsymbol{v}_o(\boldsymbol{r}', t)) \mathrm{d}\boldsymbol{r}' +$$

$$\int \mathrm{d}\boldsymbol{r}' \int_{-\infty}^{t} \mathrm{d}t' (\boldsymbol{X}_{fE}(\boldsymbol{r}, \boldsymbol{r}', t - t') \boldsymbol{E}(\boldsymbol{r}', t') + \boldsymbol{X}_{fv}(\boldsymbol{r}, \boldsymbol{r}', t - t') \boldsymbol{v}_o(\boldsymbol{r}', t')),$$

$$(5.45)$$

where the kernels $\boldsymbol{Y}_{ab}$ with $a = \{j, f\}$ and $b = \{e, v\}$ describe the instantaneous response while the analogous kernels $\boldsymbol{X}_{ab}$ describe the retarded response of the system. Instantaneous response kernels read

$$\boldsymbol{Y}_{jE}(\boldsymbol{r}, \boldsymbol{r}') = < \sum_{i,j=1}^{N} \delta(\boldsymbol{r} - \boldsymbol{R}_i) \boldsymbol{\mu}_{ij} \delta(\boldsymbol{r}' - \boldsymbol{R}_j) >,$$

$$\boldsymbol{Y}_{jv}(\boldsymbol{r}, \boldsymbol{r}') = < \sum_{i=1}^{N} \delta(\boldsymbol{r} - \boldsymbol{R}_i) [\boldsymbol{C}(\boldsymbol{r}')]_i >,$$

$$\boldsymbol{Y}_{fE}(\boldsymbol{r}, \boldsymbol{r}') = < \sum_{j=1}^{N} [\tilde{\boldsymbol{C}}(\boldsymbol{r})]_j \delta(\boldsymbol{r}' - \boldsymbol{R}_j) >,$$

$$\boldsymbol{Y}_{fv}(\boldsymbol{r}, \boldsymbol{r}') = < -\hat{\boldsymbol{Z}}(\boldsymbol{r}, \boldsymbol{r}') >, \qquad (5.46)$$

whereas the time-dependent response kernels X are given by

$$\boldsymbol{X}_{jE}(\boldsymbol{r}, \boldsymbol{r}', t) = -\beta^{-1} < \sum_{i,j=1}^{N} \delta(\boldsymbol{r} - \boldsymbol{R}_i) [\boldsymbol{\mu} \cdot \overleftarrow{\nabla}]_i e^{\mathcal{L}t} [(\overrightarrow{\nabla} + \beta \boldsymbol{\mathcal{F}}) \cdot \boldsymbol{\mu}]_j \delta(\boldsymbol{r}' - \boldsymbol{R}_j) >,$$

$$\boldsymbol{X}_{jv}(\boldsymbol{r}, \boldsymbol{r}', t) = -\beta^{-1} < \sum_{i=1}^{N} \delta(\boldsymbol{r} - \boldsymbol{R}_i) [\boldsymbol{\mu} \cdot \overleftarrow{\nabla}]_i e^{\mathcal{L}t} (\overrightarrow{\nabla} + \beta \boldsymbol{\mathcal{F}}) \cdot \boldsymbol{C}(\boldsymbol{r}') >,$$

$$\boldsymbol{X}_{fE}(\boldsymbol{r}, \boldsymbol{r}', t) = -\beta^{-1} < \tilde{\boldsymbol{C}}(\boldsymbol{r}) \cdot \overleftarrow{\nabla} e^{\mathcal{L}t} \sum_{j=1}^{N} [(\overrightarrow{\nabla} + \beta \boldsymbol{\mathcal{F}}) \cdot \boldsymbol{\mu}]_j \delta(\boldsymbol{r}' - \boldsymbol{R}_j) >,$$

$$\boldsymbol{X}_{fv}(\boldsymbol{r}, \boldsymbol{r}', t) = -\beta^{-1} < \tilde{\boldsymbol{C}}(\boldsymbol{r}) \cdot \overleftarrow{\nabla} e^{\mathcal{L}t} (\overrightarrow{\nabla} + \beta \boldsymbol{\mathcal{F}}) \cdot \boldsymbol{C}(\boldsymbol{r}') > . \qquad (5.47)$$

Additionally, in writing (5.45) we have introduced an auxiliary field $\boldsymbol{E}(\boldsymbol{r}, t)$, such that the forces $\boldsymbol{E}_i(t)$ are given by the value of $\boldsymbol{E}(\boldsymbol{r}, t)$ in the center of the i-th sphere

$$\boldsymbol{E}_i(t) = \int \delta(\boldsymbol{r} - \boldsymbol{R}_i)\boldsymbol{E}(\boldsymbol{r}, t)\mathrm{d}\boldsymbol{r}. \tag{5.48}$$

Let us notice that the equation (5.44) for the particle current in the absence of the external flow can be written in the Fourier space as

$$\boldsymbol{J}(\boldsymbol{k}, t) = <\boldsymbol{j}(\boldsymbol{k})>_t = \boldsymbol{Y}_{jE}(\boldsymbol{k})\boldsymbol{E}(\boldsymbol{k}, t) + \int_{-\infty}^{t} \mathrm{d}t' \boldsymbol{X}_{jE}(\boldsymbol{k}, t - t')\boldsymbol{E}(\boldsymbol{k}, t'), \tag{5.49}$$

where the Fourier transforms of all the objects are defined according to Eqs. (1.43)-(1.47).

To study the long time collective diffusion one considers the dynamics on the timescale t much longer than the relaxation time of $\boldsymbol{X}_{jE}$. On this timescale we get namely

$$\boldsymbol{J}(\boldsymbol{k}, t) = \left(\boldsymbol{Y}_{jE}(\boldsymbol{k}) + \int_0^{\infty} \mathrm{d}t' \boldsymbol{X}_{jE}(\boldsymbol{k}, t')\right)\boldsymbol{E}(\boldsymbol{k}, t). \tag{5.50}$$

Let us now perform the limit $\boldsymbol{k} \to 0$, which corresponds to the case of homogeneous $\boldsymbol{E}$ and $\boldsymbol{J}$, such as it was considered in section 5.1. For the isotropic system the kernels $\boldsymbol{Y}_{jE}$ and $\boldsymbol{X}_{jv}$ in the $\boldsymbol{k} \to 0$ limit are proportional to unit matrices and $\boldsymbol{J}$ is parallel to the field $\boldsymbol{E}$.

Therefore the long time collective diffusion coefficient can be identified with

$$D_c^l = \lim_{\boldsymbol{k} \to 0} \lim_{\infty} \frac{k_B T}{nS(0)} \frac{1}{3} \mathrm{Tr}\left[\boldsymbol{Y}_{jE}(\boldsymbol{k}) + \int_0^{\infty} \mathrm{d}t' \boldsymbol{X}_{jE}(\boldsymbol{k}, t')\right], \tag{5.51}$$

which, taking into account the analytical form of the response kernels $\boldsymbol{Y}_{jE}(\boldsymbol{k})$ (5.46) and $\boldsymbol{X}_{jE}(\boldsymbol{k}, t')$ (5.47), is equivalent to the expression for D_c^l derived in frames of the Zwanzig-Mori formalism (4.39).

Note that in the above definition D_c is expressed in terms of the kernel linking $\boldsymbol{E}$ with the particle current $\boldsymbol{J}$ and not the diffusion current $\boldsymbol{J}_d$ as it stands in the original definition (5.15). One should remember however that before the limit $\boldsymbol{k} \to 0$ is performed one should first apply the thermodynamic limit, which should be supplied by the condition that the system as a whole does not move (it is called sometimes "the rigid wall condition" [94], as it corresponds to the statement that the container in which the suspension is enclosed does not move). Such a thermodynamic limit assures that $\lim_{\boldsymbol{k} \to 0} \boldsymbol{v}_s(\boldsymbol{k}) = 0$, which in turn, guarantees that the two above-mentioned transport kernels approach the same limiting value as $\boldsymbol{k} \to 0$.

As far as short time diffusion coefficient is concerned, it can be obtained from (5.51) by neglecting the memory term, i.e.

$$D_c^s = \lim_{\boldsymbol{k} \to 0} \frac{k_B T}{3nS(0)} \mathrm{Tr}\boldsymbol{Y}_{jE}(\boldsymbol{k}). \tag{5.52}$$

It is important to stress here once more the fact that one cannot just put $k = 0$ in the above expressions, as the kernels $\boldsymbol{Y}_{jE}$ and $\boldsymbol{X}_{jE}$ are long-ranged, which was indicated in the Introduction and will be proved in Chapters 6 and 7. Our goal in these Chapters will be to find the local equations for the diffusion current in the sense elucidated in the Introduction. By means of the short-range kernels appearing in such equations the collective diffusion coefficient could be assessed without the cumbersome $\boldsymbol{k} \to 0$ limit.

Chapter 6

Cluster expansion for the instantaneous response

The instantaneous response kernels $\boldsymbol{Y}$ defined by Eq. (5.46) are non-local, what leads to divergences. The goal of this Chapter is to find the description of the instantaneous response of the system in terms of local kernels. It will turn out that the local equations describing the system's response are of the form

$$\boldsymbol{J}^{ins} = \boldsymbol{Y}_{jE}^{irr} \boldsymbol{E} + \boldsymbol{Y}_{jv}^{irr} \boldsymbol{v}^{ins} \tag{6.1}$$

instead of

$$\boldsymbol{J}^{ins} = \boldsymbol{Y}_{jE} \boldsymbol{E} + \boldsymbol{Y}_{jv} \boldsymbol{v}_o \tag{6.2}$$

The instantaneous suspension velocity $\boldsymbol{v}^{ins}$ that have appeared in (6.1) is defined as (cf. (2.11))

$$\boldsymbol{v}^{ins} = \boldsymbol{v}_o + \boldsymbol{G}\boldsymbol{f}^{ins} \tag{6.3}$$

We are going to prove that, in contradistinction to nonlocal kernels $\boldsymbol{Y}_{jE}$ and $\boldsymbol{Y}_{jv}$ in (6.2), the kernels $\boldsymbol{Y}_{jE}^{irr}$ and $\boldsymbol{Y}_{jv}^{irr}$ in (6.1) are short-ranged and therefore local. These kernels will allow us to find the the explicit expression for D_c^s, which does not involve the troublesome limit $k \to 0$.

In the next Chapter similar in idea (although much more complicated in practice) operations will be performed on the retarded part of the system's response (5.45).

6.1 Cluster structure

While calculating the kernels Y and X defined in (5.46) and (5.47) we have to deal with the integrals of the form

$$I = \int A(\boldsymbol{X}, \boldsymbol{r}, \boldsymbol{r}') P_{eq}(\boldsymbol{X}) d\boldsymbol{X}, \tag{6.4}$$

where A is some operator such as $\sum_{i,j=1}^{N} \delta(\boldsymbol{r} - R_i)\boldsymbol{\mu}_{ij}\delta(\boldsymbol{r}' - R_j)$ or $\hat{\boldsymbol{Z}}(\boldsymbol{r}, \boldsymbol{r}')$.

The operator A can be written in the form of the scattering sequence (cf. 2.36,2.40,2.42,2.43) and therefore can be represented as

$$A = \sum_{i} A(i) + \frac{1}{2!} \sum_{i \neq j} A(i, j) + \frac{1}{3!} \sum_{i \neq j \neq k} A(i, j, k) + ..., \tag{6.5}$$

where $A(i_1, ..., i_s)$ comprises all these terms in the scattering sequence of A which depend on the positions of exactly s particles $\{i_1, i_2...i_s\}$. For example the sequence

$$\boldsymbol{\mu}_o(1)\boldsymbol{\mathcal{P}}(1)\boldsymbol{Z}_o(1)\boldsymbol{G}_{12}\hat{\boldsymbol{Z}}_{\boldsymbol{o}}(2)\boldsymbol{G}_{21}\hat{\boldsymbol{Z}}_{\boldsymbol{o}}(1)\delta(\boldsymbol{r} - \boldsymbol{R}_1)$$

is the part of $A(1, 2)$ (as well as $A(2, 1)$) whereas

$$\boldsymbol{\mu}_o(1)\boldsymbol{\mathcal{P}}(1)\boldsymbol{Z}_o(1)\boldsymbol{G}_{12}\hat{\boldsymbol{Z}}_{\boldsymbol{o}}(2)\boldsymbol{G}_{23}\hat{\boldsymbol{Z}}_{\boldsymbol{o}}(3)\delta(\boldsymbol{r} - \boldsymbol{R}_1)$$

is the part of $A(1, 2, 3)$ (in both cases $A = \sum_{j=1}^{N}[\boldsymbol{\mathcal{C}}(\boldsymbol{r})]_j\delta(\boldsymbol{r}' - R_j)$).

Hence we get for I

$$I = \sum_{i} \int A(i) P_{eq}(\boldsymbol{X})d\boldsymbol{X} + \frac{1}{2!} \sum_{i \neq j} \int A(i, j) P_{eq}(\boldsymbol{X})d\boldsymbol{X} +$$

$$\frac{1}{3!} \sum_{i \neq j \neq k} \int A(i, j, k) P_{eq}(\boldsymbol{X})d\boldsymbol{X} + ... \tag{6.6}$$

Or, summing up the equivalent terms

$$I = \sum_{s=1}^{N} \frac{N!}{(N - s)!s!} \int A(1, 2..., s) P_{eq}(\boldsymbol{R}_1...\boldsymbol{R}_N)d\boldsymbol{R}_1...d\boldsymbol{R}_N =$$

$$= \sum_{s=1}^{N} \frac{1}{s!} \int A(1, 2..., s) n(\boldsymbol{R}_1, \boldsymbol{R}_2..., \boldsymbol{R}_s)d\boldsymbol{R}_1...d\boldsymbol{R}_s, \tag{6.7}$$

where $n(1, 2..., s)$ is the s-particle partial distribution function

$$n(1, 2, ..., s) = \frac{N!}{(N - s)!} \int P_{eq}(\boldsymbol{R}_1...\boldsymbol{R}_N)d\boldsymbol{R}_{s+1}...d\boldsymbol{R}_N. \tag{6.8}$$

Note that the s-particle partial distribution function can be also written as

$$n(\boldsymbol{r}_1, \boldsymbol{r}_2, ...\boldsymbol{r}_s) =< \sum_{i_1, i_2, ..., i_s}^{\prime} \delta(\boldsymbol{r}_1 - \boldsymbol{R}_{i_1})\delta(\boldsymbol{r}_2 - \boldsymbol{R}_{i_2})...\delta(\boldsymbol{r}_s - \boldsymbol{R}_{i_s}) >, \tag{6.9}$$

which in a shorthand notation will be also denoted as $< 1\ 2\ ...\ s >$. The sum $\sum^{\prime}$ in the above expression is supplied with the condition that all i_k, $k = 1, ..., s$ are different each from the other.

Next we assume that the correlations between the two groups of particles vanish as the distance between them goes to infinity. This means that the partial distribution function should have the group property, i.e.

$$n(1, 2..., r, r+1, .., s) \rightarrow n(1, 2..., r)n(r+1, ..., s), \tag{6.10}$$

as the distance between the particles $\{1, 2...r\}$ and $\{r+1, ..., s\}$ goes to infinity.

This property of the partial distribution function allows us to decompose $n(1, 2...s)$ as [95]

$$
\begin{aligned}
&n(1) = h(1), \\
&n(1, 2) = n(1)n(2) + h(1, 2), \\
&n(1, 2, 3) = n(1)n(2)n(3) + n(1)h(2, 3) + n(2)h(1, 3) + n(3)h(1, 2) + h(1, 2, 3), \\
&...,
\end{aligned}
\tag{6.11}
$$

where the s-particle correlation function $h(1, 2...s)$ goes to zero as one drags any subset of particles $\subset \{1, 2...s\}$ away from the rest.

For the later use we introduce after Michels [96] the "uncorrelating operator"

$$P_{unc} => <, \tag{6.12}$$

which has the property of statistically uncorrelating the variables at its left from those at its right, i.e

$$< AP_{unc}B > = < A >< B > . \tag{6.13}$$

The orthogonal complement of P_{unc} is

$$Q_{unc} = 1 - >< . \tag{6.14}$$

So, using the notation of Eq. (6.9), we get for example

$$< 1 \ Q_{unc} \ 2 > = < 1 \ 2 > - < 1 >< 2 > = n(1, 2) - n(1)n(2) = h(1, 2). \tag{6.15}$$

Using the decomposition (6.11) together with the cluster expansion (6.5) we get the representation the kernels $\boldsymbol{Y}_{jE}, \boldsymbol{Y}_{jv}, \boldsymbol{Y}_{fE}, \boldsymbol{Y}_{vv}$ as sums of many-body terms from scattering sequence multiplied by the respective correlation functions. To deal effectively with such a complicated structure we are going to introduce the diagrammatic representation.

6.2 Diagrammatic representation

We introduce the diagrammatic representation of the scattering (S) and correlation (C) structure of the $\boldsymbol{Y}$ kernels from Eq. (5.42). Such SC diagrams consist of the following elements

1. the horizontal line - - - - represents a given particle (we call it particle line)

2. the symbol $\Diamond$ stands for the operator $-\hat{\boldsymbol{Z}}_{\boldsymbol{o}}(i)$

3. the symbol $\supset$ stands for the operator $\boldsymbol{Z_o}(i)\boldsymbol{\mathcal{P}}(i)\boldsymbol{\mu}_o(i)\delta(\boldsymbol{r'} - \boldsymbol{R}_i)$

4. the symbol $\sqsubset$ stands for the operator $\delta(\boldsymbol{r} - \boldsymbol{R}_i)\boldsymbol{\mu}_o(i)\boldsymbol{\mathcal{P}}(i)\boldsymbol{Z_o}(i)$

5. the vertical line $|$ stands for the $\boldsymbol{G}$ - bond

6. double vertical line $\|$ represents the correlation function h (we call it h-bond)

Moreover we assume that the positions of all the particles in the diagrams are integrated over. Hence, for example the diagram
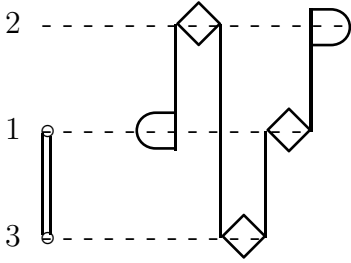
Fig. 6.1.

represents the expression

$$-\int \mathrm{d}1\mathrm{d}2\mathrm{d}3 \, h_{13}\delta(\boldsymbol{r} - \boldsymbol{R}_1)\boldsymbol{\mu}_o(1)\boldsymbol{\mathcal{P}}(1)\boldsymbol{Z_o}(1)\boldsymbol{G}(12)\hat{\boldsymbol{Z}}_{\boldsymbol{o}}(2)\boldsymbol{G}(23)\hat{\boldsymbol{Z}}_{\boldsymbol{o}}(3)\boldsymbol{G}(31)$$
$$\hat{\boldsymbol{Z}}_{\boldsymbol{o}}(1)\boldsymbol{G}(12)\boldsymbol{Z_o}(2)\boldsymbol{\mathcal{P}}(2)\boldsymbol{\mu}_o(2)\delta(\boldsymbol{r'} - \boldsymbol{R}_2), \tag{6.16}$$

which is the part of the kernel $\boldsymbol{Y}_{jE}$. Note that the diagrams should be read from left to right.

The diagram with n $\boldsymbol{G}$-bonds would be called "n-linked" diagram.

6.3   Reducibility

The $\boldsymbol{G}$ bond is called a connection line if the removal of this $\boldsymbol{G}$-bond causes the diagram to become disconnected. Diagrams with one or more connection lines will be called reducible.
    For example the diagram

Fig. 6.2.

is reducible and can be cut into two pieces by breaking the $\boldsymbol{G}$ - bond between particles 2 and 3. The connection line which is most to the left will be called **articulation line**. Note that the sub-diagram on the left of the articulation line is irreducible.

In the analogous way we can define the reducibility for the S-structure of the diagrams (S-reducibility). First of all **nodal line** is defined as a $\boldsymbol{G}$-bond which would be a connection line if there were no $h - bonds$ in a diagram. Diagrams with one or more nodal lines are called S-reducible.

Hence in the following diagram

Fig. 6.3.

the $\boldsymbol{G}$ bond between particles 2 and 3 is the nodal line but not the connection line and the diagram is S-reducible (although it is irreducible with respect to its SC-structure).

6.4 The nodal structure

The nodal lines decompose the particles in a given diagram on the set of **nodal blocks** C_i: C_1 denotes the set of particles on the left of the first nodal line, C_2 - the particles between the first and the second nodal line and so on. Note that the definition of the nodal line assures that $C_i \cap C_j = \emptyset$ if only $i \neq j$. For example the diagram

Fig. 6.4.

has the nodal structure of the form
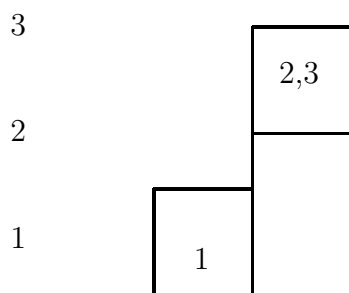
Fig. 6.5.

or simply 1|23.

The object on Fig. 6.5 is called the **nodal structure graph** (NSG). The vertices of such a graph are nodal blocks, whereas the bonds in this graph are created by nodal lines.

6.5   The block distribution function

Consider all the irreducible diagrams of the kernel Y which have the same scattering structure and differ only in correlation structure. The task of summing all of these diagrams boils down to finding the sum of all their correlation functions.

To start with, the irreducibility requires that if there is a nodal line in the diagram then particles on the left of it cannot be totally uncorrelated from particles on its right. This means that the correlation function that we are looking for is given by

$$b(C_1|C_2|...|C_k) = < C_1(1 - P_{unc})C_2(1 - P_{unc})...(1 - P_{unc})C_k > . \qquad (6.17)$$

Here $C_1|C_2|...|C_k$ describes the nodal structure of the diagram, whereas the operator P_{unc} is the "uncorrelating operator" introduced in (6.12). The function $b(C_1|C_2|...|C_k)$ defined in (6.17) is called the block distribution function [39]. Note that if there are no nodal lines in the scattering structure of a given s-particle diagram, than b would be just the full s-particle partial distribution function $n(1, 2, ..., s)$.

To get a better grip of $b(C_1|...|C_k)$ let us evaluate it for a few simple scattering sequences. For the sequence presented in Fig. 6.4 the block distribution reads:

$$b(1|23) = < 1(1 - P_{unc})23 > = < 123 > - < 1 >< 23 > = n(1, 2, 3) - n(1)n(23). \qquad (6.18)$$

We see that $b(1|23)$ goes quickly to zero when we drag particle 1 apart from the particles 2 and 3, as in this case

$$n(1, 2, 3) \to n(1)n(23). \qquad (6.19)$$

Let us consider now the scattering sequence of the form
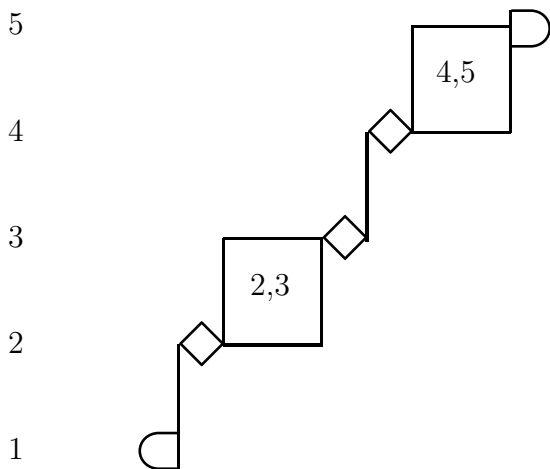
Fig. 6.6.

where
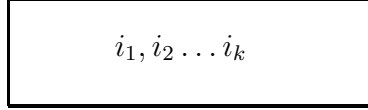
$$\boxed{i_1, i_2 \ldots i_k}$$

Fig. 6.7.

stands for any scattering sequence that involves the particles $i_1, i_2 \ldots i_k$.

The above scattering sequence has the nodal structure $(1|23|45)$. Therefore its block distribution function reads

$$
\begin{aligned}
b(1|23|45) =&< 1(1 - P_{unc})23(1 - P_{unc})45 >= \\
=&< 12345 > - < 1 >< 2345 > - < 123 >< 45 > + < 1 >< 23 >< 45 >= \\
=& \, n(1,2,3,4,5) - n(1)n(2,3,4,5) - n(1,2,3)n(4,5) + n(1)n(2,3)n(4,5),
\end{aligned}
\tag{6.20}
$$

which, as can be easily proved, vanishes whenever the particle $\{1\}$ or the group $\{4,5\}$ is dragged away from the rest of the particles.

6.6   Long-range character of the kernels

Note that the kernels $Y(\boldsymbol{r}, \boldsymbol{r}')$ in (5.46) are of a very long range: they fall off as slowly as $|\boldsymbol{r} - \boldsymbol{r}'|^{-k}$ with $k \leq 3$. It is caused by the presence of reducible diagrams in the expansion of $Y(\boldsymbol{r}, \boldsymbol{r}')$. In such a diagram we have at least one connection line: let it be $\boldsymbol{G}(ij)$ joining the particles i and j. Looking at the scattering expansions (2.36,2.42,2.43) we recognize the three possibilities

1. The connection line $\boldsymbol{G}$ joins two $\hat{\boldsymbol{Z}}_{\boldsymbol{o}}$ operators: $\hat{\boldsymbol{Z}}_{\boldsymbol{o}}(i)$ and $\hat{\boldsymbol{Z}}_{\boldsymbol{o}}(j)$. But, as we have mentioned in Chapter 2, in the multipole language all the components of $\hat{\boldsymbol{Z}}_{\boldsymbol{o}}(l = 1, m, \sigma; l' = 1, m', \sigma')$ except for $\hat{\boldsymbol{Z}}_{\boldsymbol{o}}(l = 1, m, \sigma = 2; l' = 1, m', \sigma' = 2)$ vanish. This, together with the fact that $\boldsymbol{G}_{\sigma, l; \sigma', l'}(\boldsymbol{R})$ decays as $R^{-(l+l'+\sigma+\sigma'-1)}$, leads us to the conclusion that the leading term in the connection line behaves as R^{-3} (for $l = l' = 2$ and $\sigma = \sigma' = 0$).

2. The connection line joins the $\boldsymbol{Z}_{\boldsymbol{o}}$ operator with $\hat{\boldsymbol{Z}}_{\boldsymbol{o}}$. Then, from the form of the $\boldsymbol{Z}_{\boldsymbol{o}}$ operator quoted in Appendix C follows that the leading term in the connection line behaves as R^{-2} (for $l = 1; l' = 2$ and $\sigma = 0; \sigma' = 0$). Here the prime variables refer to the $\hat{\boldsymbol{Z}}_{\boldsymbol{o}}$ operator.

3. The connection line joins two $\boldsymbol{Z}_{\boldsymbol{o}}$ operators. Then the leading term behaves as R^{-1} (for $l = l' = 1$ and $\sigma = \sigma' = 0$). It is worth noting that such a situation can happen only in case of the diagrams representing $\boldsymbol{Y}_{jE}$ (as only this kernel has more than one

$\boldsymbol{Z_o}$ operator in its scattering sequence). As there are exactly two $\boldsymbol{Z_o}$ operators in diagrams of $\boldsymbol{Y}_{jE}$, one at the beginning and one at the end of the diagram, the only scattering structure that allows for R^{-1} connector is the two-particle diagram of the form

2

R^{-1}

1
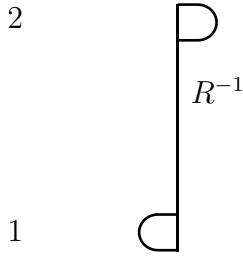
Fig. 6.8.

Such an asymptotic behavior of the connection lines may lead to the serious divergence problems. Consider for example the integral

$$\int \boldsymbol{Y}_{jE}(\boldsymbol{r}, \boldsymbol{r}')\mathrm{d}\boldsymbol{r}', \tag{6.21}$$

which one encounters while calculating the system's response to the spatially uniform disturbance ($\boldsymbol{E}(\boldsymbol{r}') = const.$). Using (5.46) we can rewrite it as

$$\sum_{s=1}^{N} \int \boldsymbol{\mu}_{11}(1, 2..., s)\delta(\boldsymbol{r} - \boldsymbol{R}_1)n(\boldsymbol{R}_1, \boldsymbol{R}_2..., \boldsymbol{R}_s)\mathrm{d}\boldsymbol{R}_1...\mathrm{d}\boldsymbol{R}_s+$$

$$+ \sum_{s=2}^{N} \int \boldsymbol{\mu}_{12}(1, 2..., s)\delta(\boldsymbol{r} - \boldsymbol{R}_1)n(\boldsymbol{R}_1, \boldsymbol{R}_2..., \boldsymbol{R}_s)\mathrm{d}\boldsymbol{R}_1...\mathrm{d}\boldsymbol{R}_s, \tag{6.22}$$

where $\boldsymbol{\mu}(1, 2, ..., s)$ are the terms in the cluster expansion of $\boldsymbol{\mu}$. Now the first term in (6.22) does not cause any problems, because there cannot be any connection lines in diagrammatic expansion of $\mu_{11}(1, 2..., s)n(\boldsymbol{R}_1, \boldsymbol{R}_2..., \boldsymbol{R}_s)$ as each diagram have to begin and end on the same particle (number 1). However the expansion of $\mu_{12}(1, 2..., s)n(\boldsymbol{R}_1, \boldsymbol{R}_2..., \boldsymbol{R}_s)$ contains the reducible diagrams. The integration over the particle at the end of the connection line in such a diagram leads to the integrals of the following kind

$$\int \frac{1}{r^k}\mathrm{d}\boldsymbol{r} \qquad k = 1, 2, 3, \tag{6.23}$$

which are clearly divergent.

It should be stressed that the long-range terms are absent in the irreducible diagrams. To see it, suppose that we came across a long-range bond linking particles i and j in an irreducible diagram K. As the diagram is irreducible, one of the following should hold

1. particles i and j are connected by a correlation function. In this case the long-range connector between i and j causes no trouble, as the correlation function decays very quickly as i wanders away from j.

2. particles i and j are connected by some other bond or the group of bonds coming through other particles. But then the diagram contains more than two bonds and therefore it is not a diagram from Fig. 6.8. This in turn implies that each of the two bonds between i and j decays at least as R^{-2}, so that the analytic expression corresponding to our diagram would contain the term decaying as R^{-4} or faster, which assures convergence.

The presence of long-ranged, reducible diagrams in the kernels under considerations is caused by the fact that the particle current $\boldsymbol{J}$, as well as the suspension velocity $\boldsymbol{v}^{ins}$ depend not only on the external disturbances $\boldsymbol{v}_o$ and $\boldsymbol{E}$ but also on the boundary conditions - i.e. the dimensions and the shape of the sample. Therefore the kernels $\boldsymbol{Y}_{jE}$, $\boldsymbol{Y}_{jv}$, $\boldsymbol{Y}_{fE}$ and $\boldsymbol{Y}_{fv}$ are not local. We will prove subsequently that the right local equations describing the response of the system in our case read (in a compact notation)

$$\boldsymbol{J} = \boldsymbol{Y}_{jE}^{irr}\boldsymbol{E} + \boldsymbol{Y}_{jv}^{irr}\boldsymbol{v}^{ins} \tag{6.24}$$

with the kernels $\boldsymbol{Y}_{jE}^{irr}$ and $\boldsymbol{Y}_{jv}^{irr}$ which are irreducible and therefore short-ranged. The reason why the kernels in (6.24) are local whereas kernels in (5.46) not, is that in (6.24) the boundary effects are accounted for by introducing the velocity $\boldsymbol{v}^{ins}$, which itself depends on the shape and dimensions of the sample. Analogous equation with local kernels will be found for the force density $\boldsymbol{f}$. The next part of this Chapter will be devoted to finding such irreducible, local kernels.

6.7   The reduction of the long-range kernels

In the following we are going to concentrate on the analysis of the diagrams of the kernel $\boldsymbol{Y}_{jE}$, the scattering structure of which is given by Eq. (2.36).

First, let us divide all the diagrams which make up $\boldsymbol{Y}_{jE}$ into two groups: reducible and irreducible ones. Then we rewrite each reducible diagram in form of a product:

$$B_{jE}(\boldsymbol{r}, \boldsymbol{r}') = \int I_{jE}(\boldsymbol{r}, \boldsymbol{r}'')\boldsymbol{G}(\boldsymbol{r}'', \boldsymbol{r}''')R_{jE}(\boldsymbol{r}''', \boldsymbol{r}')\mathrm{d}\boldsymbol{r}'\mathrm{d}\boldsymbol{r}''', \tag{6.25}$$

where B_{jE} stands for the diagram under consideration, I_{jE} is its part on the left of the articulation line and R_{jE} is the part on the right of the articulation line. Note that I_{jE} must be an irreducible diagram. For example the diagram from figure 6.2 is divided in a following way
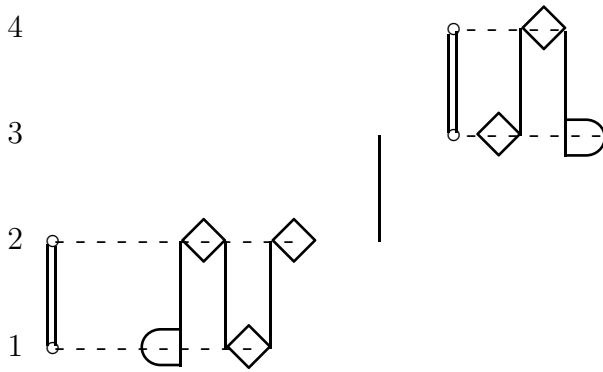
Fig. 6.9.

Here I_{jE} is given by the diagram
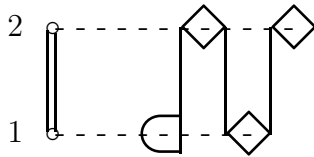
Fig. 6.10.

whereas R_{jE} is given by
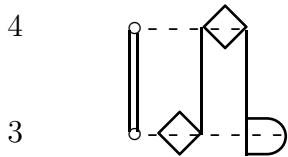
Fig. 6.11.

The n-linked diagrams of I_{jE} have the following scattering structure

$$Scatt(I_{jE}) = \boldsymbol{\mu}_o \boldsymbol{\mathcal{P}} \boldsymbol{Z}_o (-\boldsymbol{G}\hat{\boldsymbol{Z}}_o)^n \qquad n = 0, 1, \ldots, \tag{6.26}$$

whereas the correlation function which multiplies the sum of all I_{jE} diagrams with the same scattering structure is the block correlation function $b(C_1|...|C_k)$ defined in (6.17).

Now we turn to R_{jE} diagrams. Here the scattering structure of the n-linked diagram reads

$$Scatt(R_{jE}) = (-\hat{\boldsymbol{Z}}_{\boldsymbol{o}}\boldsymbol{G})^n \boldsymbol{Z}_o \boldsymbol{\mathcal{P}} \boldsymbol{\mu}_{\boldsymbol{o}}, \tag{6.27}$$

whereas the correlation structure is simple: the sum of all diagrams with the same scattering structure is multiplied simply by the function $n(i_1..i_k)$ where $\{i_1, \ldots, i_k\}$ is the set of all the particles in the diagram. The reason for it is lack of restrictions with respect to the reducibility: diagrams of R_{jE} may be reducible or not.

The scattering structure of R_{jE} given by (6.27) is just the same as the scattering structure of the diagrams of the kernel $\boldsymbol{Y}_{fE}$ (cf. Eqs. 5.46 and 2.42). Therefore in the thermodynamic limit the sum of all R_{jE} diagrams equals $\boldsymbol{Y}_{fE}(\boldsymbol{r}, \boldsymbol{r}')$.

Similarly, the scattering structure of I_{jE} is the same as that of the kernel $\boldsymbol{Y}_{jv}$ (cf. Eqs. 5.46 and 2.43), hence in the limit $N \to \infty$ the sum of all I_{jE} equals the sum of all **irreducible** diagrams making up $\boldsymbol{Y}_{jv}$: we are going to denote it by $\boldsymbol{Y}_{jv}^{irr}$.

Hence in the thermodynamic limit

$$
\int \boldsymbol{Y}_{jE}(\boldsymbol{r}, \boldsymbol{r}')\boldsymbol{E}(\boldsymbol{r}')\mathrm{d}\boldsymbol{r}' = \tag{6.28}
$$

$$
\int \boldsymbol{Y}_{jE}^{irr}(\boldsymbol{r}, \boldsymbol{r}')\boldsymbol{E}(\boldsymbol{r}')\mathrm{d}\boldsymbol{r}' + \int \boldsymbol{Y}_{jv}^{irr}(\boldsymbol{r}, \boldsymbol{r}'')\boldsymbol{G}(\boldsymbol{r}'', \boldsymbol{r}''')\boldsymbol{Y}_{fE}(\boldsymbol{r}''', \boldsymbol{r}')\boldsymbol{E}(\boldsymbol{r}')\mathrm{d}\boldsymbol{r}'\mathrm{d}\boldsymbol{r}''\mathrm{d}\boldsymbol{r}'''.
$$

The similar reduction can be performed on the kernel $\boldsymbol{Y}_{jv}$. Writing down the decompositions analogous to Eq. (6.25) we obtain the diagrams I_{jv} and R_{jv} with the following scattering structure for n-linked diagrams

$$
Scatt(I_{jv}) = \boldsymbol{\mu}_o \boldsymbol{P} \boldsymbol{Z}_o(-\boldsymbol{G}\hat{\boldsymbol{Z}}_o)^n = Scatt(I_{jE}),
$$
$$
Scatt(R_{jv}) = -(-\hat{\boldsymbol{Z}}_o\boldsymbol{G})^n \hat{\boldsymbol{Z}}_o. \tag{6.29}
$$

In the limit of the macroscopic system the sum of all R_{jv} diagrams is equal to $\boldsymbol{Y}_{fv}$ (cf. Eqs. 5.46 and 2.40). Therefore in this limit the following holds

$$
\int \boldsymbol{Y}_{jv}(\boldsymbol{r}, \boldsymbol{r}')\boldsymbol{v}_o(\boldsymbol{r}') = \tag{6.30}
$$

$$
\int \boldsymbol{Y}_{jv}^{irr}(\boldsymbol{r}, \boldsymbol{r}')\boldsymbol{v}_o(\boldsymbol{r}')\mathrm{d}\boldsymbol{r}' + \int \boldsymbol{Y}_{jv}^{irr}(\boldsymbol{r}, \boldsymbol{r}'')\boldsymbol{G}(\boldsymbol{r}'', \boldsymbol{r}''')\boldsymbol{Y}_{fv}(\boldsymbol{r}''', \boldsymbol{r}')\boldsymbol{v}_o(\boldsymbol{r}')\mathrm{d}\boldsymbol{r}''\mathrm{d}\boldsymbol{r}'.
$$

Summing up (6.28) and (6.30) we obtain

$$
< \boldsymbol{j}(\boldsymbol{r}) > = \int (\boldsymbol{Y}_{jE}(\boldsymbol{r}, \boldsymbol{r}')\boldsymbol{E}(\boldsymbol{r}') + \boldsymbol{Y}_{jv}(\boldsymbol{r}, \boldsymbol{r}')\boldsymbol{v}_o(\boldsymbol{r}'))\mathrm{d}\boldsymbol{r}' =
$$

$$
= \int (\boldsymbol{Y}_{jE}^{irr}(\boldsymbol{r}, \boldsymbol{r}')\boldsymbol{E}(\boldsymbol{r}') + \boldsymbol{Y}_{jv}^{irr}(\boldsymbol{r}, \boldsymbol{r}')\boldsymbol{v}_o(\boldsymbol{r}'))\mathrm{d}\boldsymbol{r}' + \tag{6.31}
$$

$$
+ \int \mathrm{d}\boldsymbol{r}''\mathrm{d}\boldsymbol{r}'''\boldsymbol{Y}_{jv}^{irr}(\boldsymbol{r}, \boldsymbol{r}'')\boldsymbol{G}(\boldsymbol{r}'', \boldsymbol{r}''') \left(\int \mathrm{d}\boldsymbol{r}'\boldsymbol{Y}_{fE}(\boldsymbol{r}''', \boldsymbol{r}')\boldsymbol{E}(\boldsymbol{r}') + \boldsymbol{Y}_{fv}(\boldsymbol{r}''', \boldsymbol{r}')\boldsymbol{v}_o(\boldsymbol{r}') \right).
$$

But form Eq. (5.45) the expression in brackets is just the instantaneous force density $\boldsymbol{f}^{ins}(\boldsymbol{r})$. Hence, using the fact that the instantaneous velocity can be expressed by the force density as (2.11)

$$\boldsymbol{v}^{ins}(\boldsymbol{r}) = \boldsymbol{v}_o(\boldsymbol{r}) + \int d\boldsymbol{r}' \boldsymbol{G}(\boldsymbol{r}, \boldsymbol{r}') \boldsymbol{f}^{ins}(\boldsymbol{r}') \tag{6.32}$$

we can rewrite Eq. (6.31) as

$$\boldsymbol{J}^{ins} =< \boldsymbol{j} >= \boldsymbol{Y}_{jE}^{irr} \boldsymbol{E} + \boldsymbol{Y}_{jv}^{irr} \boldsymbol{v}^{ins}, \tag{6.33}$$

where again the compact notation has been used.

Note that the kernels in the above equation are short-ranged, as all their diagrams are irreducible and therefore deployed of all solitary $\boldsymbol{G}$ connectors.

6.8 The force density

Let us now perform similar renormalization procedure on the force density kernels $\boldsymbol{Y}_{fE}$ and $\boldsymbol{Y}_{fv}$ defined by the relation

$$< \boldsymbol{f}(\boldsymbol{r}) >= \int (\boldsymbol{Y}_{fE}(\boldsymbol{r}, \boldsymbol{r}') \boldsymbol{E}(\boldsymbol{r}') + \boldsymbol{Y}_{fv}(\boldsymbol{r}, \boldsymbol{r}') \boldsymbol{v}_o(\boldsymbol{r}')) d\boldsymbol{r}'. \tag{6.34}$$

Just as before, we take the **reducible** diagrams of $\boldsymbol{Y}_{fE}$ and $\boldsymbol{Y}_{fv}$ and decompose them

$$B_{fE}(\boldsymbol{r}, \boldsymbol{r}') = \int I_{fE}(\boldsymbol{r}, \boldsymbol{r}'') \boldsymbol{G}(\boldsymbol{r}'', \boldsymbol{r}''') R_{fE}(\boldsymbol{r}''', \boldsymbol{r}') d\boldsymbol{r}'' d\boldsymbol{r}''',$$

$$B_{fv}(\boldsymbol{r}, \boldsymbol{r}') = \int I_{fv}(\boldsymbol{r}, \boldsymbol{r}'') \boldsymbol{G}(\boldsymbol{r}'', \boldsymbol{r}''') R_{fv}(\boldsymbol{r}''', \boldsymbol{r}') d\boldsymbol{r}'' d\boldsymbol{r}''', \tag{6.35}$$

with the notation analogous to that introduced in section 6.7.

The scattering structure of the n-linked diagrams I_{fE} and I_{fv} is the same and reads

$$Scatt(I_{fE}) = Scatt(I_{fv}) = \hat{\boldsymbol{Z}}_o(-\boldsymbol{G}\hat{\boldsymbol{Z}}_o)^n, \tag{6.36}$$

which is the same as the scattering structure of $\boldsymbol{Y}_{fv}$. The scattering structures of the respective R diagrams are identical to those encountered in the previous section

$$Scatt(R_{fE}) = (-\hat{\boldsymbol{Z}}_o\boldsymbol{G})^n \boldsymbol{Z}_o \mathcal{P} \boldsymbol{\mu}_o = Scatt(R_{jE}),$$

$$Scatt(R_{fv}) = (-\hat{\boldsymbol{Z}}_o\boldsymbol{G})^n \hat{\boldsymbol{Z}}_o = Scatt(R_{jv}). \tag{6.37}$$

Therefore in the limit of the macroscopic system we can write

$$\boldsymbol{f}^{ins}(\boldsymbol{r}) =< \boldsymbol{f}(\boldsymbol{r}) >= \int (\boldsymbol{Y}_{fE}(\boldsymbol{r},\boldsymbol{r}')\boldsymbol{E}(\boldsymbol{r}') + \boldsymbol{Y}_{fv}(\boldsymbol{r},\boldsymbol{r}')\boldsymbol{v}_o(\boldsymbol{r}'))\mathrm{d}\boldsymbol{r}' =$$

$$= \int \boldsymbol{Y}_{fE}^{irr}(\boldsymbol{r},\boldsymbol{r}')\boldsymbol{E}(\boldsymbol{r}')\mathrm{d}\boldsymbol{r}'+$$

$$+ \int \boldsymbol{Y}_{fv}^{irr}(\boldsymbol{r},\boldsymbol{r}') \left(\boldsymbol{v}_o(\boldsymbol{r}') + \int \boldsymbol{G}(\boldsymbol{r}',\boldsymbol{r}''') \left[\boldsymbol{Y}_{fE}(\boldsymbol{r}''',\boldsymbol{r}'')\boldsymbol{E}(\boldsymbol{r}'') + \boldsymbol{Y}_{fv}(\boldsymbol{r}''',\boldsymbol{r}'')\boldsymbol{v}_o(\boldsymbol{r}'')\right] \mathrm{d}\boldsymbol{r}''\mathrm{d}\boldsymbol{r}''' \right) \mathrm{d}\boldsymbol{r}'$$

But the expression in brackets on the right hand side of Eq. (6.38) is the instantaneous suspension velocity, so eventually

$$\boldsymbol{f}^{ins} = \boldsymbol{Y}_{fE}^{irr}\boldsymbol{E} + \boldsymbol{Y}_{fv}^{irr}\boldsymbol{v}^{ins}. \tag{6.38}$$

6.9   The short-time diffusion coefficient

We have succeeded in deriving the equations (6.33) and (6.38) for the particle current $\boldsymbol{J}^{ins}$ and the instantaneous force density $\boldsymbol{f}^{ins}$ given by the short-range kernels $\boldsymbol{Y}^{irr}$ acting on the external field $\boldsymbol{E}$ and suspension velocity $\boldsymbol{v}^{ins}$. Because of their short range, as it was argued in the Introduction, the kernels $\boldsymbol{Y}^{irr}$ are independent of the shape and size of the sample provided that it is macroscopic. But if it is so, then one can assume that the sample is infinite. It would not affect the kernels $\boldsymbol{Y}^{irr}(\boldsymbol{r},\boldsymbol{r}')$, but greatly facilitate the calculations, as then the hydrodynamic Green function for an infinite system given by (2.9) can be used.

Now we change to the $\boldsymbol{k}$ space to calculate the values of the response kernels at $k = 0$ and thereby get the diffusion coefficient. The Fourier transforms of the kernels and fields are performed according to expressions (1.44)-(1.47). In this way we obtain that the Fourier transform of the equation (6.33) for the particle current reads (in case of the homogeneous system)

$$\boldsymbol{J}^{ins}(\boldsymbol{k}) = \boldsymbol{Y}_{jE}^{irr}(\boldsymbol{k})\boldsymbol{E}(\boldsymbol{k}) + \boldsymbol{Y}_{jv}^{irr}(\boldsymbol{k})\boldsymbol{v}^{ins}(\boldsymbol{k}), \tag{6.39}$$

In the long wavelength limit ($\boldsymbol{k} \to 0$) the tensor $\boldsymbol{Y}_{jv}^{irr}$ takes a particularly simple form. We have namely from Eqs. (5.46) and (2.43)

$$\boldsymbol{Y}_{jv}^{irr}(\boldsymbol{k} = 0) = \int < \sum_{i=1}^{N} \delta(R_i)[\boldsymbol{\mu}_o\boldsymbol{P}\boldsymbol{Z}_o + \boldsymbol{\mu}_o\boldsymbol{P}\boldsymbol{Z}_o\boldsymbol{G}(1 + \hat{\boldsymbol{Z}}_o\boldsymbol{G})^{-1}\hat{\boldsymbol{Z}}_o]_i(\boldsymbol{r}') >^{irr} \mathrm{d}\boldsymbol{r}'. \tag{6.40}$$

But $\hat{\boldsymbol{Z}}_o(i)(\boldsymbol{r},\boldsymbol{r}') \neq 0$ only if $\theta_i(\boldsymbol{r}') \neq 0$ so we can write (6.40) equivalently as

$$\boldsymbol{Y}_{jv}^{irr}(\boldsymbol{k} = 0) =< \sum_{i=1}^{N} \delta(R_i)[\boldsymbol{\mu}_o\boldsymbol{P}\boldsymbol{Z}_o\boldsymbol{P}^t + \boldsymbol{\mu}_o\boldsymbol{P}\boldsymbol{Z}_o\boldsymbol{G}(1 + \hat{\boldsymbol{Z}}_o\boldsymbol{G})^{-1}\hat{\boldsymbol{Z}}_o\boldsymbol{P}^t]_i(\boldsymbol{r}') >^{irr} . \tag{6.41}$$

But, as we have proved in Chapter 2

$$\hat{\boldsymbol{\mathcal{Z}}}_o \boldsymbol{\mathcal{P}}^t = 0 \tag{6.42}$$

thus

$$\boldsymbol{Y}_{jv}^{irr}(\boldsymbol{k} = 0) = < \sum_{i=1}^{N} \delta(R_i) \boldsymbol{\mu}_o(i) \boldsymbol{\mathcal{P}}(i) \boldsymbol{Z}_o(i) \boldsymbol{\mathcal{P}}^t(i) >^{irr} = < \sum_{i=1}^{N} \delta(R_i) > \mathbf{1} = n(0)\mathbf{1} = n\mathbf{1}, \tag{6.43}$$

where in the last equality we have used once again the homogeneity of the system.

We see therefore that in the limit of small wavevectors there have appeared in a natural way in our equations the (instantaneous) diffusion current $\boldsymbol{J}_d^{ins} = \boldsymbol{J} - n\boldsymbol{v}^{ins}$. In fact in the $\boldsymbol{k} \to 0$ limit the equation (6.39) takes form (for the isotropic system)

$$\boldsymbol{J}_d^{ins} = \boldsymbol{Y}_{jE}^{irr}(\boldsymbol{k} = 0)\boldsymbol{E}, \tag{6.44}$$

where we use the fact that, because of the local character of irreducible kernels, $\lim_{k \to 0} \boldsymbol{Y}_{jE}^{irr}(\boldsymbol{k}) = \boldsymbol{Y}_{jE}^{irr}(\boldsymbol{k} = 0)$. In the isotropic system this tensor is proportional to the unit matrix, i.e.

$$\boldsymbol{Y}_{jE}^{irr}(\boldsymbol{k} = 0) = y_{jE}\mathbf{1}. \tag{6.45}$$

This allows us to identify the collective diffusion coefficient with

$$D_c^s = \frac{k_B T}{3nS(0)} \text{Tr} \boldsymbol{Y}_{jE}^{irr}(\boldsymbol{k} = 0) = \frac{k_B T}{nS(0)} y_{jE}. \tag{6.46}$$

The diffusion coefficient described by this formula is a short-time one because $\boldsymbol{Y}_{jE}^{irr}(\boldsymbol{k} = 0)$ is the proportionality factor between the instantaneous diffusion current and the external field. To calculate the long time collective diffusion coefficient we have to take into account the memory effects hidden in the retarded response part of the diffusion current.

The comparison of the above expression for D_c^s with the one obtained from the Mori-Zwanzig formalism (4.30) shows that one can extend the hydrodynamic factor $H(k)$ to $k = 0$ by defining its value in $k = 0$ as

$$H(0) = \frac{k_B T}{nD_o} y_{jE} = \frac{1}{3N\mu_o} \text{Tr} < \sum_{i,j} \boldsymbol{\mu}_{ij} >^{irr}, \tag{6.47}$$

which is equal to the limit $k \to 0$ of the function $H(k)$ defined in (4.31). Therefore the short-time diffusion coefficient can be written by analogy to (4.30) as

$$D_c^s = \frac{D_o H(0)}{S(0)}. \tag{6.48}$$

6.10   The small k limit of the equations for instantaneous velocity and diffusion current

In the expansion of $\boldsymbol{Y}_{jv}(\boldsymbol{k})$ in $\boldsymbol{k}$ around $\boldsymbol{k} = 0$ for the homogeneous system the linear term ($\sim k$) vanishes because of the isotropy so that

$$\boldsymbol{Y}_{jv}^{irr}(\boldsymbol{k}) = n\boldsymbol{1} + k^2\boldsymbol{y}_{jv} + ..., \tag{6.49}$$

where the tensor $\boldsymbol{y}_{jv}$ because of the isotropy must have the form

$$\boldsymbol{y}_{jv} = y_{jv}^l \hat{\boldsymbol{k}}\hat{\boldsymbol{k}} + y_{jv}^t(\boldsymbol{1} - \hat{\boldsymbol{k}}\hat{\boldsymbol{k}}), \tag{6.50}$$

where y_{jv}^l and y_{jv}^t are scalars. On account of the incompressibility condition

$$\boldsymbol{k} \cdot \boldsymbol{v}^{ins} = 0 \tag{6.51}$$

the first term in (6.50) does not contribute to equation (6.39). Hence in the small $\boldsymbol{k}$ limit this equation can be rewritten as

$$\boldsymbol{J}_d^{ins}(\boldsymbol{k}) = y_{jE}(\boldsymbol{k})\boldsymbol{E}(\boldsymbol{k}) + k^2 y_{jv}^t \boldsymbol{v}^{ins}(\boldsymbol{k}). \tag{6.52}$$

Let us now turn to the equations of the fluid motion. The Fourier transform of the hydrodynamic Green function for an infinite space reads

$$\boldsymbol{G}(\boldsymbol{k}) = \frac{1}{\eta k^2}(\boldsymbol{1} - \hat{\boldsymbol{k}}\hat{\boldsymbol{k}}), \tag{6.53}$$

so that the velocity in this case may be written as

$$k^2 \boldsymbol{v}^{ins}(\boldsymbol{k}) = \frac{1}{\eta}(\boldsymbol{1} - \hat{\boldsymbol{k}}\hat{\boldsymbol{k}})(\boldsymbol{f}^{ins}(\boldsymbol{k}) + \boldsymbol{f}_o(\boldsymbol{k})). \tag{6.54}$$

Now the instantaneous force density $\boldsymbol{f}^{ins}$ can be found by the Fourier transform of (6.38) and the velocity takes form

$$k^2 \boldsymbol{v}^{ins}(\boldsymbol{k}) = \frac{1}{\eta}(\boldsymbol{1} - \hat{\boldsymbol{k}}\hat{\boldsymbol{k}})(\boldsymbol{f}_o(\boldsymbol{k}) + \boldsymbol{Y}_{fE}^{irr}(\boldsymbol{k})\boldsymbol{E}(\boldsymbol{k}) + \boldsymbol{Y}_{fv}^{irr}(\boldsymbol{k})\boldsymbol{v}^{ins}(\boldsymbol{k})). \tag{6.55}$$

First let us investigate the lowest order ($O(1)$) term in $\boldsymbol{k}$ of the operators $\boldsymbol{Y}_{fE}^{irr}(\boldsymbol{k})$ and $\boldsymbol{Y}_{fv}^{irr}(\boldsymbol{k})$ around $\boldsymbol{k} = 0$. For $\boldsymbol{Y}_{fE}^{irr}$ the answer can be given immediately, as this operator is adjoint to $\boldsymbol{Y}_{jv}^{irr}$, so from (6.43) we get

$$\boldsymbol{Y}_{fE}(\boldsymbol{k} = 0) = \boldsymbol{Y}_{jv}(\boldsymbol{k} = 0) = n\boldsymbol{1}. \tag{6.56}$$

To find out the $\boldsymbol{k} = 0$ value for $\boldsymbol{Y}_{fv}^{irr}(\boldsymbol{k})$ we recall its scattering structure. From (5.46) and (2.40)

$$\boldsymbol{Y}_{fv}^{irr}(\boldsymbol{k} = 0) = -\int < \hat{\boldsymbol{\mathcal{Z}}}_o(1 + \boldsymbol{\mathcal{G}}\hat{\boldsymbol{\mathcal{Z}}}_o)^{-1}(\boldsymbol{r} = 0, \boldsymbol{r}') >^{irr} d\boldsymbol{r}'. \tag{6.57}$$

Here the scattering sequence ends on $\hat{\boldsymbol{\mathcal{Z}}}_{\boldsymbol{o}}$ operator, so the same reasoning as that after Eq.(6.40) leads us to the conclusion that

$$\boldsymbol{Y}_{fv}^{irr}(\boldsymbol{k}=0)=0. \tag{6.58}$$

Therefore the small $\boldsymbol{k}$ limit of operators $\boldsymbol{Y}_{fE}$ and $\boldsymbol{Y}_{fv}$ reads

$$\boldsymbol{Y}_{fE}^{irr}(\boldsymbol{k})=n\boldsymbol{1}+k^2\boldsymbol{y}_{fE}+...,$$
$$\boldsymbol{Y}_{fv}^{irr}(\boldsymbol{k})=-k^2\boldsymbol{y}_{fv}+... \tag{6.59}$$

The tensors $\boldsymbol{y}_{fv}$ and $\boldsymbol{y}_{fE}$ can be similarly to $\boldsymbol{y}_{jv}$ decomposed on the longitudinal and transverse parts and the equation (6.55) takes form

$$-k^2(\eta+y_{fv}^t)\boldsymbol{v}^{ins}(\boldsymbol{k})=(\boldsymbol{1}-\hat{\boldsymbol{k}}\hat{\boldsymbol{k}})(\boldsymbol{f}_{o}(\boldsymbol{k})+n\boldsymbol{E}(\boldsymbol{k})+k^2y_{fE}^t\boldsymbol{E}(\boldsymbol{k})), \tag{6.60}$$

where we have used the fact that, due to the incompressibility condition

$$(\boldsymbol{1}-\hat{\boldsymbol{k}}\hat{\boldsymbol{k}})\boldsymbol{v}(\boldsymbol{k})=\boldsymbol{v}(\boldsymbol{k}). \tag{6.61}$$

Due to the symmetry between the operators $\boldsymbol{Y}_{jv}$ and $\boldsymbol{Y}_{fE}$ the coefficient y_{fE}^t is equal to y_{jv}^t introduced earlier. This is in fact the manifestation of the Onsager symmetry guessed by Nozières [42].

We see that in above equation there appeared in a natural way the total external force (per unit volume) exerted on the suspension

$$\boldsymbol{F}_{tot}=\boldsymbol{f}_{o}+n\boldsymbol{E}, \tag{6.62}$$

which is the sum of the force $\boldsymbol{f}_{o}$ exerted on the whole suspension and the force $\boldsymbol{E}$ which acts only in the particles (hence the factor n in front of $\boldsymbol{E}$).

Now the equation (6.60) takes form

$$k^2(\eta+y_{fv}^t)\boldsymbol{v}^{ins}(\boldsymbol{k})=(\boldsymbol{1}-\hat{\boldsymbol{k}}\hat{\boldsymbol{k}})(\boldsymbol{F}_{tot}(\boldsymbol{k})+k^2y_{fE}^t\boldsymbol{E}(\boldsymbol{k})). \tag{6.63}$$

6.11 Analysis of the equations for suspension velocity and diffusion current

Let us take a closer look at the macroscopic equations for the suspension velocity (6.63) and diffusion current (6.52) derived in the previous section. To this end we are going to rewrite them in a slightly different manner, correct to the order k^2. Namely

$$\boldsymbol{J}_d^{ins}(\boldsymbol{k}) = y_{jE}\boldsymbol{E}(\boldsymbol{k}) + k^2 y_{jv}^t \boldsymbol{v}^{ins}(\boldsymbol{k}), \tag{6.64}$$

$$k^2(\eta + y_{fv}^t)\boldsymbol{v}^{ins}(\boldsymbol{k}) = (\boldsymbol{1} - \hat{\boldsymbol{k}}\hat{\boldsymbol{k}})(\boldsymbol{F}_{tot}(\boldsymbol{k}) + k^2\frac{y_{fE}^t}{y_{jE}}\boldsymbol{J}_d^{ins}),$$

or, if one transforms it back into the real space

$$\boldsymbol{J}_d^{ins} = y_{jE}\boldsymbol{E} - y_{jv}^t\nabla^2\boldsymbol{v}^{ins}, \tag{6.65}$$

$$-(\eta + y_{fv}^t)\nabla^2\boldsymbol{v}^{ins} = \boldsymbol{F}_{tot} - \mathbf{grad}\, p - \frac{y_{fE}^t}{y_{jE}}(\nabla^2\boldsymbol{J}_d^{ins} - \mathbf{grad}\,\mathrm{div}\boldsymbol{J}_d^{ins}),$$

where we have used the fact that longitudinal part of the force $\boldsymbol{F}_{tot}$ is compensated by a pressure gradient such that

$$-i\boldsymbol{k}p(\boldsymbol{k}) = \hat{\boldsymbol{k}}\hat{\boldsymbol{k}} \cdot \boldsymbol{F}_{tot}(\boldsymbol{k}) \tag{6.66}$$

which can be seen from the Fourier transform of (2.10) together with (2.8).
One sees that the above equations describe the following effects

1. Direct effects: the diffusion current is induced by the external force $\boldsymbol{E}$ applied to the particles with the coefficient of proportionality y_{jE} whereas the suspension velocity field is induced by the overall external force acting on the particles and the fluid $\boldsymbol{F}_{tot} = \boldsymbol{f}_o + n\boldsymbol{E}$. Note that the presence of the particles changes the effective viscosity of the suspension, as the role of η in (1.13) is here played by

$$\eta^{eff} = \eta + y_{fv}^t. \tag{6.67}$$

2. Cross effects linking the suspension velocity with the diffusion current. These are described by the terms $y_{jv}^t\nabla^2\boldsymbol{v}^{ins}$ and $\frac{y_{fE}^t}{y_{jE}}\nabla^2\boldsymbol{J}_d^{ins}$ respectively. They describe the processes in which the **inhomogeneities** in the suspension velocity drive the diffusion current and vice versa.

It is instructive to rewrite the equations once more, this time expressing the cross terms in terms of forces instead of the flows. One gets then (still in a small wave-vector approximation)

$$\boldsymbol{J}_d^{ins} = y_{jE}\boldsymbol{E} - \frac{y_{jv}^t}{\eta + y_{fv}^t}(\boldsymbol{F}_{tot} - \mathrm{grad}\,\boldsymbol{p}),$$

$$-(\eta + y_{fv}^t)\nabla^2\boldsymbol{v}^{ins} = \boldsymbol{F}_{tot} - \mathbf{grad}\, p - y_{fE}^t(\nabla^2\boldsymbol{E} - \mathbf{grad}\,\mathrm{div}\boldsymbol{E}), \tag{6.68}$$

Note that the force $(\boldsymbol{F}_{tot} - \mathbf{grad}\, p)$, when exists, dominates in (6.68), therefore the cross effects can be best seen in systems with $(\boldsymbol{F}_{tot} - \mathbf{grad}\, p) = 0$. In fact, the usual gravity driven sedimentation fulfills this condition, as then the gravitational force is indeed canceled by the vertical pressure gradient. Another example of such a system is the locally neutral (fluid neutralizing particles) suspension placed in the electric field. In the former case, the cross effect manifests itself in a presence of nonzero suspension flow known as backflow, intrinsic convection or the Beenaker-Mazur flow, as these two were the first to notice it [97–99]. In the second case, as it was pointed out by Noziéres the above equations provide a bulk mechanism for the electrokinetic effects (Saxen's laws): an inhomogeneous current provides convection and an inhomogeneous flow pattern may drive an electric current.

As it was already remarked, the above equations were derived first by Nozières [42] in a rather phenomenological way. The throughout derivation was given by Felderhof [43, 100] and Noetinger [23]. Felderhof used a technique called renormalized cluster expansion [101] to derive Eqs. (6.33) and (6.38) and proved that all the kernels in these equations are short-ranged. The reduction presented in this Chapter is in fact the simplified version of this technique. Felderhof gives also the explicit values of the coefficients y in the small density limit.

On the other hand, Noetinger worked from the very start in the Fourier space. He performed only the partial reduction of the kernels and therefore was left with a number of cumbersome $\boldsymbol{k} \to 0$ limits to calculate. He did it correctly and obtained the same equations as Felderhof and we here, although written in a slightly different language (as he used the hydrodynamic formalism of Mazur, van-Saarlos and Beenaker [21, 59, 102]).

As far as the short-time collective diffusion coefficient is concerned, the calculations of this quantity, as it was remarked in Introduction, has started with the papers of Burgers from 1942 [44–47], who however, did not succeed in obtaining the correct formula due to the problems with divergent integrals. Thirty years later Batchelor [49] derived his well-known formula for D_c^s to the first order in the volume fraction

$$D_c^s = D_o(1 + 1.45\phi). \tag{6.69}$$

The calculation of $k = 0$ value of the static structure factor $S(0)$ does not cause a great trouble, as the static structure factor has been throughly studied both theoretically and experimentally. In collective diffusion coefficient calculations one usually uses the Perkus-Yevick approximation, which gives the following dependence of $S(0)$ on the volume fraction

$$S(0) = \frac{(1-\phi)^4}{(1+2\phi)^2}. \tag{6.70}$$

Chapter 7

Cluster expansion for the retarded response

In this Chapter we focus our attention on the time-dependent, "retarded" part of the system's response to external perturbations (cf. Eq. 5.43). The retarded response is described by the time-dependent kernels $\boldsymbol{X}_{ab}$ given by Eq. (5.47). Those kernels are long-ranged, just as it is the case for the instantaneous kernels $\boldsymbol{Y}_{ab}$. Therefore the reduction procedure, analogous to that performed on $\boldsymbol{Y}_{ab}$ in Chapter 6 is needed. However the problem is much more difficult here, as the adjoint Smoluchowski operator $\boldsymbol{\mathcal{L}}$ governing the time-evolution of the system is long-ranged itself. Moreover, the diagrams making up $\boldsymbol{X}_{ab}$ have much more complicated structure than analogous diagrams for $\boldsymbol{Y}_{ab}$, so that such notions as block distribution function cannot be applied in a straightforward way here. It is to be stressed that there was no proof so far in a literature that the retarded response kernels $\boldsymbol{X}_{ab}$ can be reduced in a similar way as it was presented in the last Chapter for the instantaneous response. In this Chapter, using the diagrammatic technique, we perform the needed reduction. Next, we get the well-defined, explicit expression for the collective diffusion coefficient as well as for the memory contribution to this coefficient given by the factor Δ. Then, the equations for the suspension velocity and the particle current are derived. They differ from the analogous equations derived in section (6.10) by the presence of the time-dependent terms in the response kernels. Finally, the virial expansion of Δ is performed and the expression for the first nonvanishing term in the expansion, corresponding to the second order in volume fraction, is obtained.

7.1 The diagrammatic representation of the retarded response kernels

Just as in the preceding Chapter, we are going to construct the diagrammatic representation - this time of the retarded response kernels X (5.47) which are of the form $X = < A e^{\boldsymbol{\mathcal{L}}t} B >$. The task would be more difficult now, because of the time-evolution operator $e^{\boldsymbol{\mathcal{L}}t}$ sitting inside the kernels.

First of all we decompose the adjoint Smoluchowski operator

$$\mathcal{L} = [\beta^{-1} \vec{\nabla} + \mathcal{F}] \cdot \boldsymbol{\mu} \cdot \vec{\nabla} \tag{7.1}$$

as

$$\mathcal{L}(1, 2, \ldots, N) = \sum_{i,j=1}^{N} \mathcal{L}_o(i) + \delta\mathcal{L}(1, 2, \ldots, N), \tag{7.2}$$

where $\mathcal{L}_o(i)$ is the one particle operator

$$\mathcal{L}_o(i) = D_o \vec{\nabla}_i^2, \tag{7.3}$$

with $D_o = \beta^{-1}\mu_o$ denoting the one-particle diffusion coefficient. The nice thing about $\mathcal{L}_o$ is that it cannot introduce any correlations between particles. Now the evolution operator can be written as a series

$$e^{\mathcal{L}t} = S(t) + \int_0^t d\tau S(t-\tau)\delta LS(\tau) + \int_0^t d\tau \int_0^\tau d\tau' S(t-\tau)\delta LS(\tau-\tau')\delta LS(\tau) + ..., \tag{7.4}$$

where

$$S(1, 2, \ldots, N; t) = \prod_i S(i; t), \tag{7.5}$$

with

$$S(i; t) = e^{\mathcal{L}_o(i)t}. \tag{7.6}$$

In the diagrams we represent $S(i, \tau - \tau')$ as the horizontal solid line

$$\overline{\underset{\tau}{}\underset{\tau'}{}}$$

called $\boldsymbol{e}$ - bond.

To obtain the diagrammatic expansion of $< Ae^{\mathcal{L}t}B >$, we start with performing the scattering expansion of the operators A and B. In the analogous way, after representing $e^{\mathcal{L}t}$ in form of the series (7.4) we perform the expansion of the $\delta\mathcal{L}$ terms onto the sum of $\delta\mathcal{L}$ **blocks**. Then, inserting all the above expansions into $< Ae^{\mathcal{L}t}B >$ one ends up with the representation of the retarded response kernel as a sum of diagrams of the following structure (from left to right)

– on the far left of a diagram a correlation structure is placed, just as it is the case for the instantaneous diagrams of the previous Chapter

– next one places one of A-blocks

– next comes a sequence of $\boldsymbol{e}$-bonds with $\delta\mathcal{L}$ blocks in between

– finally a B-block

Just as it is in the instantaneous case, integrations $\int\mathrm{d}\boldsymbol{R}_1\ldots\int\mathrm{d}\boldsymbol{R}_N$ are performed over the coordinates of all particles. Moreover, an ordered **time integration** $\int_0^t\mathrm{d}\tau\int_0^{\tau'}\mathrm{d}\tau''$ $\int_0^{\tau''}\mathrm{d}\tau'''\ldots$ is carried out over the times of all intermediate levels (the number of integrals is equal to the number of $\delta\mathcal{L}$ blocks in a given diagram).

Note that apart from the evolution operator, there are few more elements in the retarded response kernels that were not present in the instantaneous response and therefore the "retarded" diagrams must contain some new symbols. These are:

1. a new bond: dagger line ‡ representing two-body interparticle forces ($\mathcal{F}$ - bond)

2. new vertices standing for the following operators:

$$
\begin{aligned}
\overrightarrow{\mathrm{D}} \quad &- \quad \text{standing for } \boldsymbol{Z_o}(i)\boldsymbol{\mathcal{P}}(i)\boldsymbol{\mu}_o(i)\,\overrightarrow{\nabla}_i \\[2mm]
\overrightarrow{\mathrm{C}} \quad &- \quad \text{standing for } \overrightarrow{\nabla}_i\,\boldsymbol{\mu}_o(i)\boldsymbol{\mathcal{P}}(i)\boldsymbol{Z_o}(i) \\[2mm]
\overleftarrow{\mathrm{D}} \quad &- \quad \text{standing for } \boldsymbol{Z_o}(i)\boldsymbol{\mathcal{P}}(i)\boldsymbol{\mu}_o(i)\,\overleftarrow{\nabla}_i \\[2mm]
\overrightarrow{\mathrm{C}}^{\Rightarrow} \quad &- \quad \text{standing for } \beta^{-1}\,\overrightarrow{\nabla}_i\,\boldsymbol{\mu}_o(i)\boldsymbol{\mathcal{P}}(i)\boldsymbol{Z_o}(i)
\end{aligned}
$$

(7.7)

so while $\rightarrow$ stands for ∇, the double arrow $\Rightarrow$ stands for $\beta^{-1}\nabla$

Note that the operators in (7.7) do not include the delta function $\delta(\boldsymbol{r}-\boldsymbol{R}_i)$ as it is the case for D and C .

For example the diagram

stands for the kernel
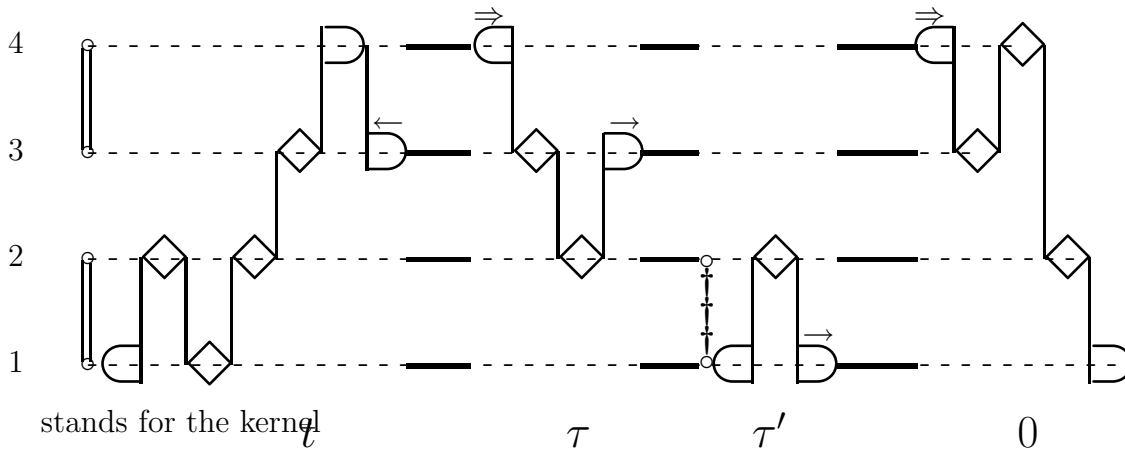
Fig. 7.1.

$$\int d1 \ldots d4 \; h(12)h(34)\tilde{A}(1,2,3,4) \int_0^t d\tau \int_0^\tau d\tau' \qquad (7.8)$$

$$S(1,2,3,4;t-\tau)\widetilde{\delta\mathcal{L}}_1(2,3,4)S(1,2,3,4;\tau-\tau')\widetilde{\delta\mathcal{L}}_2(1,2)S(1,2,3,4;\tau')\tilde{B}(1,2,3,4),$$

with the corresponding blocks given by

$$\tilde{A}(1,2,3,4) = -\delta(\boldsymbol{r}-\boldsymbol{R}_1)\mu_o(1)\boldsymbol{\mathcal{P}}(1)\boldsymbol{Z_o}(1)\boldsymbol{G}(12)\hat{\boldsymbol{Z}}_{\boldsymbol{o}}(2)\boldsymbol{G}(21)\hat{\boldsymbol{Z}}_{\boldsymbol{o}}(1)$$

$$\boldsymbol{G}(12)\hat{\boldsymbol{Z}}_{\boldsymbol{o}}(2)\boldsymbol{G}(23)\hat{\boldsymbol{Z}}_{\boldsymbol{o}}(3)\boldsymbol{G}(34)\hat{\boldsymbol{Z}}_{\boldsymbol{o}}(4)\boldsymbol{G}(43)\boldsymbol{Z_o}(3)\boldsymbol{\mathcal{P}}(3)\mu_o(3)\overleftarrow{\nabla}_3,$$

$$\widetilde{\delta\mathcal{L}}_1(2,3,4) = \overrightarrow{\nabla}_4 \, \mu_o(4)\boldsymbol{\mathcal{P}}(4)\boldsymbol{Z_o}(4)\boldsymbol{G}(43)\hat{\boldsymbol{Z}}_{\boldsymbol{o}}(3)\boldsymbol{G}(32)\hat{\boldsymbol{Z}}_{\boldsymbol{o}}(2)\boldsymbol{G}(23)\boldsymbol{Z_o}(3)\boldsymbol{\mathcal{P}}(3)\mu_o(3)\overrightarrow{\nabla}_3,$$

$$\widetilde{\delta\mathcal{L}}_2(1,2) = \boldsymbol{F}(12)\overrightarrow{\nabla}_1 \, \mu_o(1)\boldsymbol{\mathcal{P}}(1)\boldsymbol{Z_o}(1)\boldsymbol{G}(12)\hat{\boldsymbol{Z}}_{\boldsymbol{o}}(2)\boldsymbol{G}(21)\boldsymbol{Z_o}(1)\boldsymbol{\mathcal{P}}(1)\mu_o(1)\overrightarrow{\nabla}_1,$$

$$\tilde{B}(1,2,3,4) = -\overrightarrow{\nabla}_4 \, \mu_o(4)\boldsymbol{\mathcal{P}}(4)\boldsymbol{Z_o}(4)\boldsymbol{G}(43)\hat{\boldsymbol{Z}}_{\boldsymbol{o}}(3)\boldsymbol{G}(34)\hat{\boldsymbol{Z}}_{\boldsymbol{o}}(4)\boldsymbol{G}(42)$$

$$\hat{\boldsymbol{Z}}_{\boldsymbol{o}}(2)\boldsymbol{G}(21)\boldsymbol{Z_o}(1)\boldsymbol{\mathcal{P}}(1)\mu_o(1)\delta(\boldsymbol{r}-\boldsymbol{R}_1).$$

The tilde ˜ is used in the above expression to denote the fact that $\tilde{A}$, $\tilde{B}$ and $\widetilde{\delta\mathcal{L}}$ stand only for some terms in the scattering expansion of A, B and $\delta\mathcal{L}$ and not for the whole operators (see also the definition of a block in the next section).

Note that the operator $\beta^{-1}\overrightarrow{\nabla}$ appears in the kernels (cf. (5.47) and (7.1)) always together with the force $\boldsymbol{\mathcal{F}}$. Therefore every diagram in which there is $\overrightarrow{\boldsymbol{\triangleleft}}$, has a counterpart where the place of $\overrightarrow{\boldsymbol{\triangleleft}}$ is taken by the $\boldsymbol{\mathcal{F}}$ bond attached to the operator $\boldsymbol{\triangleleft}$.

7.2   Diagrammatic analysis

Let us introduce now few more definitions which are needed for further considerations.

block - a part of a diagram corresponding to some term in a scattering sequence of A, B or $\delta\mathcal{L}$ operator

first (last) vertex of a block - a vertex in a given block which is most to the left (right)

right(left) terminal block - a block with the property that the particle line passing through its last(first) vertex v does not pass through any other vertex in a diagram more to the right(left) than v

right(left) terminal $\boldsymbol{e}$ - bond - an $\boldsymbol{e}$ - bond with the property that the particle line passing through it does not pass through any vertex in a diagram on the right(left) side of that $\boldsymbol{e}$ - bond

improper block - one of the following: either a terminal $\delta\mathcal{L}$ block or a right terminal A block or a left terminal B block

proper diagram - a diagram which does not contain improper blocks

improper diagram - a diagram which is not proper

unlinked diagram - a diagram the particle lines of which can be divided into k sets C_i, $i = 1, 2...k$ with $k \geq 2$ with the property that particles in C_i are not connected by any bonds with the particles from C_j. Diagrams which are not unlinked are called **linked**. If a given diagram K is unlinked, then there always exists a unique decomposition $\tilde{C}_i$, $i = 1, 2...k$, in which all $\tilde{C}_i$ are linked. In this case, $\tilde{C}_i$ are called the components of the diagram K.

Let us illustrate the new definitions with an example. The following diagram
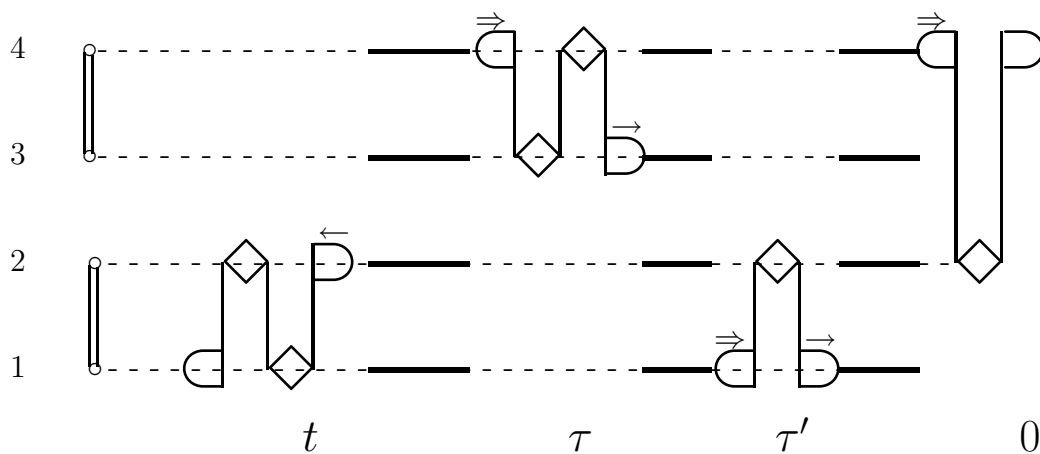
Fig. 7.2.

is a linked, improper diagram. It consists of terminal blocks only, two $\delta\mathcal{L}$ blocks among them: one right terminal $\delta\mathcal{L}$ block and one left terminal $\delta\mathcal{L}$ block.

7.3   Simplification of the diagrams

In this section we are going to simplify a bit the set of retarded response diagrams by use of few Rules. These are either **cut-off rules**, which tell us which elements of a diagram can be deleted without affecting the analytical expression to which the diagram corresponds, or The **transformation rules**, in which the prescription is given how to transform one set of diagrams into another with a simpler structure under the condition that the sum of analytic expressions corresponding to the diagrams in the former set is the same as in the latter.

The first transformation rule allows us to get rid of the diagrams in which the subdiagram of the following structure can be found
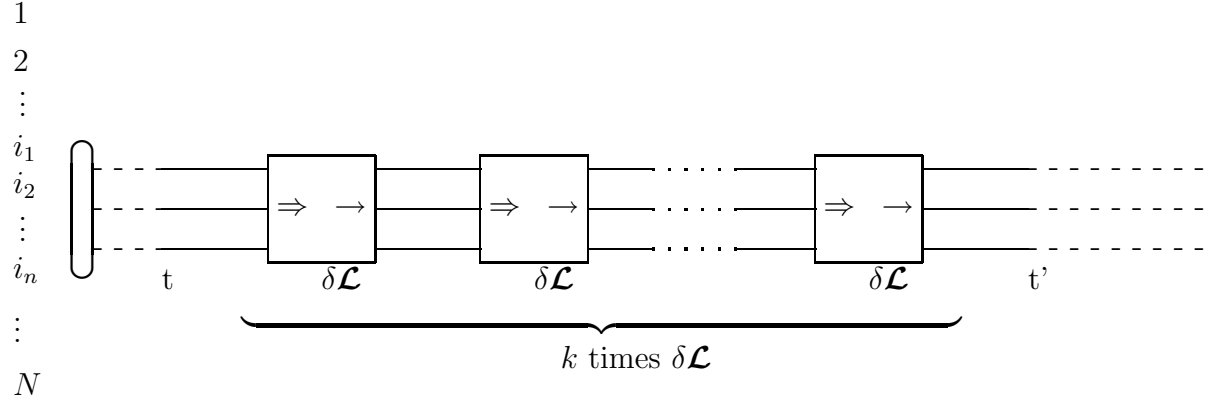
Fig. 7.3.

The oval here stands for any correlation function $\mathrm{corr}(i_1, i_2, \ldots, i_n)$ involving the particles $\{i_1, i_2, \ldots, i_n\} \subset \{1, 2, \ldots, N\}$. Note that all the $\delta\mathcal{L}$ blocks in the above Figure again must involve only $\{i_1, i_2, \ldots, i_n\}$.

Before we formulate and prove the rule, we need to introduce some formal definitions.

The set of all diagrams which contain the subdiagram of the form presented in Fig. 7.3 will be called Q. Each diagram $K \in Q$ can be divided in two parts. The first part is the above-mentioned block from Fig. 7.3, which we denote by T. The second part, containing all the elements of the diagram K which do not belong to T, will be called R ("the rest"). Note that the blocks T are characterized by

1. the starting time t' (the final time is always t)

2. the set of particles involved $\{i_1, i_2, \ldots, i_n\}$

3. the correlation function $corr(i_1, i_2, \ldots, i_n)$

4. the number of $\delta\mathcal{L}$ blocks

5. the exact scattering structure of $\delta\mathcal{L}$ blocks

Sometimes we would like to work with the set of diagrams whose T parts share some of the properties (1-5). Such a set would be denoted by $T(i, j, ..)$ where $i, j, \ldots$ stand for the respective properties that the elements of the set share. Therefore for example $K(R, T(t', \{i_1, \ldots, i_n\}))$ denotes the set of the diagrams with the given part R and the part T which involves particles $\{i_1, i_2, \ldots, i_n\}$ and starting time t'.

Let us consider now another set of diagrams which can be obtained from Q by the following transformation: one replaces the set $K(R, T(t', \{i_1, \ldots, i_n\}, corr(i_1, i_2, \ldots, i_n))$ by the single diagram $\{R, corr(i_1, i_2, \ldots, i_n; t')\}$, which has the same R part, its T part,

however, consists solely of the correlation function $corr(i_1, i_2, \ldots, i_n)$ shifted to the time t', like in the following Figure
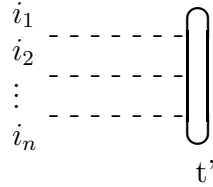
Fig. 7.4.

This new set will be called W. The following holds

Rule 1. *In the thermodynamic limit the analytic expressions corresponding to the sum of all diagrams in Q is the same as that corresponding to the sum of all the diagrams in W. Therefore in all the further considerations one may consider the diagrams W instead of Q.*

Proof. Let $K(R) \subset Q$ be the set of all diagrams in Q with the given R and different T. The task of summing the diagrams in $K(R)$ becomes simpler in the thermodynamic limit, as when the number of particles goes to infinity, the sum over all the different T's approaches

$$P_{eq}(1, \ldots, N)e^{\mathcal{L}(1,2,\ldots,N)(t-t')}, \tag{7.9}$$

which, using the invariance of P_{eq} with respect to time, can be rewritten as

$$e^{\mathcal{D}(1,2,\ldots,N)(t-t')}P_{eq}(1, 2, \ldots, N), \tag{7.10}$$

where the relation (3.23) has been used.
But now the operator $e^{\mathcal{D}(1,2,\ldots,N)(t-t')}$ stands at the far left of the diagram. However, using the integration by parts one proves that

$$\int d\boldsymbol{R}_1 \ldots d\boldsymbol{R}_N e^{\mathcal{D}(1,2,\ldots,N)(t-t')} F(1, 2, \ldots, N) = \int d\boldsymbol{R}_1 \ldots d\boldsymbol{R}_N F(1, 2, \ldots, N) \tag{7.11}$$

where $F(1, 2, \ldots, N)$ is any function of the particle positions. Therefore the evolution operator $e^{\mathcal{D}(1,2,\ldots,N)(t-t')}$ can be dropped from (7.10).

Let us now consider the sum of all diagrams in the set $W(R)$, which contains W diagrams with the same part R as the previously considered Q diagrams. From the definition of W we know that the T-parts of these diagrams contain only the correlation function $corr\{i_1, i_2, \ldots, i_n\}$. But again, in the thermodynamic limit the sum of such functions approaches $P_{eq}(1, 2, \ldots, N)$ and therefore is equal to the sum of T parts of K diagrams. Therefore the sum of $K(R)$ is equal to the sum of $W(R)$ (with the same R). The repeated application of this fact to different R structures gives the desired conclusion. $\square$

The next rule is the cut-off one, namely

Rule 2. *The right terminal $\boldsymbol{e}$-bonds in any diagram can be erased*

Proof. The proof here stems from the fact that the differential operator $\overrightarrow{\nabla}_i$ in the right terminal $\boldsymbol{e}$-bond of the form $S(i, t_1 - t_2) = e^{D_o \overrightarrow{\nabla}_i^2 (t_1 - t_2)}$ has nothing on its right to act on and so in this case $S(i, t_1 - t_2)$ is reduced to the identity operator and can be omitted without changing the value of the diagram. $\qquad\square$

Note that with the use of the two above Rules we have arrived at the diagrams deployed of all terminal $\boldsymbol{e}$-bonds. The following rule allows us in a similar way to get rid of improper blocks in the diagrams.

Rule 3. *The sum of all improper diagrams vanishes. Therefore in the further analysis one can replace the set of all (i.e. improper as well as proper) diagrams by the set of proper diagrams only.*

As we know, an improper diagram must contain one of the following: either a right (or left) terminal $\delta\mathcal{L}$ block or a right terminal A block or a left terminal B block. To proof the above theorem, we are going to tackle these cases one by one.

The case when a diagram contains a right terminal $\delta\mathcal{L}$ block is simple: every $\delta\mathcal{L}$ block ends with the $\overrightarrow{\boldsymbol{\mathsf{d}}}$ operator, in case of right terminal $\delta\mathcal{L}$ block the divergence has nothing to act on and so the value of such a diagram vanishes. Therefore we get

Lemma 1. *Every diagram with a right terminal $\delta\mathcal{L}$ block vanishes*

The case of left terminal $\delta\mathcal{L}$ block is a bit more complicated. Although it is not true that each diagram with a left terminal $\delta\mathcal{L}$ block vanishes separately, one can nevertheless prove that

Lemma 2. *Let $\boldsymbol{K}_{C;S}$ be a set of diagrams $\boldsymbol{K}$ with the correlation structure C and scattering structure S, such that $\boldsymbol{K}$ contains at least one left terminal $\delta\mathcal{L}$ block. Then*

$$\sum_C \boldsymbol{K}_{C;S} = 0,$$

Proof. Let us consider one of the left terminal $\delta\mathcal{L}$ blocks of the diagram $\boldsymbol{K}_{C;S}$ and denote it by $\boldsymbol{L_b}$. There are two possibilities:

a) $\boldsymbol{L_b}$ begins with $\overrightarrow{\overrightarrow{\boldsymbol{\mathsf{d}}}}$ operator i.e. $\beta^{-1} \overrightarrow{\nabla}_i \boldsymbol{\mu}_o(i)\boldsymbol{\mathcal{P}}(i)\boldsymbol{Z_o}(i)$

b) $\boldsymbol{L_b}$ begins with $\boldsymbol{F}_{ji}\boldsymbol{\mu}_o(i)\boldsymbol{\mathcal{P}}(i)\boldsymbol{Z_o}(i)$

Here i denotes the particle with which $\boldsymbol{L_b}$ begins whereas j is some particle from the diagram different from i. Therefore we can divide the diagrams $\boldsymbol{K_{C;S}}$ into two groups: $\boldsymbol{K_{Ca;S}}$ and $\boldsymbol{K_{Cb;S}}$ depending on whether $\boldsymbol{L_b}$ have the form (a) or (b). In the first group, using the integration by parts we can change $\overrightarrow{\boldsymbol{\Game}}$ operator at the beginning of $\boldsymbol{L_b}$ for $-1 \cdot \overleftarrow{\boldsymbol{\Game}}$ operator. But, as $\boldsymbol{L_b}$ is the left terminal block, after such operation, the differentiation in $-1 \cdot \overleftarrow{\boldsymbol{\Game}}$ acts only on the correlation function on the far left of the diagram. But the sum of all the correlation structures gives just the equilibrium distribution P_{eq}. However

$$\nabla_i P_{eq} = \beta \sum_j \boldsymbol{F}(ij) P_{eq}(\boldsymbol{X}), \tag{7.12}$$

from which one sees that the sum of all $\boldsymbol{K_{Ca;S}}$ diagrams is equal to the sum of all $\boldsymbol{K_{Cb;S}}$ diagrams taken with the opposite sign, which gives the desired conclusion. $\qquad\square$

To complete the proof of Theorem 3 we need to consider two more cases: the diagrams with a right terminal A-block and those with left terminal B-block. However, in the first case, it suffices to change $\overleftarrow{\boldsymbol{\Game}}$ operator at the end of A-block to $-1 \cdot \overrightarrow{\boldsymbol{\Game}}$ using integration by parts, and then, using Lemma 1, one sees that the given diagram vanishes. Eventually, in case of diagrams with left terminal B-block, the proof is analogous to the proof of Lemma 2.

A very attractive property of proper diagrams which greatly facilitates all the analysis is that

Theorem 1. *Proper diagrams are connected.*

Proof. Let us assume that a given proper diagram D of the form $< Ae^{\mathcal{L}t}B >$ is not connected, which means that it consists of at least two components. There are two possibilities

1. The blocks A and B are in the same component of the diagram D.

   Let us denote the above-mentioned component which contains both A and B by C_1. Then consider another component: C_2, the existence of which is assured by the fact that D is not connected. Note that C_2 can contain only $\delta\mathcal{L}$ blocks. The last block on the right of C_2 is therefore the right terminal $\delta\mathcal{L}$ block. Therefore the graph D is improper which contradicts the assumptions of the Theorem.

2. The blocks A and B are in the different components of the diagram D.

   In this case let us consider a component which contains A and call it C_1. Let us see which block stands at the right end of C_1. It can either A-block or one of the $\delta\mathcal{L}$ blocks but not B-block as it should be disconnected from A. In all cases the diagram D is improper: in the first case because of the right terminal A block, in the second one - because of the right terminal $\delta\mathcal{L}$ block. Therefore there is again a contradiction with respect to the assumption of the Theorem.

$\qquad\square$

7.4   The nodal structure of the evolution diagrams

As the evolution diagrams consist of many different building blocks (A, B and $\delta\mathcal{L}$) no wonder that their nodal structure is much more complicated than that of the instantaneous response diagrams analyzed in Chapter 6. For example the diagram
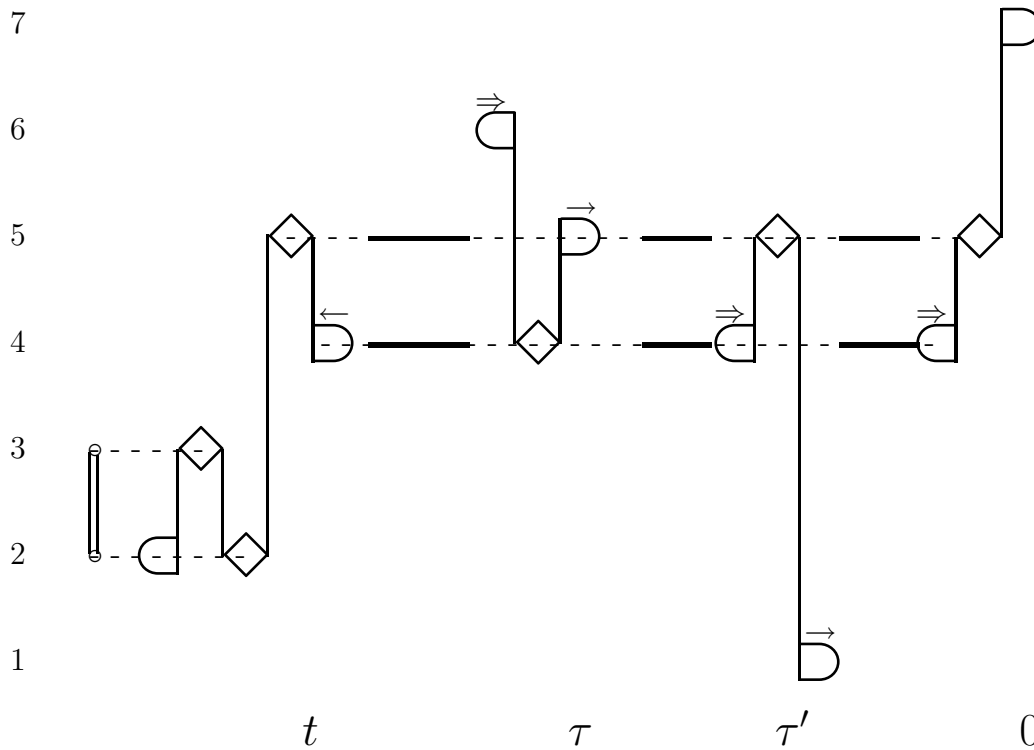
Fig. 7.5.

has the nodal structure graph (NSG) of the form
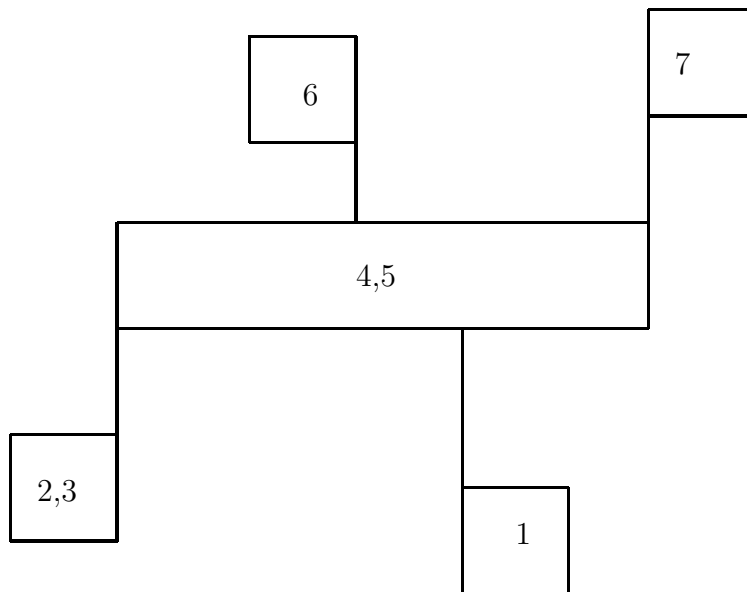
Fig. 7.6.

We see that the nodal graph can have quite a complicated tree-like structure and it may be not easy to apply in this case the methods developed in Chapter 6. In particular, the block distribution function cannot be defined on the nodal structure like that in Fig. 7.6, as it lacks the linear ordering crucial for the block distribution function and "uncorrelating operator" P_{unc} concepts (remember that P_{unc} has the property of statistically uncorrelating the particle blocks at its left from those at its right, but which block is on the left side of which in Fig. 7.6 ?). The rest of this section would be devoted to the proof that if we consider only NSG's of nonvanishing proper diagrams then the situation looks far more brightly: in fact such NSG's are linearly ordered and all the concepts of Chapter 6 can be applied in this case. Restricting ourselves to the set of proper diagrams only would not affects the analytic expressions for the kernels X, given by the sum of all diagrams, as due to the Rule 3 the overall effect of the improper diagrams vanishes.

To begin with, let us introduce some notions from the graph theory (see for example [103]). To stress the difference between nodal structure graphs and diagrams we are going to call the vertices in NSG **nodes** and the bonds in NSG - **edges**. The new notions are

path - a sequence of nodes and edges in a diagram of the form $n_1 E(n_1, n_2) n_2 ... E(n_{k-1}, n_k) n_k$, where n_i are the nodes and $E(n_i, n_{i+1})$ stands for the edge linking nodes n_i and n_{i+1}.

cycle - a path $n_1 E(n_1, n_2) n_2 ... E(n_{k-1}, n_k) n_k$ with $k \geq 3$ in which all the edges are different and the first node is the same as the last one: $n_k = n_1$

tree - an acyclic (i.e. not containing any cycles) connected graph

terminal node - a node which has less than two edges coming out of it

chain - a tree which has not more than two terminal nodes

For example the NSG in Fig. 7.6 is a tree with 4 terminal nodes, therefore it is not a chain.

First of all we notice that

Lemma 3. *The nodal structure graph of a connected diagram is a tree.*

Proof. Suppose that in NSG of a given diagram D there is a cycle: i_1 $E(i_1, i_2)$ i_2 ... $E(i_{k-1}, i_k)$ i_k $E(i_k i_1)$ i_1, $k \geq 2$ (here i_m denotes the nodes of a graph whereas $E(i_n, i_{n+1})$ stands for the nodal line linking the node i_n with the node i_{n+1}). If we remove $E(i_1, i_2)$ we notice that the graph remains connected as there still remains a path between i_1 and i_2 going through $i_k i_{k-1}...i_3$, which contradicts the fact that $E(i_1, i_2)$ is a nodal line. Therefore there cannot be any cycles in the NSG, so it is a tree. $\square$

The simple statement that every diagram of $X = < Ae^{\mathcal{L}t} B >$ begins with the A block and ends with B leads to the following property of NSG graph:

Lemma 4. *In every NSG graph there should be one terminal node N_{first} containing the first operator in the A block and one terminal node N_{last} containing the last operator in B block. It may happen that $N_{first} = N_{last}$.*

Now we are ready to formulate and prove the theorem

Theorem 2. *The nodal structure graph of a proper diagram is a chain.*

Proof. If the NSG for the given proper diagram D, which from Lemma 3 is a tree, would not be a chain, then it should have more than two terminal nodes. Therefore there is at least one terminal node N_o different from N_{first} and N_{last} defined in Lemma 4. But such a N_o node must begin (or end) with a left (right) $\delta\mathcal{L}$ block, which contradicts the assumption that D is proper. $\square$

The chain structure induces the **complete ordering** in a NSG graph: we say that the node N_i precedes the node N_j ($N_i < N_j$) in a given NSG if in the path joining N_{first} with N_{last} the block N_i comes before N_j. Note that we need here Theorem 2, because if NSG would not be a chain it might happen that N_i or/and N_j would not lie on the path joining N_{first} with N_{last}.

The final theorem in this section states that the above ordering is compatible with time order in the following sense:

Theorem 3. *If Q is the NSG graph of a nonvanishing proper diagram and N_i, $i = 1, 2 \ldots M$ - its nodes numbered in such a way that $N_i < N_j$ for $i < j$, then time coordinates of the vertices of the node N_i are larger or equal to time coordinates of the vertices of N_{i+1}*

Proof. The theorem has a clear geometrical interpretation, namely that

> The node N_i lies entirely to the left of the nodal line N_{ii+1} whereas the node N_{i+1} lies entirely to the right of it.

This means that there should be no vertices in the dashed areas on the below scheme denoted by M_i and M_{i+1}.
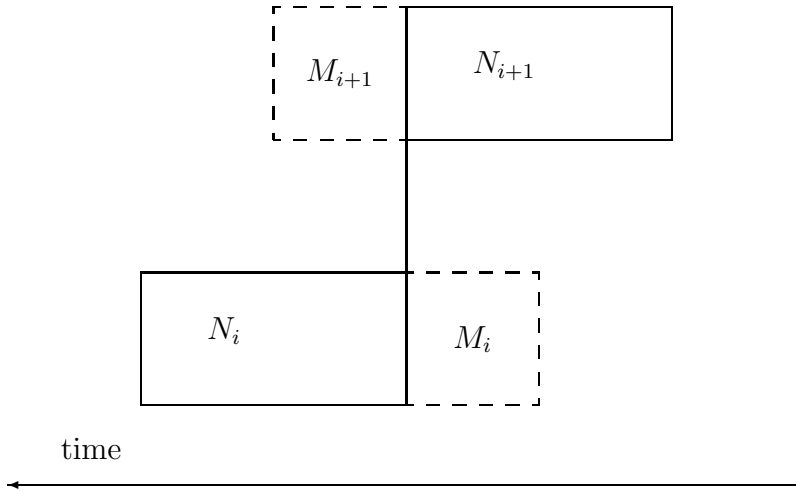
But if there would be vertices in M_i (M_{i+1}) then the node N_i (N_{i+1}) would end (begin) with an improper block, which contradicts the assumption that the diagram is proper. $\square$

The fact that the nodal graphs are ordered and that this ordering agrees with the ordering imposed by time coordinate allows us to apply the reduction formalism introduced in the previous Chapter to the case of retarded response kernels.

7.5 The reduction of the evolution diagrams

Now that we have the linear ordering of NSG graphs, we perform the reduction of the evolution diagrams analogous to that presented in section 6.7 for the case of instantaneous diagrams.

Let us start with the diagrams making up the kernel $\boldsymbol{X}_{jE}$ (5.47). We divide them into four groups

1. Diagrams with the articulation line in A-block

2. Diagrams with the articulation line in δL -block

3. Diagrams with the articulation line in B-block

4. Irreducible diagrams.

Let us tackle them one by one

1. Theorem 3 implies that all the nonvanishing diagrams with the articulation line inside A-block must be of the form

where the ovals stand for correlation functions and we have denoted in each block the respective divergence operators.

The diagram A_1 has the scattering structure $\boldsymbol{\mu}_o \boldsymbol{\mathcal{P}} \boldsymbol{Z}_o (\boldsymbol{G}\hat{\boldsymbol{Z}}_o)^{n-1}$, which we have encountered before while analyzing I_{jE} and I_{jv} in Chapter 6 (see (6.26) and (6.29)). Therefore in the limit of the macroscopic system the sum of all A_1's equals $\boldsymbol{Y}_{jv}^{irr}$, just as in case of I_{jE} and I_{jv}.

Next we notice that the upper part of the diagram has the same structure as diagrams of the kernel $\boldsymbol{X}_{fE}$. Therefore, the analogous reasoning to that presented in section 6.7 leads us to the conclusion that in the limit of the macroscopic system the sum of all the diagrams with the articulation line in the A-block is equal to

$$\boldsymbol{Y}_{jv}^{irr} \boldsymbol{G} \boldsymbol{X}_{fE}(t), \tag{7.13}$$

where we have again used the compact notation in which the dependence of the quantities on the space variables as well as integration over these variables is suppressed.

2. All the nonvanishing diagrams with the articulation line inside $\delta\boldsymbol{\mathcal{L}}$-block are of the form

Here we recognize in the lower part of the diagram the structure of the diagrams of $\boldsymbol{X}_{jv}^{irr}$, while the upper part, after changing the direction of divergence in $\delta\boldsymbol{\mathcal{L}}_2$ (by integration by parts) recovers the structure of the diagrams of $\boldsymbol{X}_{fE}$. Therefore in the limit of the macroscopic system the sum of all the diagrams with the articulation line in the $\delta\boldsymbol{\mathcal{L}}$-block is equal to

$$\int_0^t \mathrm{d}\tau\, \boldsymbol{X}_{jv}^{irr}(t-\tau)\boldsymbol{G}\boldsymbol{X}_{fE}(\tau). \tag{7.14}$$

3. Finally all the nonvanishing diagrams with articulation line inside B-block must are of the form
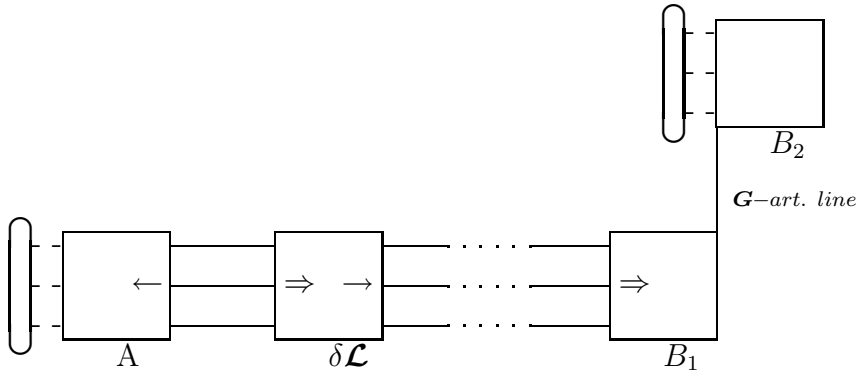
Here in the limit of the macroscopic system the sum is equal to

$$\boldsymbol{X}_{jv}^{irr}(t)\boldsymbol{G}\boldsymbol{Y}_{fE}. \tag{7.15}$$

4. The irreducible diagrams do not need any reduction, their sum is just

$$\boldsymbol{X}_{jE}^{irr}(t). \tag{7.16}$$

Eventually, summing up (7.13-7.16) we get for the kernel $\boldsymbol{X}_{jE}$ in the limit of the macroscopic system the following expression

$$
\begin{aligned}
\boldsymbol{X}_{jE}(t) = {}& \boldsymbol{X}_{jE}^{irr}(t) + \boldsymbol{Y}_{jv}^{irr}\boldsymbol{G}\boldsymbol{X}_{fE}(t) + \int_0^t \mathrm{d}\tau\,\boldsymbol{X}_{jv}^{irr}(t-\tau)\boldsymbol{G}\boldsymbol{X}_{fE}(\tau)+ \\
& + \boldsymbol{X}_{jv}^{irr}(t)\boldsymbol{G}\boldsymbol{Y}_{fE}.
\end{aligned}
\tag{7.17}
$$

In an analogous way we prove that

$$
\boldsymbol{X}_{jv}(t) = \boldsymbol{X}_{jv}^{irr}(t) + \boldsymbol{Y}_{jv}^{irr}\boldsymbol{G}\boldsymbol{X}_{fv}(t) + \int_0^t \mathrm{d}\tau\,\boldsymbol{X}_{jv}^{irr}(t-\tau)\boldsymbol{G}\boldsymbol{X}_{fv}(\tau) + \boldsymbol{X}_{jv}^{irr}(t)\boldsymbol{G}\boldsymbol{Y}_{fv}.
\tag{7.18}
$$

Inserting these equations into (5.45) we get for the retarded current

$$
\begin{aligned}
\boldsymbol{J}_{ret}(t) = {}& \int_{-\infty}^t \mathrm{d}t'(\boldsymbol{X}_{jE}^{irr}(t-t')\boldsymbol{E}(t') + \boldsymbol{X}_{jv}^{irr}(t-t')\boldsymbol{v}_o(t'))+ \\
& + \boldsymbol{Y}_{jv}^{irr}\boldsymbol{G}\int_{-\infty}^t \mathrm{d}t'\Big(\boldsymbol{X}_{fE}(t-t')\boldsymbol{E}(t') + \boldsymbol{X}_{fv}(t-t')\boldsymbol{v}_o(t')\Big)+ \\
& + \int_{-\infty}^t \mathrm{d}t'\int_0^{t-t'}\mathrm{d}\tau\,\boldsymbol{X}_{jv}^{irr}(t-t'-\tau)\boldsymbol{G}\Big(\boldsymbol{X}_{fE}(\tau)\boldsymbol{E}(t') + \boldsymbol{X}_{fv}(\tau)\boldsymbol{v}_o(t')\Big)+ \\
& + \int_{-\infty}^t \mathrm{d}t'\boldsymbol{X}_{jv}^{irr}(t-t')\boldsymbol{G}\Big(\boldsymbol{Y}_{fE}\boldsymbol{E}(t') + \boldsymbol{Y}_{fv}\boldsymbol{v}_o(t')\Big).
\end{aligned}
\tag{7.19}
$$

Changing the variables of integration in the third term to $(t', t'' = t' + \tau)$, reversing the order of the integrations and using the fact that (5.45)

$$
\int_{-\infty}^{t''} \mathrm{d}t'\Big(\boldsymbol{X}_{fE}(t''-t')\boldsymbol{E}(t') + \boldsymbol{X}_{fv}(t''-t')\boldsymbol{v}_o(t')\Big) = \boldsymbol{f}_{ret}(t''),
\tag{7.20}
$$

we can write the above-mentioned term as

$$
\int_{-\infty}^t \mathrm{d}t''\,\boldsymbol{X}_{jv}^{irr}(t-t'')\boldsymbol{G}\boldsymbol{f}_{ret}(t'').
\tag{7.21}
$$

We can further simplify (7.19) by noticing that due to Eqs. (6.32) and (5.45)

$$
\boldsymbol{G}(\boldsymbol{Y}_{fE}\boldsymbol{E} + \boldsymbol{Y}_{fv}\boldsymbol{v}_o) = \boldsymbol{v}_{ins} - \boldsymbol{v}_o,
\tag{7.22}
$$

so that (7.19) takes form

$$\boldsymbol{J}_{ret}(t) = \int_{-\infty}^{t} \mathrm{d}t' (\boldsymbol{X}_{jE}^{irr}(t-t')\boldsymbol{E}(t') + \boldsymbol{X}_{jv}^{irr}(t-t')\boldsymbol{v}_{ins}(t')) +$$

$$+ \boldsymbol{Y}_{jv}^{irr}\boldsymbol{v}_{ret}(t) + \int_{-\infty}^{t} \mathrm{d}t' \boldsymbol{X}_{jv}^{irr}(t-t')\boldsymbol{v}_{ret}(t') = \qquad (7.23)$$

$$= \int_{-\infty}^{t} \mathrm{d}t' \left(\boldsymbol{X}_{jE}^{irr}(t-t')\boldsymbol{E}(t') + \boldsymbol{X}_{jv}^{irr}(t-t')\boldsymbol{v}_{s}(t') \right) + \boldsymbol{Y}_{jv}^{irr}\boldsymbol{v}_{ret},$$

where we have introduced the "retarded" velocity given by

$$\boldsymbol{v}_{ret} = \boldsymbol{G}\boldsymbol{f}_{ret} \qquad (7.24)$$

and used the fact that the total suspension velocity is given by

$$\boldsymbol{v}_s(t) = <\boldsymbol{v}>_t = \boldsymbol{v}_{ins}(t) + \boldsymbol{v}_{ret}(t). \qquad (7.25)$$

If we add to the $\boldsymbol{J}_{ret}$ obtained above the expression (6.33) for the instantaneous particle current we can write the total particle current as

$$\boldsymbol{J}(t) = \boldsymbol{J}_{ins}(t) + \boldsymbol{J}_{ret}(t) = \boldsymbol{Y}_{jE}^{irr}\boldsymbol{E}(t) + \boldsymbol{Y}_{jv}^{irr}\boldsymbol{v}_s(t) +$$

$$+ \int_{-\infty}^{t} \mathrm{d}t' \left(\boldsymbol{X}_{jE}^{irr}(t-t')\boldsymbol{E}(t') + \boldsymbol{X}_{jv}^{irr}(t-t')\boldsymbol{v}_s(t') \right). \qquad (7.26)$$

7.6   Force density

The same decomposition procedure can be performed on the kernels $\boldsymbol{X}_{fE}$ and $\boldsymbol{X}_{fv}$ (5.47). Proceeding just as in the last section we obtain for them

$$\boldsymbol{X}_{fE}(t) = \boldsymbol{X}_{fE}^{irr}(t) + \boldsymbol{Y}_{fv}^{irr}\boldsymbol{G}\boldsymbol{X}_{fE}(t) + \int_{0}^{t} \mathrm{d}\tau \boldsymbol{X}_{fv}^{irr}(t-\tau)\boldsymbol{G}\boldsymbol{X}_{fE}(\tau) + \boldsymbol{X}_{fv}^{irr}(t)\boldsymbol{G}\boldsymbol{Y}_{fE}.$$

$$\boldsymbol{X}_{fv}(t) = \boldsymbol{X}_{fv}^{irr}(t) + \boldsymbol{Y}_{fv}^{irr}\boldsymbol{G}\boldsymbol{X}_{fv}(t) + \int_{0}^{t} \mathrm{d}\tau \boldsymbol{X}_{fv}^{irr}(t-\tau)\boldsymbol{G}\boldsymbol{X}_{fv}(\tau) + \boldsymbol{X}_{fv}^{irr}(t)\boldsymbol{G}\boldsymbol{Y}_{fv}.$$

$$(7.27)$$

and for the retarded force density

$$\boldsymbol{f}_{ret}(t) = \int_{-\infty}^{t} \mathrm{d}t' \boldsymbol{X}_{jv}^{irr}(t-t')\boldsymbol{v}_{ret}(t') =$$

$$= \int_{-\infty}^{t} \mathrm{d}t' (\boldsymbol{X}_{fE}^{irr}(t-t')\boldsymbol{E}(t') + \boldsymbol{X}_{fv}^{irr}(t-t')\boldsymbol{v}_s(t')) + \boldsymbol{Y}_{fv}^{irr}\boldsymbol{v}_{ret}. \qquad (7.28)$$

Adding this to the expression (6.38) for $\boldsymbol{f}_{ins}$ we get for the total force density

$$
\begin{aligned}
< \boldsymbol{f} >_t = \; & \boldsymbol{f}_{ins}(t) + \boldsymbol{f}_{ret}(t) = \boldsymbol{Y}_{fE}^{irr}\boldsymbol{E}(t) + \boldsymbol{Y}_{fv}^{irr}\boldsymbol{v}_s(t) + \\
& + \int_{-\infty}^{t} \mathrm{d}t' \Big(\boldsymbol{X}_{fE}^{irr}(t-t')\boldsymbol{E}(t') + \boldsymbol{X}_{fv}^{irr}(t-t')\boldsymbol{v}_s(t') \Big).
\end{aligned}
\tag{7.29}
$$

The above result can be inserted into the Stokes equation to yield, after the Fourier transform

$$
\begin{aligned}
k^2 \boldsymbol{v}_s(\boldsymbol{k},t) = \; & \frac{1}{\eta}(\boldsymbol{1} - \hat{\boldsymbol{k}}\hat{\boldsymbol{k}})\Big(\boldsymbol{f}_o(\boldsymbol{k},t) + \boldsymbol{Y}_{fE}^{irr}\boldsymbol{E}(\boldsymbol{k},t) + \boldsymbol{Y}_{fv}^{irr}\boldsymbol{v}_s(\boldsymbol{k},t) + \\
& + \int_{-\infty}^{t} \mathrm{d}t' \Big(\boldsymbol{X}_{fE}^{irr}(\boldsymbol{k},t-t')\boldsymbol{E}(t') + \boldsymbol{X}_{fv}^{irr}(\boldsymbol{k},t-t')\boldsymbol{v}_s(\boldsymbol{k},t') \Big) \Big),
\end{aligned}
\tag{7.30}
$$

where again the homogeneity of the system has been assumed.

7.7   The long-time diffusion coefficient

Now we are ready to write down the expression for the total (i.e. instantaneous + retarded) diffusion current

$$
\begin{aligned}
\boldsymbol{J}_d(t) = \; & \boldsymbol{J}(t) - n\boldsymbol{v}_s(t) = \boldsymbol{Y}_{jE}^{irr}\boldsymbol{E}(t) + (\boldsymbol{Y}_{jv}^{irr} - n)\boldsymbol{v}_s(t) + \\
& + \int_{-\infty}^{t} \mathrm{d}t' \Big(\boldsymbol{X}_{jE}^{irr}(t-t')\boldsymbol{E}(t') + \boldsymbol{X}_{jv}^{irr}(t-t')\boldsymbol{v}_s(t') \Big).
\end{aligned}
$$

The long time collective diffusion coefficient can be obtained by considering the small k limit of the Fourier transform of the above relation. The Fourier transform reads (for a homogeneous system)

$$
\begin{aligned}
\boldsymbol{J}_d(\boldsymbol{k},t) = \; & \Big(\boldsymbol{Y}_{jE}^{irr}(\boldsymbol{k})\boldsymbol{E}(\boldsymbol{k},t) + (\boldsymbol{Y}_{jv}^{irr}(\boldsymbol{k}) - n)\boldsymbol{v}_s(\boldsymbol{k},t) \Big) + \\
& + \int_{-\infty}^{t} \mathrm{d}t' \Big(\boldsymbol{X}_{jE}^{irr}(\boldsymbol{k},t-t')\boldsymbol{E}(\boldsymbol{k},t') + \boldsymbol{X}_{jv}^{irr}(\boldsymbol{k},t-t')\boldsymbol{v}_s(\boldsymbol{k},t') \Big).
\end{aligned}
\tag{7.31}
$$

By the similar reasoning as that applied in Chapter 6 to the analysis of the small-$\boldsymbol{k}$ limit of Y kernels one can prove that in the limit $\boldsymbol{k} \to 0$ the kernel $\boldsymbol{X}_{jv}(\boldsymbol{k},t)$ vanishes. Therefore in this limit Eq. (7.31) takes form

$$
\boldsymbol{J}_d(t) = y_{jE}\boldsymbol{E}(t) + \int_{-\infty}^{t} \mathrm{d}t' \boldsymbol{X}_{jE}^{irr}(\boldsymbol{k}=0,t-t')\boldsymbol{E}(t'),
\tag{7.32}
$$

where we have used (6.43).

If one is interested in the dynamics in the timescale t long compared to the relaxation time of the kernel $\boldsymbol{X}_{jE}$ then one can write

$$\boldsymbol{J}_d(t) = y_{jE}\boldsymbol{E}(t) + \int_0^\infty \mathrm{d}t' \boldsymbol{X}_{jE}^{irr}(\boldsymbol{k}=0,t')\boldsymbol{E}(t) \tag{7.33}$$

Therefore the long-time collective diffusion coefficient can be identified with

$$D_c^l = \frac{k_B T}{3nS(0)}\mathrm{Tr}\Big[y_{jE}\boldsymbol{1} + \int_0^\infty \boldsymbol{X}_{jE}^{irr}(\boldsymbol{k}=0,t')\mathrm{d}t'\Big] = D_c^s(1-\Delta),$$

where D_c^s is given by (6.46) and Δ is the measure of the memory contribution to the long-time diffusion coefficient given by

$$\begin{aligned}
\Delta &= -\frac{1}{3y_{jE}}\int_0^\infty \mathrm{Tr}\boldsymbol{X}_{jE}^{irr}(\boldsymbol{k}=0,t')\mathrm{d}t' = \\
&\frac{k_B T}{\mu_o H(0)}\int_0^\infty \mathrm{d}t'\frac{1}{3N} < \Big(\sum_{i,j,k}[\nabla_i + \beta\boldsymbol{F}_{ji}]\cdot\boldsymbol{\mu}_{ik}\Big)\cdot\Big(\sum_{l,m,p}[\nabla_l + \beta\boldsymbol{F}_{ml}]\cdot\boldsymbol{\mu}_{lp}(t')\Big) >^{irr},
\end{aligned} \tag{7.34}$$

where we have used the fact that the trace of a tensor product of two vectors is equal to their scalar product.

By comparison of (7.34) with the earlier expression for Δ (1.30) one sees that we can continue analytically the memory function $M(k,t)$ to $k=0$ by putting

$$M(k=0,t) = \frac{k_B T}{3N\mu_o H(0)} < \Big(\sum_{i,j,k}[\nabla_i+\beta\boldsymbol{F}_{ji}]\cdot\boldsymbol{\mu}_{ik}\Big)\cdot\Big(\sum_{l,m,p}[\nabla_l+\beta\boldsymbol{F}_{ml}]\boldsymbol{\mu}_{lp}(t')\Big) >^{irr}. \tag{7.35}$$

Now we turn to the case of finite but small $\boldsymbol{k}$ to derive the equations for the diffusion current and suspension velocity analogous to (6.68) but this time with inclusion of the retarded response terms.

7.8 The small $\boldsymbol{k}$ limit of the equations for the velocity and diffusion current

The structure of the equations for the suspension velocity and diffusion current can be seen most clearly after the Fourier transform in time

$$\begin{aligned}
\boldsymbol{J}_d(\boldsymbol{k},\omega) &= \boldsymbol{Y}_{jE}^{irr}(\boldsymbol{k})\boldsymbol{E}(\boldsymbol{k},\omega) + (\boldsymbol{Y}_{jv}^{irr}(\boldsymbol{k})-n)\boldsymbol{v}_s(\boldsymbol{k},\omega) + \boldsymbol{X}_{jE}^{irr}(\boldsymbol{k},\omega)\boldsymbol{E}(\boldsymbol{k},\omega) + \\
&+ \boldsymbol{X}_{jv}^{irr}(\boldsymbol{k},\omega)\boldsymbol{v}_s(\boldsymbol{k},\omega), \\
-k^2\boldsymbol{v}_s(\boldsymbol{k},\omega) &= \frac{1}{\eta}(\boldsymbol{1}-\hat{\boldsymbol{k}}\hat{\boldsymbol{k}})\Big(\boldsymbol{f}_o(\boldsymbol{k},\omega) + \boldsymbol{Y}_{fE}^{irr}(\boldsymbol{k})\boldsymbol{E}(\boldsymbol{k},\omega) + \boldsymbol{Y}_{fv}^{irr}(\boldsymbol{k})\boldsymbol{v}_s(\boldsymbol{k},\omega) \\
&+ \boldsymbol{X}_{fE}^{irr}(\boldsymbol{k},\omega)\boldsymbol{E}(\boldsymbol{k},\omega) + \boldsymbol{X}_{fv}^{irr}(\omega)\boldsymbol{v}_s(\boldsymbol{k},\omega)\Big), \tag{7.36}
\end{aligned}$$

where the vector quantities such as $\boldsymbol{v}_s$, $\boldsymbol{E}$, $\boldsymbol{f}$ or $\boldsymbol{J}$ are transformed as

$$\boldsymbol{C}(\boldsymbol{k}, t) = \int_{-\infty}^{\infty} \boldsymbol{C}(\boldsymbol{k}, t) e^{-i\omega t} \mathrm{d}\omega \quad \boldsymbol{C}(\boldsymbol{k}, w) = \frac{1}{2\pi} \int_{-\infty}^{\infty} \boldsymbol{C}(\boldsymbol{k}, \omega) e^{i\omega t} \mathrm{d}\omega, \tag{7.37}$$

while the Fourier transform of the kernels $X = <Ae^{Lt}B>$ reads

$$X(\omega) = \int_{0}^{\infty} <Ae^{Lt}B> e^{i\omega t} \mathrm{d}t. \tag{7.38}$$

Using the expansion in $\boldsymbol{k}$ of the kernels $Y(\boldsymbol{k})$ derived in section 6.10 together with the analogous expansions for the kernels $X(\boldsymbol{k})$

$$\boldsymbol{X}_{jE}^{irr}(\boldsymbol{k}, \omega) = x_{jE}(\omega)\boldsymbol{1} + \dots, \tag{7.39}$$
$$\boldsymbol{X}_{jv}^{irr}(\boldsymbol{k}, \omega) = k^2 \boldsymbol{x}_{jv}(\omega) + \dots, \tag{7.40}$$
$$\boldsymbol{X}_{fv}^{irr}(\boldsymbol{k}, \omega) = -k^2 \boldsymbol{x}_{fv}(\omega) + \dots, \tag{7.41}$$
$$\boldsymbol{X}_{fE}^{irr}(\boldsymbol{k}, \omega) = k^2 \boldsymbol{x}_{fE}(\omega) + \dots, \tag{7.42}$$

we can write the equations for the diffusion current and force density for small but finite $\boldsymbol{k}$ as

$$\boldsymbol{J}_d(\boldsymbol{k}, \omega) = \left(y_{jE} + x_{jE}(\omega)\right)\boldsymbol{E}(\boldsymbol{k}, \omega) + k^2(\boldsymbol{1} - \hat{\boldsymbol{k}}\hat{\boldsymbol{k}})\left(y_{jv}^t + x_{jv}^t(\omega)\right)\boldsymbol{v}_s(\boldsymbol{k}, \omega), \tag{7.43}$$

$$k^2(\eta + y_{fv}^t + x_{fv}^t(\omega))\boldsymbol{v}_s(\boldsymbol{k}, \omega) = (\boldsymbol{1} - \hat{\boldsymbol{k}}\hat{\boldsymbol{k}})\left(\boldsymbol{f}_o(\boldsymbol{k}, \omega) + n\boldsymbol{E}(\boldsymbol{k}, \omega) + k^2(y_{fE}^t + x_{fE}^t(\omega))\boldsymbol{E}(\boldsymbol{k}, \omega)\right), \tag{7.44}$$

where x_{ab}^t denotes as before the transversal part of the operator $\boldsymbol{x}_{ab}$ whereas x_{ab}^l stands for its longitudinal part.
Once again we can change to the real space and transform equations to the form analogous to (6.68), getting

$$\boldsymbol{J}_d(\omega) = \left(y_{jE} + x_{jE}(\omega)\right)\boldsymbol{E}(\omega) - \frac{y_{jv}^t + x_{jv}^t(\omega)}{\eta + y_{fv}^t + x_{fv}^t(\omega)}\left(\boldsymbol{F}_{tot}(\omega) - \mathbf{grad}\, p(\omega)\right),$$

$$-\left(\eta + y_{fv}^t + x_{fv}^t(\omega)\right)\nabla^2 \boldsymbol{v}_s(\boldsymbol{k}, \omega) = \boldsymbol{F}_{tot}(\omega) - \mathbf{grad}\, p(\omega)$$

$$-\left(y_{fE}^t + x_{fE}^t(\omega)\right)\left(\nabla^2 \boldsymbol{E}(\omega) - \mathbf{grad}\, \mathrm{div}\boldsymbol{E}(\omega)\right), \tag{7.45}$$

where as before (cf. Eq. 6.62)

$$\boldsymbol{F}_{tot}(\omega) = \boldsymbol{f}_o(\omega) + n\boldsymbol{E}(\omega). \tag{7.46}$$

Note that the instantaneous response equations (6.68) can be obtained from (7.45) by taking the limit $\omega \to \infty$.

As it can be seen, the inclusion of the retarded response terms in the equations adds new elements in comparison with the instantaneous response described by (6.68): the effective viscosity and the diffusion coefficient attain the frequency-dependent terms x^t_{fv} and x_{jE} respectively. Also the cross terms linking $\boldsymbol{J}_d$ with the Laplacian of $\boldsymbol{v}_s$ and the Laplacian of $\boldsymbol{v}_s$ with $\boldsymbol{E}$ gain the new, frequency-dependent contributions x^t_{jv} and x^t_{fE}, which are equal each to the other due to the Onsager symmetry. The overall picture remains essentially the same: we get the equation for the velocity supplemented by the boundary conditions which must be solved first. Then, once we have $\boldsymbol{v}_s$, we calculate the particle current with respect to it with use of the equation (7.43). Note that all the coefficients in the above equations are obtained from the short-range response kernels and therefore they are well-defined, local characteristics of the system.

7.9 The collective diffusion memory function - virial expansion

In this section the memory contribution to the long-time diffusion coefficient is studied by means of the virial expansion in the density of the spheres. It is found that the first two terms in this expansion, corresponding to contributions of one- and two-particle clusters, vanish. The explicit expression for the first nonvanishing term, which gives the contribution of three-particle clusters, is found.

To start with, let us calculate the memory factor Δ in the absence of hydrodynamic interactions, i.e. when the mobility matrix is of the form

$$\boldsymbol{\mu}_{ij} = \boldsymbol{\mu}_o \delta_{ij}. \tag{7.47}$$

In this limit Δ reads simply

$$\frac{1}{3N\mu_o} \int_0^\infty \mathrm{d}t' < \sum_{i,j=1} \boldsymbol{F}_{ij} \cdot \sum_{k,l=1} \boldsymbol{F}_{kl} >, \tag{7.48}$$

where the irreducibility requirement is relaxed, as when there are no hydrodynamic interactions the diagrams are deployed of all the $\boldsymbol{G}$ connectors not only the solitary ones.

But the sums in vertices of (7.48) vanish, as the sum of all interparticle forces is equal to zero. Therefore in systems without hydrodynamic interactions the short- and long- time collective diffusion coefficients are equal.

In order to find Δ for a diluted suspension with the volume fraction $\phi = \frac{4}{3}\pi a^3 n \ll 1$ one may use the virial expansion. However, as it can be seen from the expression (7.34) the factor Δ can be written as

$$\Delta = \frac{\tilde{\Delta}}{H(0)} \tag{7.49}$$

where we have singled out the contributions of a different nature: instantaneous response described by the hydrodynamic factor $H(0)$ and the retarded one given by

$$\tilde{\Delta} = \frac{k_B T}{3N\mu_o} \int_0^\infty \mathrm{d}t' < T(t') >^{irr} \tag{7.50}$$

with $T(t)$ given by

$$T(t) = \left[\sum_{i,j,k} (\nabla_i + \beta \boldsymbol{F}_{ji}) \cdot \boldsymbol{\mu}_{ik} \right] \cdot \left[\sum_{l,m,p} (\nabla_l + \beta \boldsymbol{F}_{ml}) \cdot \boldsymbol{\mu}_{lp}(t) \right], \tag{7.51}$$

These two terms behave differently as functions of the volume fraction and therefore it is more convenient to look for the virial expansion of $H(0)$ and $\tilde{\Delta}$ separately. In fact, the virial expansion for $H(0)$ is well-established theoretically [48]. It reads

$$H(0) = 1 + \lambda\phi + \mathcal{O}(\phi^2), \tag{7.52}$$

where the value of the parameter λ for hard-sphere suspensions reads [48, 104, 105]

$$\lambda \approx -6.546. \tag{7.53}$$

We can therefore concentrate on finding the virial expansion of $\tilde{\Delta}$ in the form

$$\tilde{\Delta} = d_1 + d_2\phi + d_3\phi^2 + \dots \tag{7.54}$$

To obtain it one starts with the cluster expansion of the operator $< T(t) >^{irr}$

$$< T(1, 2, \dots, N; t) >^{irr} = \sum_i < T(i; t) >^{irr} + \sum_{i,j} < T(i, j; t) >^{irr} + \dots =$$

$$N < T(1; t) >^{irr} + \frac{N(N-1)}{2!} < T(1, 2; t) >^{irr} + \dots \tag{7.55}$$

By inspecting Eq. (7.50) one concludes that the s-th virial coefficient is given by

$$d_s = \frac{N! k_B T}{3(N-s)! s! N \mu_o \phi^{s-1}} \int_0^\infty \mathrm{d}t < T(1, 2, \dots, s; t) >^{irr} \tag{7.56}$$

Let us analyze now the first few terms. The first term, which is determined by the one-particle contributions to $T(t)$, vanishes as in this case $\boldsymbol{\mu}$ again has the form (7.47). The second term, multiplying ϕ vanishes from the symmetry of the two-body hydrodynamic interactions as shown in Appendix D.

The first nonvanishing term in the cluster expansion of $< T(t) >$ is therefore the three-particle one. Let us analyze it in more detail. First of all

Theorem 4. *All the nonzero three particle diagrams making up $< T(1, 2, 3; t) >$ are irreducible and therefore $< T(1, 2, 3; t) >^{irr} = < T(1, 2, 3; t) >$*

Proof. The kernel $< T(t) >$ can be written as $< A(1,2,3)e^{Lt}B(1,2,3) >$. However the sum of all the diagrams, in which either A or B does not depend on the positions of all three particles but only one or two of them, vanishes (the proof is essentially the same as the proof that d_2 vanishes, given in the Appendix D). What remains are the diagrams in which the particles (1,2,3) are connected with each other by at least one bond in A and one in B. All such diagrams are irreducible. $\qquad\square$

Therefore we can relax the irreducibility condition while calculating the virial coefficient d_3. The explicit expression for it reads

$$d_3 = \frac{k_B T}{32\pi^2 \mu_o a^6} \int_0^\infty dt' d\boldsymbol{R}_{12} \, d\boldsymbol{R}_{13} \Big[\sum_{i,j,k=1}^3 (\nabla_i + \beta \boldsymbol{F}_{ji}) \cdot \boldsymbol{\mu}_{ik} \Big] \cdot \Big[\sum_{l,m,p=1}^3 (\nabla_l + \beta \boldsymbol{F}_{pl}) \cdot \boldsymbol{\mu}_{lp}(t') \Big] g(1,2,3),$$

(7.57)

where

$$g(1,2,3) = \frac{n(1,2,3)}{n^3},$$

(7.58)

with the 3-particle distribution function $n(1,2,3)$ defined by Eq. (6.7).

Note that due to the fact that the virial expansion of H(0) is of the form (7.52) the coefficient d_3 describes also the first nonvanishing term in the cluster expansion of Δ itself.

7.10 The expression for Δ for hard spheres

In Chapter 3 it is shown that in case of hard spheres one should replace in all the expressions the forces $\boldsymbol{F}_{ij}$ with the functions $\boldsymbol{\mathcal{T}}_{ij}$ given by (3.28). However, the terms involving $\boldsymbol{\mathcal{T}}_{ij}$ can be further simplified if one makes use of the fact that [13] the part of the mobility matrix corresponding to the motion along the line of the centers of spheres i and j goes to zero as the spheres approach each other, i.e.

$$\lim_{|\boldsymbol{R}_i - \boldsymbol{R}_j| \to 0} \hat{\boldsymbol{R}}_{ij} \cdot \sum_k (\boldsymbol{\mu}_{ik} - \boldsymbol{\mu}_{jk}).$$

(7.59)

Then, from the definition of $\boldsymbol{\mathcal{T}}_{ij}$ (3.28) one gets

$$\sum_{i,j,k} \boldsymbol{\mathcal{T}}_{ij} \boldsymbol{\mu}_{jk} = 0$$

(7.60)

Using the above fact one rewrites the expression for Δ (7.34) for the case of the hard sphere potential as

$$\Delta = \frac{k_B T}{\mu_o H(0)} \int_0^\infty dt' \frac{1}{3N} < \Big(\sum_{i,j} \nabla_i \cdot \boldsymbol{\mu}_{ij} \Big) \cdot \Big(\sum_{l,m} \nabla_l \cdot \boldsymbol{\mu}_{lm}(t') \Big) >^{irr},$$

(7.61)

Moreover, the equilibrium distribution of N hard spheres is given by the characteristic function of the nonoverlapping configurations of the spheres, i.e.

$$P_{eq}(\boldsymbol{X}) \sim W(1, 2, \ldots, N) = \prod_{i \neq j} W(R_{ij}) \qquad W(x) = \begin{cases} 0 & x < 2a \\ \\ 1 & x \geq 2a, \end{cases} \qquad (7.62)$$

so that the three-particle coefficient d_3 for the hard sphere system reads

$$d_3 = \frac{k_B T}{32\pi^2 a^6 \mu_o} \int_0^\infty dt' \int d\boldsymbol{R}_{12} \, d\boldsymbol{R}_{13} \Big(\sum_{i,j=1}^3 \nabla_i \cdot \boldsymbol{\mu}_{ij} \Big) \cdot \Big(\sum_{l,m=1}^3 \nabla_l \cdot \boldsymbol{\mu}_{lm}(t') \Big) W(1, 2, 3). \quad (7.63)$$

Chapter 8

The numerical computation of the memory function

This Chapter is devoted to the numerical estimation of the memory contribution Δ to the long-time collective diffusion coefficient D_c^l for the hard sphere system. The factor Δ is given (see (1.30) and (1.34)) by

$$\Delta = \int_{t'=0}^{\infty} M(k=0, t')dt'. \tag{8.1}$$

For the hard sphere system, the memory function $M(k, t)$ at $k = 0$ is given by (7.35)

$$M(t) = \frac{k_B T}{3N\mu_o H(0)} < \left(\sum_{i,j=1}^{N} \nabla_j \cdot \boldsymbol{\mu}_{ij}\right) \cdot \left(\sum_{k,l=1}^{N} \nabla_l \cdot \boldsymbol{\mu}_{kl}(t)\right) >^{irr} \tag{8.2}$$

Subsequently we are going to denote $M(k = 0, t)$ simply by $M(t)$.

It is reasonable to divide the task of estimating Δ into two stages

1. calculations of the initial value of the memory function $M(t = 0)$. As this is the dimensional quantity (measured in 1/time) it is convenient to consider rather the dimensionless one, eg. $M_o = \tau_R M(t = 0)$ where $\tau_R = a^2/D_o$ is the structural relaxation time (1.6). Then

$$M_o = \frac{a^2}{3N\mu_o^2 H(0)} < \left(\sum_{i,j=1}^{N} \nabla_j \cdot \boldsymbol{\mu}_{ij}\right) \cdot \left(\sum_{k,l}^{N} \nabla_l \cdot \boldsymbol{\mu}_{kl}\right) >^{irr}. \tag{8.3}$$

2. calculations of the relaxation time of the memory function, given by

$$\tau_M = \frac{1}{M(t = 0)} \int_{t'=0}^{\infty} M(t')dt'. \tag{8.4}$$

103

The reason why we have singled the initial value of the memory function is that it can be estimated by means of equilibrium averaging only, which can be done with much greater accuracy than the calculations of τ_M, which require Brownian dynamic simulations. Then, even without the Brownian dynamics simulations, we can estimate the value of Δ provided we assume that the relaxation time of M would not be very different from the relaxation times for other memory functions for Brownian particles (e.g. the viscosity memory function, whose relaxation time is assessed experimentally in [106]).

This Chapter is devoted to the first part of the task - i.e. to the calculation of M_o, whereas the next one presents results of the Brownian dynamics simulation performed to estimate τ_M.

We start with the calculations of M_o for very small volume fractions, when the virial expansion (7.57) can be used.

8.1 Virial expansion of M_o for hard spheres

In section 7.9 we have proved that the first nonvanishing term in the virial expansion of Δ is the one related to the three-particle clusters (7.63). The analogous expansion can be performed for the initial value M_o, i.e.

$$M_o = m_1 + m_2\phi + m_3\phi^2 + \dots \tag{8.5}$$

The results of section 7.9 imply that also in this case $m_1 = m_2 = 0$, whereas the three-particle term m_3 is given by

$$m_3 = \frac{1}{32\pi^2 a^4 \mu_o^2} \int \mathrm{d}\boldsymbol{R}_{12}\,\mathrm{d}\boldsymbol{R}_{13}\Big(\sum_{i,j=1}^{3} \nabla_j \cdot \boldsymbol{\mu}_{ij}\Big)^2 W(1,2,3). \tag{8.6}$$

Our goal now would be to calculate the above integral. To do it, we adopt an algorithm analogous to the one used by Cichocki et al. in [75]. First of all let us restrict the integral to the triangles $\Delta 123$ obeying

$$R_{23} \geq R_{13} \geq R_{12}. \tag{8.7}$$

Due to the symmetry the integral over such triangles is equal to one sixth of the value of the total integral. Next, the integration variables are changed to $\boldsymbol{R}_{12}$, α - the angle at the particle 1 and β - the angle at the particle 2.

The Jacobian of such a transformation reads

$$\mathrm{d}\boldsymbol{R}_{12}\mathrm{d}\boldsymbol{R}_{13} = 8\pi^2 \frac{\sin^2\alpha \sin^2\beta}{\sin^4(\alpha+\beta)} R_{12}^5 \mathrm{d}\boldsymbol{R}_{12}\mathrm{d}\alpha\mathrm{d}\beta$$

and so the integral (8.6) takes form

$$m_3 = \frac{3}{2a^4\mu_o^2} \int_{\pi-\beta \geq \alpha \geq \beta \geq \pi-(\alpha+\beta)} d\alpha\, d\beta \frac{\sin^2 \alpha \sin^2 \beta}{\sin^4(\alpha+\beta)} \cdot$$
$$\cdot \int_{2a}^{\infty} R_{12}^5 d\boldsymbol{R}_{12} \Big(\sum_{i,j=1}^{3} \nabla_j \cdot \boldsymbol{\mu}_{ij} \Big)^2. \tag{8.8}$$

The main problem in calculating numerically the above integral lies in computing the divergence of the mobility matrix $\boldsymbol{\mu}$, as it may considerably increase the numerical complexity of the algorithm. For example, if one wants to obtain $\nabla \cdot \boldsymbol{\mu}$ in a crudest possible way using the formula

$$\frac{\partial}{\partial R_{i\alpha}} \mu_{ij\alpha\beta}(\boldsymbol{R}_1, \ldots, \boldsymbol{R}_i, \ldots, \boldsymbol{R}_N) \approx \frac{1}{\Delta r} \big(\mu_{ij\alpha\beta}(\boldsymbol{R}_1, \ldots, \boldsymbol{R}_i + \Delta r \boldsymbol{e}_\alpha, \ldots, \boldsymbol{R}_N) -$$
$$\mu_{ij\alpha\beta}(\boldsymbol{R}_1, \ldots, \boldsymbol{R}_i, \ldots, \boldsymbol{R}_N) \big)$$

for some sufficiently small Δr, then one needs to calculate $\boldsymbol{\mu}$ $3N$ times to obtain $\nabla \cdot \boldsymbol{\mu}$ for a given configuration. The formula (8.9) is very inaccurate; more accurate finite-difference methods exist [107] but they need even more calculations of $\boldsymbol{\mu}$, which is unacceptable from the point of view of numerical efficiency.

As the divergence of mobility matrix is a crucial object for computations of the collective diffusion memory function we have derived an alternative, analytical scheme of calculating it based on the multipole expansion method.

We start with the expression (2.31) for the mobility matrix. This, together with the relations (2.20) and (2.27) gives for $\boldsymbol{\mu}$

$$\boldsymbol{\mu} = \Big[\mathcal{P} \frac{1}{\mathcal{Z}_o^{-1} + \mathcal{G}} \mathcal{P} \Big]^{-1}. \tag{8.9}$$

Using now the following tensor differentiation rule

$$\delta A^{-1} = -A^{-1} \delta A A^{-1} \tag{8.10}$$

we can represent the derivative of $\boldsymbol{\mu}$ as

$$\frac{\partial}{\partial \boldsymbol{X}} \boldsymbol{\mu} = -\boldsymbol{\mu} \Big(\frac{\partial}{\partial \boldsymbol{X}} \cdot \Big[\mathcal{P} \frac{1}{\mathcal{Z}_o^{-1} + \mathcal{G}} \mathcal{P} \Big] \Big) \boldsymbol{\mu}. \tag{8.11}$$

The tensor $\mathcal{Z}_o$ is the one-particle operator, so it does not depend on the positions of particles given by $\boldsymbol{X}$. Therefore

$$\frac{\partial}{\partial \boldsymbol{X}} \boldsymbol{\mu} = -\boldsymbol{\mu} \Big[\mathcal{P} \frac{1}{\mathcal{Z}_o^{-1} + \mathcal{G}} \Big(\frac{\partial}{\partial \boldsymbol{X}} \mathcal{G} \Big) \frac{1}{\mathcal{Z}_o^{-1} + \mathcal{G}} \mathcal{P} \Big] \boldsymbol{\mu}. \tag{8.12}$$

We see that finding the derivative of the mobility matrix boils down to differentiation of the connectors $\mathcal{G}$. However, in the multipole formalism, the derivative of

$G(l, \sigma, m; l', \sigma', m')$ can be expressed as the linear combination of the G matrices linking different multipoles. Therefore

$$\frac{\partial}{\partial X} \mathcal{G} = \mathcal{R} \mathcal{G}, \qquad (8.13)$$

where $\mathcal{R}$ is a well-defined matrix. The exact form of $\mathcal{R}$ can be found with use of the representation of $\mathcal{G}$ by means of the vector spherical harmonics [108].

In this way we obtain the analytical expression for the divergence of the mobility matrix. Naturally in the numerical calculations one truncates the multipoles at $l = L$ (see Chapter 2) and obtains the truncated matrix $\frac{\partial}{\partial X} \boldsymbol{\mu}_L$. The program deriving $\frac{\partial}{\partial X} \boldsymbol{\mu}$ from (8.12) and (8.13) is only approximately 3 times slower than the program calculating solely $\boldsymbol{\mu}$ for the same configuration of particles, whereas the explicit techniques based on finite difference methods are at least $3N$ times slower! Moreover the calculations of $\frac{\partial}{\partial X} \boldsymbol{\mu}$ by the above procedure are as accurate as the analogous calculations of $\boldsymbol{\zeta}$ and $\boldsymbol{\mu}$, i.e. for $L = 3$ it is expected that the accuracy of $\frac{\partial}{\partial X} \boldsymbol{\mu}$ obtained from (8.12) is about 1% with respect to the exact value.

The above algorithm for calculation of $\frac{\partial}{\partial X} \boldsymbol{\mu}$ was implemented numerically by E.Wajnryb and incorporated into the CFW package described in Chapter 2.

The integral (8.8) is carried out as follows. First the integration over R_{12} is performed by the simple Simpson method, as for the fixed angles α and β the integrand is non-oscillating function of R_{12}. Then the resulting function of α and β is integrated by means of the Monte Carlo technique.

After 100 000 Monte Carlo trials we have arrived at the following result for the initial value of the memory function

$$m_3 = 1.42 \pm 0.02, \qquad (8.14)$$

where the error corresponds to the standard deviation due to all the Monte Carlo trials.

8.2   The asymptotic part of m_3

In this section we study the asymptotic part of the integrand in (8.8), that is the part that becomes dominant when the triangle $\Delta 123$ grows, i.e. when its longest side R_{23} goes to infinity. We know that the integrand is short ranged, so the asymptotic part should decay at least as fast as R_{23}^{-4} or even faster. By examining the 3-particle scattering diagrams making up $\left(\sum_{i,j=1}^{3} \nabla_j \cdot \boldsymbol{\mu}_{ij} \right)^2$ one concludes that there indeed are contributions that behave asymptotically as R_{23}^{-4}. They are given by the diagrams of the form $< A|B >$ with both A and B of one of the following four kinds $\{L_1, L_2, L_3, L_4\}$. Here L_1 and L_2 given by
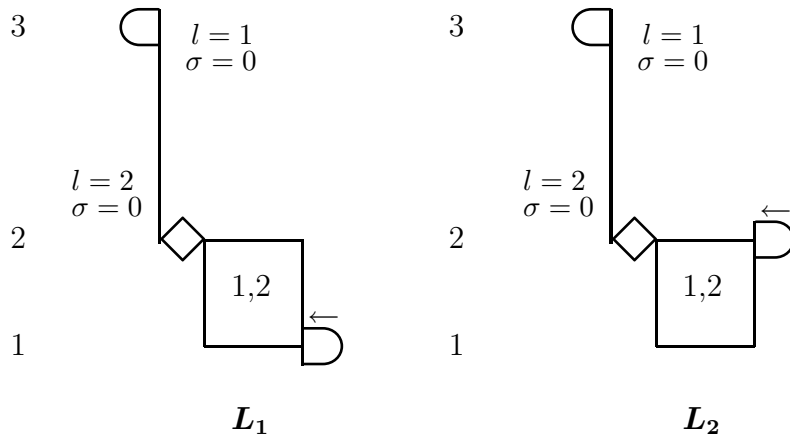
Fig. 8.1.

and L_3 and L_4 are obtained from the above ones by interchanging the positions of particles 1 and 2. In the above diagrams the rectangular box with $(1, 2)$ inside stands for any scattering sequence of the form $\boldsymbol{G\hat{Z}_oG\hat{Z}_o...G}$ involving the particles 1 and 2. Note that for a given length of the longest side R_{23} the diagrams L_i would give the biggest contribution if particles 1 and 2 are close to each other, therefore the main contribution to the asymptotic part is given by the long, thin triangles $\Delta123$, for which $R_{23} \approx R_{13} >> R_{12}$. The sum of all sequences of the form
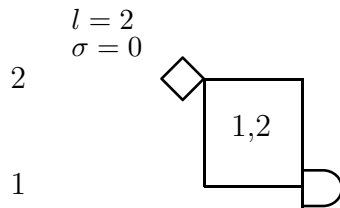
Fig. 8.2.

is known in hydrodynamics as $\boldsymbol{\mu}_{21}^{dt}(1, 2)$ (see eg. [67]). Here "t" denotes as always the first multipole of the force density i.e. the total force acting on the particle 1, whereas "d" stands for the symmetrized dipole of the force density on particle 2, i.e.

$$\boldsymbol{f}^d(j) = \int [\boldsymbol{f}(\boldsymbol{r}; i)(\boldsymbol{r} - \boldsymbol{R}_i)]^s d\boldsymbol{r}, \tag{8.15}$$

where the symbol "s" stands for the symmetrization. In the multipole notation introduced in section 2.5 the "d" multipole corresponds to $l = 2, \sigma = 0$. The tensorial form of $\boldsymbol{\mu}_{1i}^{dt}$ with $i = 1, 2$ reads [109]

$$\mu_{1i_{\alpha\beta\nu}}^{dt}(\boldsymbol{R}) = \alpha_{1i}(R)(\hat{R}_\alpha \hat{R}_\beta - \frac{1}{3}\delta_{\alpha\beta})\hat{R}_\nu + \beta_{1i}(R)[\frac{1}{2}(\hat{R}_\alpha \delta_{\beta\nu} + \hat{R}_\beta \delta_{\alpha\nu}) - \hat{R}_\alpha \hat{R}_\beta \hat{R}_\nu], \quad (8.16)$$

where α and β are the scalar functions and $\boldsymbol{R} = \boldsymbol{R}_i - \boldsymbol{R}_2$. Therefore the sum of all diagrams with the scattering sequences like that on the left in Fig. 8.1 can be written as

$$\frac{\partial}{\partial R_{1_\nu}} \frac{3}{8\pi\eta R_{32}^2} \hat{R}_{32_\alpha}(\hat{R}_{32_\beta} \hat{R}_{32_\gamma} - \frac{1}{3}\delta_{\beta\gamma})\mu_{21_{\beta\gamma\mu}}^{dt}(R_{21}), \quad (8.17)$$

where we used the expressions for $\boldsymbol{G}$ from Appendix C.

After inserting (8.16) and differentiation one obtains

$$\boldsymbol{L}_1 = -\frac{3\hat{\boldsymbol{R}}_{23}}{8\pi\eta R_{23}^2}(\alpha'_{12}(R_{12}) + \frac{2\alpha_{12}(R_{12}) - 3\beta_{12}(R_{12})}{R_{12}})[(\hat{\boldsymbol{R}}_{12} \cdot \hat{\boldsymbol{R}}_{23})^2 - \frac{1}{3}]. \quad (8.18)$$

Adding up the analogous expressions for the other $\boldsymbol{L}_i$ we get eventually the expression

$$\left(\sum_{i,j=1}^3 \nabla_j \cdot \boldsymbol{\mu}_{ij}\right) = -\sum_{i=1,2} \frac{3\hat{\boldsymbol{R}}_{i3}}{8\pi\eta R_{i3}^2} \sum_{j=1,2}(\alpha'_{1j}(R_{12}) + \frac{2\alpha_{1j}(R_{12}) - 3\beta_{1j}(R_{12})}{R_{12}})[(\hat{\boldsymbol{R}}_{12}\cdot\hat{\boldsymbol{R}}_{i3})^2 - \frac{1}{3}] = I_{(1,2),3}$$

$$(8.19)$$

We use here the subscript "$(1,2),3$" to emphasize the fact that the above expression gives a good asymptotic for the situation in which the particle 3 is far away from particles 1 and 2. In principle we could insert now the expression (8.19) into (8.8) and, after the integration, obtain the estimation of he contribution of the asymptotic diagrams to m_3. However, the problem with the above asymptotic expression is that it gives completely wrong estimation of $\left(\sum_{i,j=1}^3 \nabla_j \cdot \boldsymbol{\mu}_{ij}\right)$ for smaller triangles $\Delta 123$ (small here means such that their sides are not much longer than 2a). It stems from the asymmetric nature of the expression (8.19): note that for the case when $\Delta 123$ is a small equilateral triangle (8.19) yields a nonzero value of $\left(\sum_{i,j=1}^3 \nabla_j \cdot \boldsymbol{\mu}_{ij}\right)$, whereas the real value is, due to the symmetry, zero. As m_3 is given by the integral of $\left(\sum_{i,j=1}^3 \nabla_j \cdot \boldsymbol{\mu}_{ij}\right)^2$, we conclude from the above that the expression (8.19) would give the value of m_3 overestimated to a large extend.

To avoid this artifact in our calculations of the contribution of the asymptotic diagrams to the value of m_3 we have used the symmetrized version of (8.19), namely

$$\left(\sum_{i,j=1}^3 \nabla_j \cdot \boldsymbol{\mu}_{ij}\right) \approx I_{(1,2),3} + I_{(1,3),2} + I_{(2,3),1} \quad (8.20)$$

where $I_{(1,3),2}$ is given by the expression analogous to (8.19) in which, however, the particle indexes 2 and 3 are interchanged and analogous hold for $I_{(2,3),1}$. The expression (8.20) has the same asymptotic behavior as (8.19), and, at the same time, due to the symmetrization with respect to the particle indexes, behaves much better for smaller triangles.

Before we calculate m_3 from (8.20) using (8.8) we should first have the expression for the hydrodynamic functions $\alpha(R_{12})$ and $\beta(R_{12})$. This may be achieved by means of the scheme devised by Cichocki, Felderhof and Schmitz [67], which allows one to find the expansion of different functions describing the two-body hydrodynamic interactions in powers of the inverse interparticle distance. Following their algorithm, we have found the series expansion of $\alpha(R_{12})$ and $\beta(R_{12})$ up to terms $(1/R_{12})^{500})$. The first 20 terms of these series can also be found in [109].

The calculations of the asymptotic contribution to m_3 were performed with use of *Mathematica* and yielded

$$m_3^{asym} \approx 1.90$$

which is of the order of m_3 itself (cf. (8.14)), which shows that the asymptotic terms give an important contribution to the initial value of the memory function in the three-body approximation.

8.3 Monte Carlo calculation of M_o for concentrated suspensions

The calculations of M_o based on the virial expansion presented above are applicable only to very diluted suspensions. To find M_o for larger volume fractions, where clusters of more than 3 hydrodynamically interacting particles become important we have used the method of Monte Carlo averaging. It consists in generating several thousand statistically independent configurations of N hard spheres in periodic boundary conditions for a given volume fraction and the subsequent calculation of M_o for each configuration. Monte Carlo averaging techniques have previously been used in theory of colloidal suspensions to calculate several transport coefficients such as viscosity, permeability or self-diffusion coefficient [78,80,81]. The use of periodic boundary conditions gets rid of the boundary effects in the simulated sample, giving rise at the same time to some artificial effects caused by introducing periodicity in the sample. These are however less severe and easier to account for than the boundary effects for the finite sample (see also section 8.6 below). Moreover, when deriving the periodic Green function [69,94,110] one supplements the equations with the condition that the net suspension velocity in a whole sample is equal to zero, as otherwise the divergences in the fluid velocity field would appear. The resulting formulae for the hydrodynamic matrixes in the periodic boundary conditions guarantee therefore that $\boldsymbol{v}_s(\boldsymbol{k} = 0) = 0$, what, in turn, implies that the limits $\boldsymbol{k} \to 0$ of the unreduced kernels $\boldsymbol{Y}_{jE}(\boldsymbol{k})$ and $\boldsymbol{X}_{jE}(\boldsymbol{k}, t)$ are equal to their values in $k = 0$ which means that we can relax the irreducibility condition in Δ and calculate M_o as

$$M_o = \frac{a^2}{3N\mu_o^2 H(0)} < \Big(\sum_{i,j=1}^{N} \nabla_j \cdot \boldsymbol{\mu}_{ij} \Big)^2 > . \tag{8.21}$$

As we have already remarked in section 7.9, for some purposes it may be reasonable to separate out the instantaneous response effects described by the hydrodynamic factor

$H(0)$ and study (in analogy with $\tilde{\Delta}$ introduced in section 7.9) the retarded response in the form

$$\tilde{M}_o = \frac{a^2}{3N\mu_o^2} < \Big(\sum_{i,j=1}^{N} \nabla_j \cdot \boldsymbol{\mu}_{ij}\Big)^2 > . \tag{8.22}$$

As these two terms ($H(0)$ and $\tilde{M}_o$) behave differently as functions of ϕ and N, calculating them separately is more convenient (especially for the analysis of the finite- size effects presented in the section 8.6 below). In fact, for the hydrodynamic factor a very good numerical data has been obtained by Ladd [78], so there is no need to repeat these calculations here. Hence subsequently we are going to concentrate on calculations of $\tilde{M}_o$.

In the next section we dwell on the subject of generating statistically independent configurations for Monte-Carlo averaging.

8.4   Sample-generating technique

To be able to calculate an equilibrium average of a given quantity C one must first generate a large set of nonoverlapping configuration of spheres which are statistically independent. Then one calculates C for all of the configurations in the set and finally the mean of those values as well as the mean deviation is found.

Our sample generation technique for a suspension of N spheres inside the volume V (with the volume fraction $\phi = \frac{4N}{3V}\pi a^3$) is the following: For very small volume fractions ($\phi < 0.01$) we just generate random positions of the spheres and check if they overlap or not. If they do, we discard the positions and generate new configuration. We keep on trying till we finally obtain a non-overlapping configuration. Usually for $\phi = 0.01$ one must perform no more than 10 trials. To obtain the configurations for larger ϕ we start with the previously prepared configuration for $\phi = 0.01$ and then use the following **random-stepping routine**

1. choose one sphere at random (let us denote it by i)

2. move the sphere i. The displacement on every coordinate is given by the Gaussian random variable whose standard deviation is equal to $(L/N)^{1/3} - 1$ where $L = V^{1/3}$ is the side of the box.

3. check if the new position of the sphere is not taken by any other sphere. If it is so, the move is not performed.

4. go to 1

After every successful move we shrink the side of the box by δL sufficiently small to ensure that the spheres would not overlap with the displaced walls. By such "rattling & shrinking" procedure we can obtain a nonoverlapping configuration of the sphere for any volume fraction up $\phi = 0.49$, which corresponds to the fluid-solid transition for hard

N	t_{PC}	t_{CR}	memory
30	50 s	15 s	10MB
100	34 min	9 min	150MB
200	4.5 h	67 min	340MB

Table 8.1: The amount of time and RAM needed to calculate the divergence of the mobility matrix for N spherical particles in periodic boundary conditions taking into account the multipoles up to $L = 3$. The divergence was calculated from (8.12). In the above PC stands for the standard PC Pentium-III 500MHz 512 MB RAM computer with Lahey Fortran 95 compiler while CR is the Cray SV1-A in the Interdisciplinary Centre for Mathematical and Computational Modelling (ICM) at the Warsaw University. As it is seen the computational time grows approximately like N^3 while the memory consumption grows like N^2.

sphere system [111]. To generate more configurations for a given volume fraction, we use once again the random stepping routine, this time without shrinking. The algorithm is performed $5000N$ times to assure that the final configuration is statistically independent form the initial one.

8.5   Numerical efficiency

The CFW package with the mobility divergence algorithm incorporated provides us with **virtually exact** way of calculating both $\boldsymbol{\mu}$ and $\nabla \cdot \boldsymbol{\mu}$. Unfortunately for such a throughout treatment of the hydrodynamic interactions one is bound to pay a price, as the time needed to calculate $\boldsymbol{\mu}$ and $\frac{\partial}{\partial \boldsymbol{X}} \boldsymbol{\mu}$ for one configuration by our program is quite considerable and the same holds form the amount of RAM needed (in contradistinction to schemes based on the Oseen or Rote-Pragner approximations, in which the mobility matrix is calculated with use of the Eq. (2.54) or (2.55) and the divergence of such an object is simply zero). These characteristics for the calculations of $\nabla \cdot \boldsymbol{\mu}$ in frames of $L = 3$ scheme are given in Table 8.1. We see that the computational time grows approximately like N^3 while the memory consumption grows like N^2.

This means that it is more feasible computationally to perform the calculations for the smaller number of particles than the larger one, even if we take into consideration the fact that, due to the self-averaging, the results obtained for the larger systems would generally be less fluctuating than those of the smaller ones. Of course from the physical point of view the situation is quite the reverse: we want as many particles as possible, because in case of small number of particles in the periodic boundary conditions there is rather a strong interaction of a given particle with its periodic images which can affect the properties of the system in a considerable way.
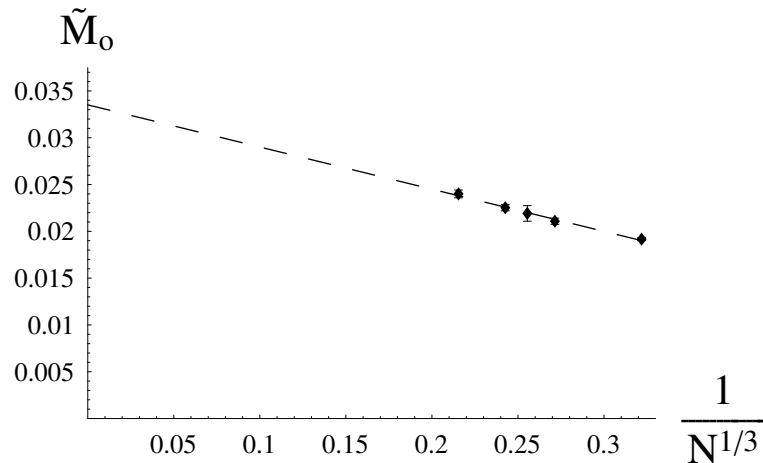
Figure 8.1: The initial value of the memory function $\tilde{M}_o$ as a function of the inverse cube root of the number of particles in the periodic cell N.

8.6   The complications associated with introducing periodicity in the model

The use of periodic boundary conditions allows us to get rid of the boundary effects but at the same time introduces periodicity into the model of disordered medium, which can affect the result of our calculations. Similar phenomenon was reported in case of Monte Carlo calculations of collective mobility of colloidal particles [78, 80, 81], when the periodicity effects caused a strong dependence of the result on the number of particles used in simulations. In order to investigate this effect, we have performed the simulations for several values of N - the number of particles in a periodic cell while keeping the volume fraction constant. In this way we have obtained the set of $\tilde{M}_o(N, \Phi)$ - the values of $\tilde{M}_o$ for the hard sphere suspension of volume fraction ϕ with N spheres in the periodic cell. Then we looked into the data to see if some scaling of the results with N can be observed. It turned out that the data scales with N as $N^{-1/3}$ - see Fig. 8.1 for the data for $\phi = 0.3$ and $N = 30, 50, 60, 70$ and 100. Below we present the possible explanation, why $\tilde{M}_o(N, \phi)$ should scale with N in such a way.

Looking at the expression (8.3) we notice that $\tilde{M}_o$ measures the square of the length of a vector $\boldsymbol{U}_{tot}$

$$\boldsymbol{U}_{tot} = \sum_{i,j=1}^{N} \nabla_j \cdot \boldsymbol{\mu}_{ij} = \sum_i \boldsymbol{U}_i^I \tag{8.23}$$

which is the sum of the Smoluchowski velocities (5.21) of all the particles in the absence of interparticle and external forces as well as the ambient flow.

Due to the symmetry $\boldsymbol{U}_{tot}$ vanishes for all the regular configurations of the particles, therefore $\tilde{M}_o$ is equal zero for the cubic arrays of hard spheres (fcc, bcc or sc). But the

periodic boundary conditions impose the regular, periodic structure on our problem, which is expected to lead to decrease of $\tilde{M}_o$. As an example of such a decrease caused by the periodicity let us consider the asymptotic three-body term (8.19) described in section 8.2. As we remember, these asymptotic terms come from the triangles Δabc in which two particles, say a and b are close to each other, whereas $R_{ca} \approx R_{cb} >> R_{ab}$. In Fig. (8.3) we have pictured such a situation (the particles a and b are not too close to each other for sake of the clarity of the picture). Now we consider the contributions to U_a^I from all the triangles $\Delta abc'$ where c' is the periodic image of c. Note that only the c' from cells relatively close to c give the contribution to U_a^I which behaves like R_{ac}^{-2}, because the contribution from c_1' situated further away is practically exactly balanced by the contribution from some c_2' situated on the opposite side of the central cell to c_1'. The difference between the two behaves as R_{ac}^{-4} and not as R_{ac}^{-2}!
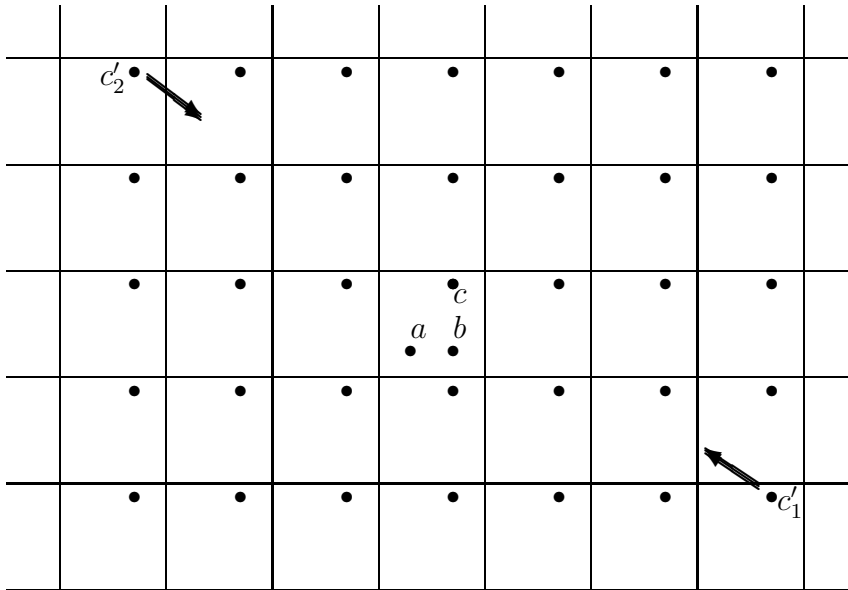
Figure 8.3: The effect of periodicity on the value of the memory function. Shown are two particles **a** and **b** lying close to each other and the third particle **c** together with its periodic images **c'**. The contribution from the triangles $\Delta abc_1'$ with c_1' lying far away from the central cell are almost completely counterbalanced by the contribution from the triangle $\Delta abc_2'$ with c_2' from the cell on the opposite side.

Therefore the effective volume which gives the contribution to $\boldsymbol{U}_a^I$ is limited to the periodic cell itself and few of its nearby copies and is therefore proportional to L^3, where L is the side of periodic cell.

On the other hand the contribution to $\left(\sum_{i,j=1}^3 \nabla_j \cdot \boldsymbol{\mu}_{ij}\right)^2$ from the clusters of particles of large linear dimensions $R \gg a$ behave as R^{-4}. Basing on this observation, one can

estimate the contribution to $\tilde{M}$ from all the clusters with $R \geq R_o \gg a$ to be proportional to R_o^{-1}.

Taking into account the above statements one concludes that the following relation should hold

$$\tilde{M}_o(L, \phi) = \tilde{M}_o(\phi) - A(\phi)L^{-1}, \tag{8.24}$$

where $\tilde{M}_o(L, \phi)$ is the value of $\tilde{M}_o$ for the hard sphere suspension of volume fraction ϕ in a periodic cell with side L. For the given volume fraction L is proportional to $N^{1/3}$, hence we expect that $\tilde{M}_o$ should depend on N in the following way

$$\tilde{M}_o(N, \phi) = \tilde{M}_o(\phi) - B(\phi)N^{-1/3}, \tag{8.25}$$

where $B(\phi)$ is some (unfortunately unknown) function of ϕ. In this way we have arrived at the desired result.

This means that by fitting the values of $\tilde{M}_o$ obtained for different number of spheres N in the periodic cell to the dependence (8.25) one can estimate the value of $\tilde{M}_o(\phi)$. We see from the above reasoning why it is more convenient to calculate $\tilde{M}_o$ separately from $H(0)$: if we would consider their ratio, the finite size effects from $H(0)$ and $\tilde{M}_o$ would be mixed and it would be harder to analyze the effects and obtain the asymptotic value.

For the data presented in Fig. 8.1 by fitting the dependence (8.25) one obtains the following asymptotic value of $\tilde{M}_o(N = \infty)$ for $\phi = 0.3$

$$\tilde{M}_o(\phi = 0.3) = 0.035 \pm 0.002. \tag{8.26}$$

8.7 Calculation details and analysis of the data

The calculations of $\tilde{M}_o$ were performed for six volume fractions: $\phi = 0.01$, 0.1, 0.2, 0.3, 0.4 and 0.45. In order to investigate the influence of system size on the value of $\tilde{M}_o$ for the volume fraction $\phi = 0.3$ the simulations were performed for several values of N: namely for 30,50,60,70 and 100 particles in the unit cell. For all the other volume fractions the calculations were performed only for three values of N, namely for $N = 30$, 50 and 100. The results together with $\tilde{M}_o(\infty)$ calculated by fitting them into (8.25) can be found in Table (8.2).

In the Fig. 8.4 the results for different volume fraction are presented, together with the $\tilde{M}_o(\phi)$ dependence given by the virial expansion (7.63).

The first thing that strikes oneself in this Figure is that the Monte Carlo data diverges very quickly from the virial expansion predictions. This means that the many-body hydrodynamic interactions affect the value of $\tilde{M}_o$ even for very small densities, so the range of applicability of the virial expansion is limited in principle to very dilute suspensions with $\phi \ll 0.1$ (for $\phi = 0.1$ the error of the value given by the virial expansion amounts to about 40 %!) This behavior of $\tilde{M}_o(\phi)$ can be understood when we remember that the largest contribution to m_3 is due to the asymptotic diagrams of the form $< L_i | L_j >$, where the

ϕ	N	number of trials	$\tilde{M}_o(N)$	$\tilde{M}_o(N = \infty)$	M_o
$\phi = 0.01$	N=50	16689	$(9.63 \pm 0.15) \cdot 10^{-5}$	$(1.46 \pm 0.05) \cdot 10^{-4}$	$(1.55 \pm 0.05) \cdot 10^{-4}$
	N=70	5490	$(1.00 \pm 0.03) \cdot 10^{-4}$		
	N=100	12017	$(1.07 \pm 0.015) \cdot 10^{-4}$		
$\phi = 0.1$	N=50	5617	$(5.40 \pm 0.08) \cdot 10^{-3}$	$(9.1 \pm 0.5) \cdot 10^{-3}$	$(1.7 \pm 0.1) \cdot 10^{-2}$
	N=70	2139	$(5.80 \pm 0.15) \cdot 10^{-3}$		
	N=100	6433	$(6.18 \pm 0.08) \cdot 10^{-3}$		
$\phi = 0.2$	N=50	4712	$(1.37 \pm 0.02) \cdot 10^{-2}$	$(2.61 \pm 0.08) \cdot 10^{-2}$	$(9.2 \pm 0.3) \cdot 10^{-2}$
	N=70	7001	$(1.48 \pm 0.02) \cdot 10^{-2}$		
	N=100	3549	$(1.625 \pm 0.03) \cdot 10^{-2}$		
$\phi = 0.3$	N=30	18572	$(1.917 \pm 0.015) \cdot 10^{-2}$	$(3.35 \pm 0.2) \cdot 10^{-2}$	0.24 ± 0.015
	N=50	3381	$(2.11 \pm 0.03) \cdot 10^{-2}$		
	N=60	476	$(2.19 \pm 0.08) \cdot 10^{-2}$		
	N=70	3396	$(2.25 \pm 0.03) \cdot 10^{-2}$		
	N=100	1987	$(2.40 \pm 0.04) \cdot 10^{-2}$		
$\phi = 0.4$	N=50	29733	$(2.55 \pm 0.01) \cdot 10^{-2}$	$(3.6 \pm 0.2) \cdot 10^{-2}$	0.54 ± 0.03
	N=70	4030	$(2.64 \pm 0.04) \cdot 10^{-2}$		
	N=100	3726	$(2.77 \pm 0.04) \cdot 10^{-2}$		
$\phi = 0.45$	N=50	6436	$(2.68 \pm 0.04) \cdot 10^{-2}$	$(3.09 \pm 0.01) \cdot 10^{-2}$	0.67 ± 0.02
	N=70	5029	$(2.73 \pm 0.04) \cdot 10^{-2}$		
	N=100	5744	$(2.77 \pm 0.04) \cdot 10^{-2}$		

Table 8.2: The results of the Monte Carlo calculations of the initial value of the memory function. Shown are the number of Monte Carlo trials for each volume fraction ϕ and number of particles N, the calculated values of $\tilde{M}_o(N, \phi)$ (8.22), the estimated values of $\tilde{M}_o(N = \infty, \phi)$ and finally the values of $M_o(\phi)$ (8.3), obtained by dividing $\tilde{M}_o$ by the hydrodynamic factor taken from [78]
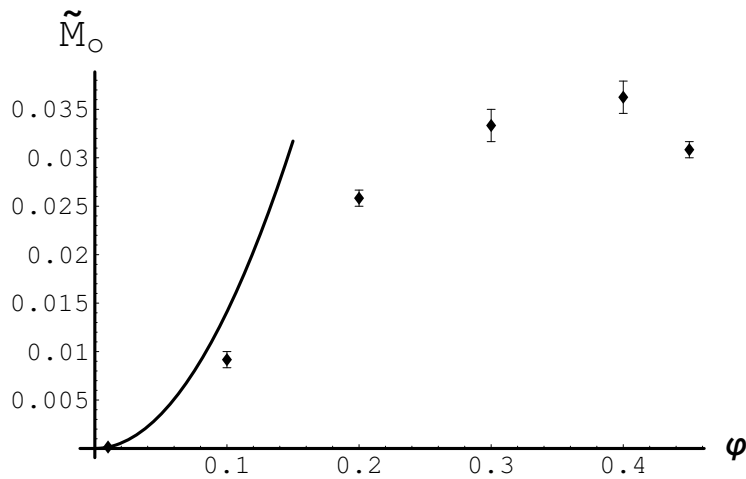
Figure 8.4: The initial value of the memory function $\tilde{M}_o$ as a function of the volume fraction (points) together with the small ϕ expansion results given by Eq. (8.14) (solid line)

subdiagrams $L_i, \quad i = 1, \ldots, 4$ are described in section 8.2 (see Fig. 8.1). Note that these diagrams are S-reducible, as they include a solitary connector (which decays like R^{-2}). If the suspension is so dilute that only the 3- particle diagrams are important, then as it has already been mentioned in section 7.9, the diagram $< L_i|L_j >$ will be irreducible, as any two particles will be linked by at least one bond in L_i and one in L_j. On the other hand, for more dense suspensions, when many-particle clusters become important, the diagrams $< L_i|L_j >$ will generally be **reducible**, as in the majority of cases L_i and L_j would involve different particles. In this case the above-mentioned solitary connectors will not only be nodal, but also articulation lines, which means that the whole diagram will be reducible and therefore will not contribute to $\tilde{M}_o$. This would lead to decrease of $\tilde{M}_o$ for the suspensions which are not very diluted in comparison with the predictions of the virial expansion.

The other characteristic feature of $\tilde{M}_o(\phi)$ which can be seen in Fig. 8.4 is that for large volume fractions the function seems to be decreasing. This can be understood if one remembers the discussion in section 8.6, in which it is argued that $\tilde{M}_o$ essentially measures the asymmetry of the configuration of the particles and vanishes for all the regular configurations. On the other hand, for the large volume fraction, the spheres have not much place to move and they become more ordered [112], which is a probable reason why $\tilde{M}_o$ decreases.

As it is said at the beginning of this Chapter, the mere knowledge of the initial value of the memory function allows one to estimate the value of Δ provided one makes some assumptions about the relaxation time τ_M. To obtain the characteristic relaxation time for the collective processes in a suspension we use the semi-phenomenological reasoning due to Medina-Noyola [113] and de Schepper et al. [114, 115]. They argued namely that the effect of hydrodynamic interactions on the dynamics of a suspension can be taken into account by replacing in the formulae the one-particle diffusion coefficient D_o, which

ϕ	$\frac{\tau_c}{\tau_R}$	Δ
0.01	0.94	0.01 %
0.1	0.55	1 %
0.2	0.32	3 %
0.3	0.20	5 %
0.4	0.13	7 %
0.45	0.10	7 %

Table 8.3: The estimate of the memory contribution to the long-time collective diffusion co-efficient Δ from the initial values of the memory function (Table 8.2) and the characteristic relaxation time τ_c (8.29) (here given in units of structural relaxation time τ_R)

describes the diffusion in the absence of hydrodynamic interactions by the short-time self diffusion coefficient D_s^s. The latter is defined as

$$D_s^s = \lim_{k \to \infty} \lim_{z \to \infty} D(k, z), \tag{8.27}$$

and characterizes the short-time decay of the "self" intermediate scattering function

$$F_s(k, t) = < e^{i\boldsymbol{k} \cdot (\boldsymbol{R}_1(t) - \boldsymbol{R}_1(0))} >, \tag{8.28}$$

describing the single particle motions in a suspension.

As the characteristic time for the collective phenomena in the absence of the hydro-dynamic interactions reads simply $\tau_c^o = a^2 S(0)/D_o$, the above reasoning would give the characteristic time for the collective processes for systems with hydrodynamic interactions to be

$$\tau_c \approx a^2 S(0)/D_s^s \tag{8.29}$$

Assuming that the relaxation time of our memory function τ_M is not very different from τ_c and taking the values of D_s^s from the numerical simulations of Ladd [78], we get the estimations of the integral of the memory function Δ, which together with the values of τ_c are presented in Table 8.3. One concludes from inspecting the Table that the memory function effect is expected to be quite small (less than 10 %) but it is growing with the volume fraction.

In the next Chapter our estimation will be given a more firm ground, as we would perform the Brownian dynamics simulations and study the time-dependence of the memory function, from which another estimate of τ_M will be calculated.

Chapter 9

Brownian dynamics calculations of the memory function

In this section we estimate the relaxation time τ_M of the memory function M for three volume fractions $\phi = 0.2$, 0.3 and 0.4 by means of the Brownian dynamics simulations. This is the largest and most time-consuming part of the numerical calculations in the Thesis.

9.1 The method

The Smoluchowski equation (3.10) is a good starting point for deriving the algorithm of the dynamic simulation of a suspension of Brownian particles. Let us namely integrate this equation over the small time interval Δt with the condition that the positions of the particles for $t = 0$ are known (so that the initial distribution is given by $P_o(\boldsymbol{X}) = \delta(\boldsymbol{X} - \boldsymbol{X}^0) = \prod_i \delta(\boldsymbol{R}_i - \boldsymbol{R}_i^o)$. To the first order in Δt the solution of the Smoluchowski equation is given by the multivariate Gaussian distribution uniquely defined by the moments

$$< \Delta \boldsymbol{X} >_{\Delta t} = \int \boldsymbol{X} D P_o(\boldsymbol{X}) \Delta t \, \mathrm{d}\boldsymbol{X} = \int (\boldsymbol{\mathcal{L}} \boldsymbol{X}) P_o(\boldsymbol{X}) \Delta t \, \mathrm{d}\boldsymbol{X} =$$

$$(9.1)$$

$$= (\beta^{-1} \frac{\partial}{\partial \boldsymbol{X}} \cdot \boldsymbol{\mu} + \boldsymbol{\mu} \boldsymbol{\mathcal{F}}) \Delta t$$

and

$$< \Delta \boldsymbol{X} \Delta \boldsymbol{X} >_{\Delta t} = 2\beta^{-1} \boldsymbol{\mu} \Delta t, \qquad (9.2)$$

where the absence of external disturbances is supposed ($\boldsymbol{v}_o = \boldsymbol{\mathcal{E}} = 0$). In the above formula the mobility matrix as well as the forces are calculated at the initial configuration (for $t = 0$). In the numerical implementation one constructs the configuration space

trajectories, which are chosen according to the distribution function given by (9.1) and (9.2). Therefore the trajectory of the particle i is given by

$$\boldsymbol{R}_i = \boldsymbol{R}_i^o + \beta^{-1} \sum_j \left(\nabla_j \cdot \boldsymbol{\mu}_{ij}^o\right)\Delta t + \sum_j \boldsymbol{\mu}_{ij}^o \cdot \boldsymbol{F}_j^o \Delta t + \gamma_i(\Delta t), \qquad (9.3)$$

where $\gamma_i(\Delta t)$ is the random displacement given by the Gaussian distribution with the average value zero and covariance obeying

$$< \gamma_i(\Delta t)\gamma_j(\Delta t) >= 2\beta^{-1}\boldsymbol{\mu}_{ij}\Delta t. \qquad (9.4)$$

The above algorithm was derived for the first time by Ermak and McCammon in 1978 [116]. Since then many groups have tried to use this algorithm to calculate the dynamic properties of the colloidal suspensions. In spite of the apparently simple structure of (9.3), if one wants to implement numerically this algorithm, one is immediately faced with two complex problems. The first is calculation of the mobility matrix $\boldsymbol{\mu}$, the second, even more complex, is to obtain the divergence of $\boldsymbol{\mu}$ needed in (9.3). Therefore it is no wonder that various groups working on the numerical implementation of the Brownian dynamics have tried to adopt a number of approximations to reduce the complexity of the problem. For example Ermak and McCammon in the above-mentioned paper [116], Dickinson and co-workers [117–121] as well as van Megen, Snook and Gaylor [122, 123] used the Oseen and Rote-Pragner approximations (2.54,2.55) of the mobility matrix, which, as it was already mentioned in Chapter 2, are very crude.

Much more elaborate are the numerical simulations of Brady and co-workers presented in a series of papers (see for example [74, 124–126]). They have included more multipoles in calculations of $\boldsymbol{\mu}$. Unfortunately, as it was mentioned in Chapter 2, they still do not take into account all the long-range contributions to $\boldsymbol{\mu}$, which makes their scheme not satisfactory.

9.2   The implementation

In our numerical implementation of the Brownian dynamics algorithm we use the CFW package together with the procedure for calculating the divergence of the mobility matrix as described in Chapter 8.

The next step needed in the Brownian dynamics simulations is to obtain the values for the set of 3N displacements M_i obeying (9.4). To this end the multivariate normal deviate generator from the NAG numerical library is used (G05EAF/G05EZF procedures in the library).

Now we turn to the question of choosing the appropriate time step in the Brownian dynamics simulations. On the one hand the smaller the timestep, the more precise the simulation is, on the other hand when one uses shorter timestep, one needs more computer time to get the Brownian trajectory of the same length. We have performed a number of tests to determine the optimal timestep and finally decided on $\Delta t = 10^{-4}d^2/D_o$ where

$d = 2a$ is the diameter of the spheres. The discrepancy between the results obtained with this timestep and with $\Delta t = 10^{-5}d^2/D_o$ is found to be less than 7% (which is almost always less than the error of the value itself).

There is one more problem with which each numerical implementation of Brownian dynamics must cope somehow. Namely because of the finite timestep it may happen that after displacing the particles according to (9.3) one would end up with the configuration in which some of the spheres overlap. This would violate the boundary condition (3.25) stating that the probability current coming through the surfaces $R_{ij} = 2a$ (which correspond to the touching of spheres i and j) vanishes. We must stress that such a behavior is an artifact coming solely from the finite time step - the dynamic itself does not allow overlapping of the spheres, as when the two spheres approach each other there emerges a divergence in the part of the friction tensor $\boldsymbol{\zeta}$ corresponding to the motion along the line of centers, as described in section 2.6. Therefore the mobility for such a motion goes to zero as $|\boldsymbol{R}_i - \boldsymbol{R}_j| \to 2a$. From (9.2) we see that the vanishing of the mobility results also in vanishing of the probability that the spheres will be pushed towards each other by a Brownian force.

Nevertheless as the timestep in simulation is finite, the problem persists and have to be coped with. The other groups tried to solve this problem by the following two alternative schemes

1. rejecting the displacements $\Delta \boldsymbol{R}_i = \boldsymbol{R}_i - \boldsymbol{R}_i^o$ (9.3) that lead to the overlapping configurations

2. moving the spheres that have overlapped a bit backwards along their trajectories, so that their distance would be equal to $|\boldsymbol{R}_i - \boldsymbol{R}_j| = 2a + \epsilon$. This method is used by Brady and co-workers.

We feel that both the above methods are artificial and can disturb in a considerable way the dynamics of the Brownian particles that one wants to investigate. Our own way of dealing with the problem is to counterbalance the artificial current at $R_{ij} = 2a$ by adding the current of the same magnitude but opposite sign by means of the following algorithm

1. Calculate the displacements $\Delta \boldsymbol{X}$ from the formula (9.1) for a given timestep Δt

2. associate with every sphere an auxiliary velocity $\boldsymbol{u}_i$ given by

$$\boldsymbol{u}_i = \frac{\Delta \boldsymbol{R}_i}{\Delta t} \tag{9.5}$$

3. solve a classical molecular dynamic problem of finding the evolution of N hard spheres with the velocities $\boldsymbol{u}_i$ over the time period Δt [112,127,128]. The numerical procedure applied here locates time, collision partners and all the impact parameters for every collision occurring in the system in chronological order.

4. go to 1

ϕ	N	number of trajectories	total length of trajectories
	N=30	13	110276
$\phi = 0.2$	N=50	12	30535
	N=100	24	24298
	N=30	7	124703
$\phi = 0.3$	N=40	7	46103
	N=100	10	10680
	N=30	15	134915
$\phi = 0.4$	N=50	9	51567
	N=100	12	12093

Table 9.1: The statistics and results of the Brownian dynamics simulations. Shown are: the number of trajectories obtained for different volume fractions and number of particles and the total length of these trajectories in timesteps $\Delta t = 4 \cdot 10^{-4} a^2 / D_o$

By applying the hard-sphere collision dynamics over the time interval Δt we assure that the probability current flowing through the surface $R_{ij} = 2a$ is zero, because during the collisions of the spheres i and j the component of the relative velocity $\boldsymbol{u}_{ij}$, which is parallel to the line of the centers of the colliding pair changes sign. Note that the component of $\boldsymbol{u}_{ij}$ perpendicular to $\boldsymbol{R}_{ij}$ remains unchanged as it should be, because the boundary condition (3.25) affects only the parallel component.

9.3 Numerical results

The Brownian dynamics simulations using the above-described algorithm were performed for three volume fractions $\phi = 0.2, 0.3$ and 0.4. Table 9.1 gives some statistics of the calculations such as the number of trajectories $\boldsymbol{X}(t)$ which were obtained for each volume fraction ϕ and number of particles N, the length of these trajectories measured in timesteps $\Delta t = 4 \cdot 10^{-4} a^2 / D_o$ and the total number of timesteps for each ϕ and N.

The simulations for N up to 50 were performed on Pentium III PC (500 MHz) computers whereas the simulations for $N = 100$ - on Cray SV1-A machine in the Interdisciplinary Centre of Modelling (ICM) at the Warsaw University.

As we are looking for the integral of $M(t)$ divided by the initial value $M(t = 0)$ all the time-independent quantities in the expression for $M(t)$ (8.2) are of no interest for us here. Therefore in the simulations it is enough to measure the quantity $T(t)$ given by (cf Eqs. (7.51) and (8.23))

$$T(t) =< \boldsymbol{U}_{tot}(0)\boldsymbol{U}_{tot}(t) > \tag{9.6}$$

as naturally

$$\frac{1}{M(t = 0)} \int_{t=0}^{\infty} M(t')dt' = \frac{1}{T(t = 0)} \int_{t=0}^{\infty} T(t')dt'. \tag{9.7}$$

The raw data of the form $\boldsymbol{U}_{tot}(K\Delta t) = \sum_{i,j=1}^{N} \nabla_j \cdot \boldsymbol{\mu}_{ij}(K\Delta t)$ with $K = 1, 2, \ldots$ were averaged to yield the correlation function according to [128, 129]

$$T(\tau) = \frac{1}{K_{max}(\tau)} \sum_{K=1}^{K_{max}(\tau)} \boldsymbol{U}_{tot}(K\Delta t)\boldsymbol{U}_{tot}(\tau + K\Delta t), \quad \tau = m\Delta t, \quad m = 1, 2, 3\ldots \tag{9.8}$$

Here $K_{max}\Delta t$ gives the last possible time origin for which the calculation of $T(\tau)$ makes sense. It is given by the condition that $K_{max}(\tau)\Delta t + \tau$ must never exceed the total time of a given trajectory, i.e.

$$K_{max}(\tau) + \frac{\tau}{\Delta t} = K_{traj}, \tag{9.9}$$

where K_{traj} is the total number of timesteps in a given trajectory. From Eq. (9.8) one sees that the statistics for the longer times τ gets worse. Finally, the last step is to average $T(\tau)$ over all the trajectories obtained for the given volume fraction ϕ and number of particles N.

9.4   The long-time tail fitting

As we are essentially interested in the value of the time integral of the memory function, a key question for us concerns the behavior of $M(t)/M(t = 0)$ for long times. It can not be assessed by means of the Brownian dynamics simulations and therefore some kind of conjecture as to the behavior of the memory function when $t \to \infty$ is needed. Some indications can be found in theoretical studies on the memory function of the **self** diffusion problem in a suspension [9, 17, 130–132], in which it was predicted that the self-diffusion memory function have an algebraic long time tail (namely $t^{-5/2}$) and the amplitude of this tail was calculated for a number of limiting cases (e.g. the dilute suspension, lack of hydrodynamic interactions etc.). This is connected with the fact that the Fourier transform of the memory function $\hat{M}(\omega)$ is a meromorphic function of the square root of ω. Therefore one gets the following expansion [131, 132]

$$\hat{M}(\alpha) = \hat{M}(0) + \hat{M}_1\alpha + \hat{M}_2\alpha^2 + \hat{M}_3\alpha^3 + \ldots,$$

with

$$\alpha = \sqrt{\omega}. \tag{9.10}$$

The first coefficient in the above expansion is closely connected with the relaxation time, as

$$\tau_M = \frac{\hat{M}(\alpha = 0)}{M(t = 0)}, \tag{9.11}$$

whereas the second gives the amplitude of the long-time tail $t^{-3/2}$ in the function $M(t)$ (which stems from the properties of the Fourier transform). If, however M_1 vanishes then $M(t)$ has the long-time tail of the form $t^{-5/2}$ with the amplitude determined by M_3.

It is not unreasonable to expect that such an algebraic long-time tail will be present also in our case. However, because of the complicated form of the memory function in our case and particularly the fact that the two-body contributions to M vanish, the techniques applied in the above-cited papers to determine the coefficients in (9.10) are not directly applicable in our case.

Therefore we decided on semi-empirical way of accounting for the long-time behavior of the memory function. Namely we have tried to fit to our data the tail of the form $At^{-(2n+1)/2}$ with $n = 1, 2, 3....$ The fitting was performed only for trajectories with $N \leq 50$, as in case of $N = 100$ the errors of the data are too large to obtain any reasonable fit. In all the cases the best fit was obtained for the tail of the form $t^{-3/2}$ (see Fig. 9.1 for the fit of the $t^{-3/2}$ tail of the $M(t)$ for $\phi = 0.4$ and $N = 50$).
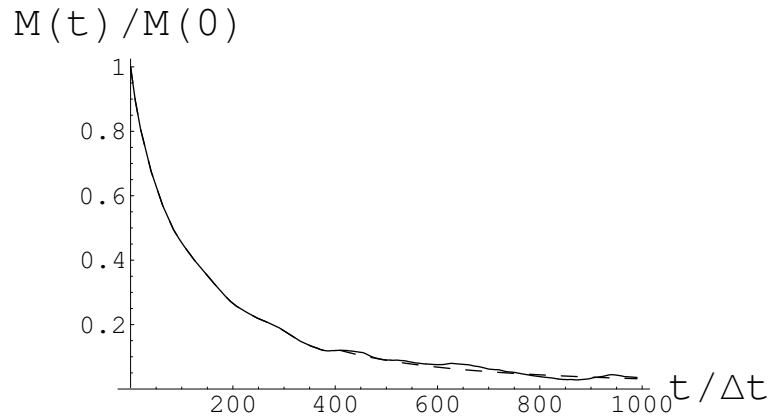
Figure 9.1: The memory function $\frac{M(t)}{M(0)}$ for N=50 and $\phi = 0.4$ (solid line) together with the fit of the long-time tail $At^{-3/2}$ starting from $t = 400\Delta t$ on (dashed).

Such a fitting cannot serve as a proof that the collective diffusion memory function has indeed the $t^{-3/2}$ long time-tail. Nevertheless fitting of the $t^{-3/2}$ tail to the data gives the upper bound of the value of τ_M, as the $At^{-(2n+1)/2}$ with $n > 1$ decay faster.

Now that we have a long-time fit, we can calculate the relaxation time τ_M given by (8.4). The results are the following

$$
\begin{aligned}
&\text{for } \phi = 0.2 && \tau_M = (315 \pm 60)\Delta t = (0.126 \pm 0.025)\tau_R \\
&\text{for } \phi = 0.3 && \tau_M = (300 \pm 40)\Delta t = (0.120 \pm 0.015)\tau_R && (9.12) \\
&\text{for } \phi = 0.4 && \tau_M = (220 \pm 50)\Delta t = (0.09 \pm 0.02)\tau_R
\end{aligned}
$$

From the relaxation time we can estimate the errors $\delta(\frac{M(t)}{M(0)})$ of the correlation function itself using the Zwanzig-Ailawadi formula [129, 133, 134]

$$
\delta\left(\frac{M(t)}{M(0)}\right) = \sqrt{\frac{2\tau_2}{T}}\left[1 - \frac{M(t)}{M(0)}\right] \tag{9.13}
$$

where T stands for the total simulation time and τ_2 is given by

$$
\tau_2 = 2\int_0^\infty \left(\frac{M(t)}{M(0)}\right)^2 dt. \tag{9.14}
$$

Figures 9.2 and 9.3 show the memory functions together with the errors for 30 and 100 particles respectively for the volume fraction $\phi = 0.3$.
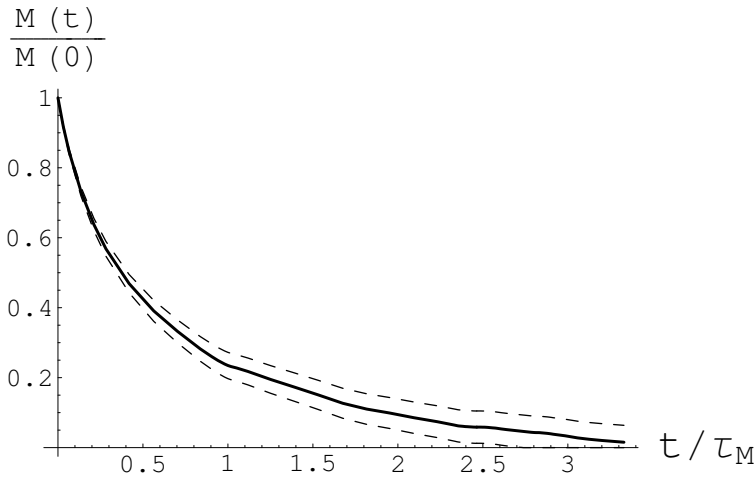
Figure 9.2: The memory function M as a function of time (in units of relaxation time τ_M) for the volume fraction $\phi = 0.3$ and the number of particles $N = 30$. The function is normalized by its initial value $M(t = 0)$. Dashed lines mark the accuracy of the result calculated according to Zwanzig-Ailawadi formula (9.13) supplemented by the condition that the memory function is positive.

M(t)/M(0)
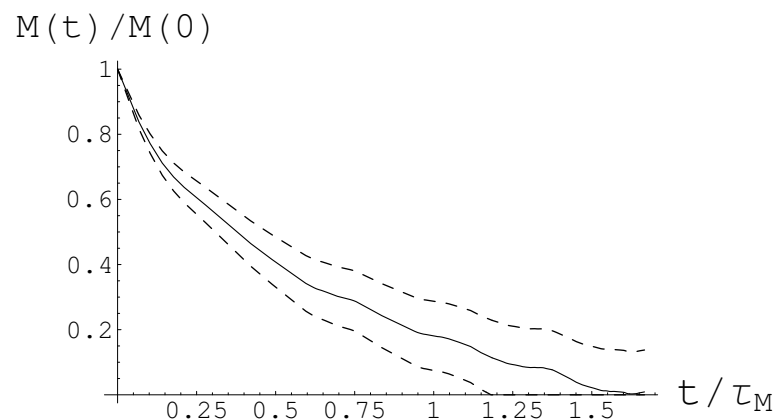
Figure 9.3: Same as in Fig. 9.2 but for 100 particles

9.5   Finite size effects

One can expect that just as it was for M_o, also in the case of the τ_M calculations the periodicity introduced by the boundary conditions can affect the result and make it dependent on N. To this end it is reasonable to analyze the $\frac{M(t)}{M(0)}$ curves for the same density and different number of particles to seek for the possible scaling effects. It is best to look at the curves for small t, as then the errors are not too big. Having all the above in mind we have looked into the short time form of the memory functions for different number of particles N for $\phi = 0.2, 0.3$ and 0.4. As an example, in Fig. 9.4 the memory functions for $\phi = 0.3$ and $N = 30, 40$ and 100 are presented.
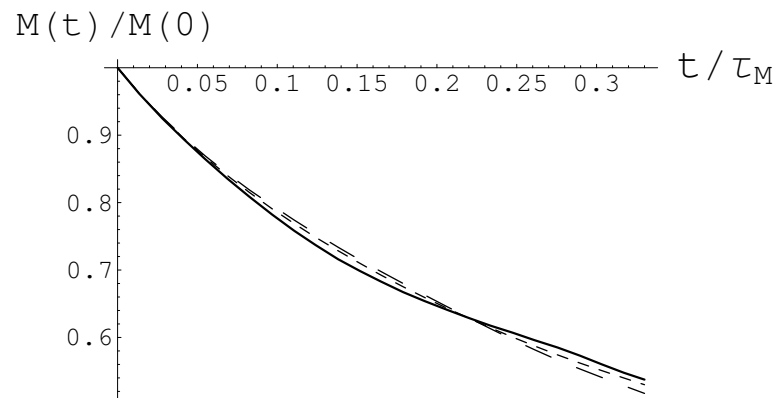
M(t)/M(0)

Figure 9.4: The memory function $\frac{M(t)}{M(0)}$ for $\phi = 0.3$ and N=30, 40 and 100 (short-dashed, long-dashed and solid lines respectively).

ϕ	Δ
0.2	0.01 ± 0.003
0.3	0.03 ± 0.01
0.4	0.05 ± 0.015

Table 9.2: The final results for the memory contribution to the long-time collective diffusion coefficient Δ. The values of Δ for $\phi = 0.2, 0.3$ and 0.4 are calculated from M_o computed in Chapter 8 (Table 8.2) and τ_M calculated in this Chapter.

As can be seen, within the range of errors no scaling is observed. From the results for $\phi = 0.2$ and $\phi = 0.4$ the similar conclusions can be drawn, which may indicate that the relaxation time is not sensitive to the system's size. However, on the other hand, it may also mean that our data is not accurate enough for the scaling to be seen. This fact augments further the uncertainty with which the results (9.12) are given.

9.6   Final results

By combining the above results for τ_M with the values of M_o obtained in the Chapter 8, we calculate the values of Δ for the volume fractions $\phi = 0.2, 0.3$ and $\phi = 0.4$. The results obtained in this way are given in Table 9.2.

We see that the estimations of Δ from the initial value of the memory function and characteristic time of the collective relaxation processes τ_c presented in the previous Chapter were essentially correct. They gave the values of Δ which are of the same magnitude as these calculated from the Brownian dynamics for the volume fractions $\phi = 0.2$, 0.3 and 0.4. Moreover, the estimations based on τ_c captured yet another important feature of the memory function, namely that its relaxation time τ_M gets shorter with the increase of the volume fraction. This phenomenon can be understood when we remember that the quantity $\sum_j \nabla_j \cdot \boldsymbol{\mu}_{ij}$ which plays the major role in $M(t)$ is very sensitive to particle configurations. And naturally the more dense the suspension is, the smaller particle displacement is needed to change the overall configuration in the considerable way, what results in the rapid changes in $M(t)$.

Chapter 10

Comparison with the experimental data

From the final results for Δ presented in the last section, one concludes that the contribution of the memory function to the long-time collective diffusion coefficient is nonzero but relatively small in comparison with the short time diffusion coefficient D_c^s. One may ask, however, if this results agree with the experimental measurements of the long- and short-time diffusion coefficient. However, in our case the quantitative comparison with the experimental data is almost impossible because of the very large errors of the measurements of the diffusion coefficient.

Pusey [8] in his review paper on colloidal suspensions, while discussing the problem of the memory contributions to D_c^l, quotes the experimental results of Kops-Werkhoven and Fijnaut [135] on the short time collective diffusion coefficient together with the results obtained by van Megen et. al [136] on the long-time collective diffusion coefficient. We reproduce the both sets of data in Fig. 10.1.
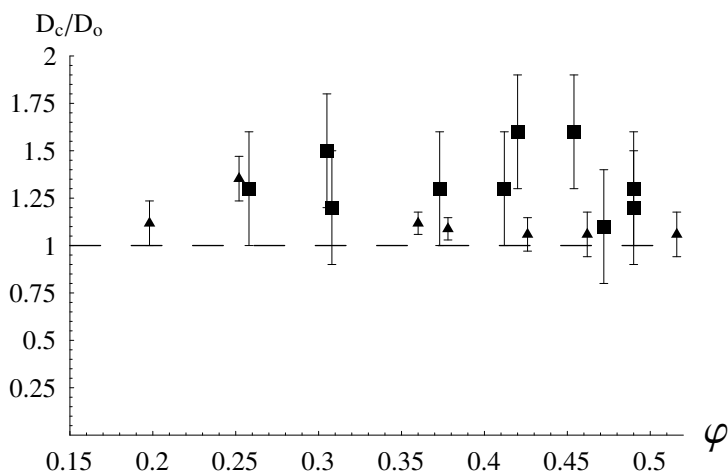
Figure 10.1: Short (squares) and long-time (triangles) diffusion coefficient normalized by the one particle value taken from [136] and [135] respectively

Pusey comments that "while the short-time results appear to be slightly larger than the long-term ones, the difference is hardly significant given the large error bars". He concludes that "the extant experimental evidence indicates that the memory contribution to collective diffusion is relatively small at least at concentrations below freezing". It is hard to believe but since 1991 when those words were written, despite the development of the experimental techniques, there is still a lack of valuable data from which the memory contribution could be estimated [137]. This is caused by the fact (see eg. [136]) that it is very hard for the experimentalists to get accurate results for small wave vectors. Therefore to get the collective diffusion coefficient they usually extrapolate the results obtained for small wave numbers down to $k = 0$, which gives rise to quite a large error.

Another way of approaching D_c^l is the sedimentation phenomena [10], i.e. the experiments in which the flux of the particles induced by an external force (e.g. gravity or centrifugal force) is measured. As it is shown in section 5.1 the collective diffusion coefficient is related to the sedimentation coefficient by

$$D_c = \frac{k_B T}{S(0)} K. \tag{10.1}$$

As the experimental timescale in sedimentation experiments is almost always much larger than τ_R one concludes that D_c calculated from (10.1) can be identified with the long-time collective diffusion coefficient. Unfortunately the errors of the diffusion coefficient obtained in such a way are at least as large as these of the light scattering experiments and they get larger with the increase of the volume fraction. It is caused by the fact that for large volume fractions the sedimentation velocity is small and hence hard to be measured with good accuracy. It is a pity, because the suspensions with large volume fractions are systems in which we expect the memory effects to be visible most clearly.

There is one more phenomenon that must be mentioned in connection with the small wavevector measurements of the diffusion coefficient. Namely in the Thesis we have performed calculations for **monodisperse** systems - i.e. such, in which all particles are of the same size. In reality, however, colloidal particles inevitably have some distribution of size: **"polydispersity"**. For the spherical particles a good measure of polydispersity is the standard deviation of the particle size distribution $P(a)$ divided by its mean [8]

$$\sigma \equiv \frac{\sqrt{\overline{a^2} - \overline{a}^2}}{\overline{a}} \tag{10.2}$$

where

$$\overline{a^n} = \int a^n P(a) \mathrm{d}a \tag{10.3}$$

Even the systems which are referred to in the papers as "monodisperse" have usually small ($\sigma = 0.01 - 0.05$) degree of polydispersity. It is important for our problem as it has been shown [53] that the polydispersity leads in general to the nonzero value of Δ even in the absence of the hydrodynamic interactions. Therefore in the experiments these two effects are usually mixed. Unfortunately, the theories which allow one to calculate the

contribution of polydispersity to Δ [8, 53] are not well developed (they are based on the number of rather arbitrary approximations). We hope that the present work, giving the estimate of memory effects for the monodisperse, hydrodynamically interacting suspension, would be a help for the experimentalists in a hard task of separating these two effects.

To sum up: the numerical estimation of the memory contribution to the long-time collective diffusion coefficient seems to be in a qualitative agreement with the experimental results. Both suggest that the memory factor Δ is nonzero but small and grows with the volume fraction. However the quantitative comparison of the numerical results with experiment is hard because of the considerable errors of the data.

Summary

The subject of the Thesis has been the analysis of the memory contribution to the collective diffusion coefficient of interacting Brownian particles. It has been suggested more than twenty years ago by Ackerson [51] that this contribution may give rise to a difference between short- and long-time diffusion coefficient in colloidal suspensions. The theoretical analysis of these quantities is obstructed by the infinite range hydrodynamic interactions in the system, because of which some of the transport kernels are non-local. These difficulties has been overcome by deriving the local equations with the short-range kernels, giving the diffusion current in terms of the external force and the velocity of a suspension as a whole. It is to be stressed that so far in the literature on the subject, the similar procedure was performed only for the instantaneous response case [23, 42, 43] . The generalization of this scheme to include the memory effects, which come from the relaxation of the distribution function, is a nontrivial task. It is the main theoretical result of the Thesis. It is worth to point out that a number of other problems can be worked out using the formalism presented here. In the Thesis we have concentrated on the memory function for the collective diffusion process, but we have simultaneously derived the expressions for other memory functions such as the viscosity memory function giving rise to the frequency-dependent contribution to the effective viscosity of the suspension (7.45).

The second part of the work is concerned with the numerical estimation of the above-mentioned memory contribution to D_c. This is achieved by means of extensive computer simulations with use of the Monte-Carlo averaging and the Brownian dynamics technique. The overall result of these calculations is that the relative memory contribution to the collective diffusion coefficient is growing with the volume fraction but never exceeds 10 %. These results agree qualitatively with the experimental data, the quantitative comparison being impossible because of the large experimental errors. It is to be hoped that the present results would stimulate the precise experimental measurements of the collective diffusion coefficient.

Acknowledgements

Appendix A

The scattering sequences

In this appendix we give the derivation of the scattering sequences (2.41) and (2.42) of the operators $\boldsymbol{\mu}$ and $\tilde{\boldsymbol{\mathcal{C}}}$ respectively.

Let us begin with $\boldsymbol{\mu}$. From (2.20), (2.27) and (2.31)

$$\boldsymbol{\mu} = \boldsymbol{\zeta}^{-1} = [\boldsymbol{\mathcal{P}}\boldsymbol{\mathcal{Z}}_o \frac{1}{1+\boldsymbol{\mathcal{G}}\boldsymbol{\mathcal{Z}}_o}\boldsymbol{\mathcal{P}}]^{-1} = [\boldsymbol{\mathcal{P}}\boldsymbol{\mathcal{Z}}_o\boldsymbol{\mathcal{P}} - \boldsymbol{\mathcal{P}}\boldsymbol{\mathcal{Z}}_o\frac{1}{1+\boldsymbol{\mathcal{G}}\boldsymbol{\mathcal{Z}}_o}\boldsymbol{\mathcal{G}}\boldsymbol{\mathcal{Z}}_o\boldsymbol{\mathcal{P}}]^{-1} =$$

$$= [\boldsymbol{\zeta}_o(1 - \boldsymbol{\zeta}_o^{-1}\boldsymbol{\mathcal{P}}\boldsymbol{\mathcal{Z}}_o\frac{1}{1+\boldsymbol{\mathcal{G}}\boldsymbol{\mathcal{Z}}_o}\boldsymbol{\mathcal{G}}\boldsymbol{\mathcal{Z}}_o\boldsymbol{\mathcal{P}})]^{-1}, \tag{A.1}$$

where

$$\boldsymbol{\zeta}_o = \boldsymbol{\mathcal{P}}\boldsymbol{\mathcal{Z}}_o\boldsymbol{\mathcal{P}} \tag{A.2}$$

is the one-particle friction matrix. Expressing the inverse in Eq. (A.1) as a series we get

$$\boldsymbol{\mu} = \boldsymbol{\mu}_o + \boldsymbol{\mu}_o\boldsymbol{\mathcal{P}}\boldsymbol{\mathcal{Z}}_o\frac{1}{1+\boldsymbol{\mathcal{G}}\boldsymbol{\mathcal{Z}}_o}[1 + \boldsymbol{\mathcal{G}}\boldsymbol{\mathcal{Z}}_o\boldsymbol{\mathcal{P}}\boldsymbol{\mu}_o\boldsymbol{\mathcal{P}}\boldsymbol{\mathcal{Z}}_o\frac{1}{1+\boldsymbol{\mathcal{G}}\boldsymbol{\mathcal{Z}}_o} +$$

$$\boldsymbol{\mathcal{G}}\boldsymbol{\mathcal{Z}}_o\boldsymbol{\mathcal{P}}\boldsymbol{\mu}_o\boldsymbol{\mathcal{P}}\boldsymbol{\mathcal{Z}}_o\frac{1}{1+\boldsymbol{\mathcal{G}}\boldsymbol{\mathcal{Z}}_o}\boldsymbol{\mathcal{G}}\boldsymbol{\mathcal{Z}}_o\boldsymbol{\mathcal{P}}\boldsymbol{\mu}_o\boldsymbol{\mathcal{P}}\boldsymbol{\mathcal{Z}}_o\frac{1}{1+\boldsymbol{\mathcal{G}}\boldsymbol{\mathcal{Z}}_o} + ...]\boldsymbol{\mathcal{G}}\boldsymbol{\mathcal{Z}}_o\boldsymbol{\mathcal{P}}\boldsymbol{\mu}_o, \tag{A.3}$$

where the one-particle mobility matrix is given by

$$\boldsymbol{\mu}_o = \boldsymbol{\zeta}_o^{-1}. \tag{A.4}$$

The series in square brackets in (A.3) can be summed to yield

$$\boldsymbol{\mu} = \boldsymbol{\mu}_o + \boldsymbol{\mu}_o\boldsymbol{\mathcal{P}}\boldsymbol{\mathcal{Z}}_o\frac{1}{1+\boldsymbol{\mathcal{G}}\boldsymbol{\mathcal{Z}}_o} \frac{1}{1 - \boldsymbol{\mathcal{G}}\boldsymbol{\mathcal{Z}}_o\boldsymbol{\mathcal{P}}\boldsymbol{\mu}_o\boldsymbol{\mathcal{P}}\boldsymbol{\mathcal{Z}}_o\frac{1}{1+\boldsymbol{\mathcal{G}}\boldsymbol{\mathcal{Z}}_o}}\boldsymbol{\mathcal{G}}\boldsymbol{\mathcal{Z}}_o\boldsymbol{\mathcal{P}}\boldsymbol{\mu}_o =$$

$$= \boldsymbol{\mu}_o + \boldsymbol{\mu}_o\boldsymbol{\mathcal{P}}\boldsymbol{\mathcal{Z}}_o\frac{1}{1+\boldsymbol{\mathcal{G}}(\boldsymbol{\mathcal{Z}}_o - \boldsymbol{\mathcal{Z}}_o\boldsymbol{\mathcal{P}}\boldsymbol{\mu}_o\boldsymbol{\mathcal{P}}\boldsymbol{\mathcal{Z}}_o)}\boldsymbol{\mathcal{G}}\boldsymbol{\mathcal{Z}}_o\boldsymbol{\mathcal{P}}\boldsymbol{\mu}_o \tag{A.5}$$

and the scattering expansion of $\boldsymbol{\mu}$ takes form

$$\boldsymbol{\mu} = \boldsymbol{\mu}_o + \boldsymbol{\mu}_o \mathcal{P} \boldsymbol{\mathcal{Z}}_o \frac{1}{1 + \mathcal{G}\hat{\boldsymbol{\mathcal{Z}}}_o} \mathcal{G}\boldsymbol{\mathcal{Z}}_o \mathcal{P}\boldsymbol{\mu}_o, \tag{A.6}$$

where the convective extended friction matrix [64] is defined as

$$\hat{\boldsymbol{\mathcal{Z}}}_o = \boldsymbol{\mathcal{Z}}_o - \boldsymbol{\mathcal{Z}}_o \mathcal{P}\boldsymbol{\mu}_o \mathcal{P}\boldsymbol{\mathcal{Z}}_o. \tag{A.7}$$

Therefore we have succeded in deriving (2.41).

Next we turn to the $\tilde{\mathcal{C}}$ operator. From (2.33) together with (2.20) and the above-derived (A.6) one obtains

$$\begin{aligned}
\tilde{\mathcal{C}} &= \boldsymbol{\mathcal{Z}}_o(1 + \mathcal{G}\boldsymbol{\mathcal{Z}}_o)^{-1}\mathcal{P}[\boldsymbol{\mu}_o + \boldsymbol{\mu}_o \mathcal{P}\boldsymbol{\mathcal{Z}}_o(1 + \mathcal{G}\hat{\boldsymbol{\mathcal{Z}}}_o)^{-1}\mathcal{G}\boldsymbol{\mathcal{Z}}_o\mathcal{P}\boldsymbol{\mu}_o] = \\
&= \boldsymbol{\mathcal{Z}}_o(1 + \mathcal{G}\boldsymbol{\mathcal{Z}}_o)^{-1}\mathcal{P}\boldsymbol{\mu}_o + \boldsymbol{\mathcal{Z}}_o(1 + \mathcal{G}\boldsymbol{\mathcal{Z}}_o)^{-1}\mathcal{P}\boldsymbol{\mu}_o\mathcal{P}\boldsymbol{\mathcal{Z}}_o(1 + \mathcal{G}\hat{\boldsymbol{\mathcal{Z}}}_o)^{-1}\mathcal{G}\boldsymbol{\mathcal{Z}}_o\mathcal{P}\boldsymbol{\mu}_o = \\
&= (1 + \boldsymbol{\mathcal{Z}}_o\mathcal{G})^{-1}\mathcal{P}\boldsymbol{\mu}_o + (1 + \boldsymbol{\mathcal{Z}}_o\mathcal{G})^{-1}\boldsymbol{\mathcal{Z}}_o\mathcal{P}\boldsymbol{\mu}_o\mathcal{P}\boldsymbol{\mathcal{Z}}_o\mathcal{G}(1 + \hat{\boldsymbol{\mathcal{Z}}}_o\mathcal{G})^{-1}\boldsymbol{\mathcal{Z}}_o\mathcal{P}\boldsymbol{\mu}_o. \tag{A.8}
\end{aligned}$$

Using the matrix identity

$$(1 + A)^{-1}(B - A)(1 + B)^{-1} = (1 + A)^{-1} - (1 + B)^{-1} \tag{A.9}$$

for

$$\begin{aligned}
A &= \boldsymbol{\mathcal{Z}}_o\mathcal{G}, \\
B &= \hat{\boldsymbol{\mathcal{Z}}}_o\mathcal{G}, \\
B - A &= -\boldsymbol{\mathcal{Z}}_o\mathcal{P}\boldsymbol{\mu}_o\mathcal{P}\boldsymbol{\mathcal{Z}}_o\mathcal{G} \tag{A.10}
\end{aligned}$$

we arrive at

$$\tilde{\mathcal{C}} = (1 + \hat{\boldsymbol{\mathcal{Z}}}_o\mathcal{G})^{-1}\boldsymbol{\mathcal{Z}}_o\mathcal{P}\boldsymbol{\mu}_o = \boldsymbol{\mathcal{Z}}_o\mathcal{P}\boldsymbol{\mu}_o - \hat{\boldsymbol{\mathcal{Z}}}_o(1 + \mathcal{G}\hat{\boldsymbol{\mathcal{Z}}}_o)^{-1}\mathcal{G}\boldsymbol{\mathcal{Z}}_o\mathcal{P}\boldsymbol{\mu}_o, \tag{A.11}$$

which after inserting $\hat{\boldsymbol{\mathcal{Z}}}$ yields the desired result (2.42).

Appendix B

The irreducible multipoles of the force density and velocity

In this appendix we give the explicit expression for the set of the irreducible multipoles in terms of which the multipole moments of the velocity around the i-th sphere (2.45) as well as the force density on the surface on the sphere can be expressed.

To begin with, $\nabla^l(\boldsymbol{v}(\boldsymbol{r}) - \boldsymbol{v}_o(\boldsymbol{r}))$ can be written in terms of irreducible tensors as [72]

$$\frac{1}{l!}\partial^l_{\gamma_1...\gamma_l}\boldsymbol{v}_\alpha(\boldsymbol{r}) = (h_{0,l+1})_{\alpha\gamma_1...\gamma_l} + (h_{1,l+1})_{\alpha\gamma_1...\gamma_l} + (h_{2,l+1})_{\alpha\gamma_1...\gamma_l}, \tag{B.1}$$

where

$$
\begin{aligned}
(h_{0,l+1})_{\alpha\gamma_1...\gamma_l} &= (\boldsymbol{c}_{0,l+1})_{\alpha\gamma_1...\gamma_l} \\
(h_{1,l+1})_{\alpha\gamma_1...\gamma_l} &= -\frac{l}{l+1}(\varepsilon_{\alpha\gamma_1\lambda}(\boldsymbol{c}_{1,l})_{\lambda\gamma_2...\gamma_l})^{S(\gamma)} \\
(h_{2,l+1})_{\alpha\gamma_1...\gamma_l} &= \frac{(l-1)(l+2)}{2(2l+1)}((\boldsymbol{c}_{2,l-1})_{\alpha\gamma_1...\gamma_l}\delta_{\gamma_1\gamma_2}) - \frac{l-1}{2l+1}(\delta_{\alpha\gamma_1}(\boldsymbol{c}_{2,l-1})_{\gamma_2...\gamma_l}),
\end{aligned}
\tag{B.2}
$$

where $S(\gamma)$ stands for the symmetrization over in the γ indices. The irreducible velocity multipoles $\boldsymbol{c}_{\sigma,l}$ read

$$
\begin{aligned}
(\boldsymbol{c}_{0,l})_{\alpha\gamma_1...\gamma_{l-1}} &= \frac{1}{(l-1)!}\,\overline{\partial^{l-1}_{\gamma_1...\gamma_{l-1}}\boldsymbol{v}_\alpha(\boldsymbol{r})} = \overline{\boldsymbol{c}^l_{\alpha\gamma_1...\gamma_l}} \\
(\boldsymbol{c}_{1,l})_{\alpha\gamma_2...\gamma_l} &= \frac{1}{l!}\,\overline{\partial^{l-1}_{\gamma_2...\gamma_l}\boldsymbol{\omega}_\alpha(\boldsymbol{r})} = \overline{l\varepsilon_{\alpha\lambda\mu}\boldsymbol{c}^{(l+1)}_{\lambda\gamma_2...\gamma_l\mu}} \\
(\boldsymbol{c}_{2,l})_{\alpha\gamma_3...\gamma_{l+1}} &= \frac{1}{(l+1)!}\,\overline{\partial^{l-1}_{\gamma_3...\gamma_l}\nabla^2\boldsymbol{v}_\alpha(\boldsymbol{r})} = \overline{l(l+1)\delta_{\lambda\mu}\boldsymbol{c}^{(l+2)}_{\lambda\mu\gamma_3...\gamma_{l+1}}},
\end{aligned}
\tag{B.3}
$$

where $\boldsymbol{\omega} = \nabla \times \boldsymbol{v}$ and the overline stands for the symmetric and traceless (and hence irreducible) part of the tensor.

Similarly the force multipoles can be written as a sum of the irreducible multipoles $\boldsymbol{f}_{\sigma,l}$ of the form

$$(\boldsymbol{f}_{0,l})_{\alpha\gamma_1...\gamma_{l-1}} = \overline{\boldsymbol{f}^l_{\alpha\gamma_1...\gamma_l}} \tag{B.4}$$

$$(\boldsymbol{f}_{1,l})_{\alpha\gamma_2...\gamma_l} = \frac{l}{l+1}\varepsilon_{\alpha\lambda\mu}\overline{\boldsymbol{f}^{(l+1)}_{\lambda\gamma_2...\gamma_l\mu}} \tag{B.5}$$

$$(\boldsymbol{f}_{2,l})_{\alpha\gamma_3...\gamma_{l+1}} = \frac{l(l+1)}{2(2l+1)}\delta_{\lambda\mu}\overline{\boldsymbol{f}^{(l+2)}_{\lambda\mu\gamma_3...\gamma_{l+1}}}. \tag{B.6}$$

Appendix C

The explicit formulae for hydrodynamic matrices

In this appendix we give the explicit form of the hydrodynamic matrices $\boldsymbol{G}$ and $\boldsymbol{Z}_o$ in frames of the multipole formalism. The formulae are reproduced after [71].

The single-particle friction operator $\boldsymbol{Z}_o$ reads in this case

$$\boldsymbol{Z}_{o;l\sigma\mu_1\ldots\mu_l,l'\sigma'\mu'_1\ldots\mu'_{l'}} = \delta_{ll'}\delta_{\mu_1\mu'_1}\ldots\delta_{\mu_l\mu'_l}z_{l;\sigma\sigma'}, \tag{C.1}$$

where the matrix $z_{l;\sigma\sigma'}$ reads

$$z_{l;\sigma\sigma'} = \frac{8\pi\eta}{(l+1)(2l-3)!!}\begin{pmatrix} A_{l0} & 0 & \dfrac{A_{l2}}{2(2l+3)} \\ 0 & \dfrac{A_{l1}}{2(2l-1)} & 0 \\ \dfrac{A_{l2}}{2(2l+3)} & 0 & \dfrac{B_{l2}}{4(2l-1)(2l+3)}. \end{pmatrix} \tag{C.2}$$

The values of the coefficients A and B depend on the specific model under consideration. For the hard spheres with stick boundary conditions they read

$$\begin{aligned} A_{l0} &= \frac{2l+1}{2}a^{2l-1}, & A_{l1} &= a^{2l+1}, \\ A_{l2} &= \frac{2l+3}{2}a^{2l+1}, & B_{l2} &= \frac{2l+1}{2}a^{2l+3}. \end{aligned} \tag{C.3}$$

The elements of the Green operator $\boldsymbol{G}$ read

$$\boldsymbol{G}_{l0\mu_1...\mu_l,l'0\mu'_1...\mu'_{l'}}(ij) = (-1)^{l'-1}\overline{\partial^{l-1}_{\mu_2...\mu_l}\partial^{l'-1}_{\mu'_2...\mu'_{l'}}\boldsymbol{T}_{\mu_1\mu_{1'}}(\boldsymbol{R})}^{(\mu')^{(\mu)}}\big|_{\boldsymbol{R}=\boldsymbol{R}_i-\boldsymbol{R}_j},$$

$$\boldsymbol{G}_{l0\mu_1...\mu_l,l'1\mu'_1...\mu'_{l'}}(ij) = (-1)^{l'-1}\overline{\partial^{l-1}_{\mu_2...\mu_l}\partial^{l'}_{\nu\mu'_2...\mu'_{l'}}\boldsymbol{T}_{\mu_1\kappa}\varepsilon_{\kappa\nu\mu'_1}(\boldsymbol{R})}^{(\mu')^{(\mu)}}\big|_{\boldsymbol{R}=\boldsymbol{R}_i-\boldsymbol{R}_j},$$

$$\boldsymbol{G}_{l0\mu_1...\mu_l,l'0\mu'_1...\mu'_{l'}}(ij) = (-1)^{l'-1}\overline{\partial^{l-1}_{\mu_2...\mu_l}\partial^{l'-1}_{\mu'_2...\mu'_{l'}}\nabla^2\boldsymbol{T}_{\mu_1\mu_{1'}}(\boldsymbol{R})}^{(\mu')^{(\mu)}}\big|_{\boldsymbol{R}=\boldsymbol{R}_i-\boldsymbol{R}_j},$$

$$\boldsymbol{G}_{l1,l'0}(ij) = \boldsymbol{G}_{l0,l'1}(ij),$$

$$\boldsymbol{G}_{l2,l'0}(ij) = \boldsymbol{G}_{l0,l'22}(ij), \qquad\qquad\qquad\qquad (C.4)$$

$$\boldsymbol{G}_{l1,l'1}(ij) = -\boldsymbol{G}_{l0,l'2}(ij),$$

$$\boldsymbol{G}_{l1,l'2}(ij) = \boldsymbol{G}_{l2,l'1}(ij) = \boldsymbol{G}_{l2,l'2}(ij),$$

where $\overline{\boldsymbol{a}}^{\mu}$ indicates the irreducible part of the Cartesian tensor $\boldsymbol{a}$ with respect to the indices $\mu_1 \ldots \mu_l$. The above expressions can be simplified to

$$\boldsymbol{G}_{l0,l'0}(ij) = (-1)^{l'-1}\frac{(-1)^{l+l'-2}}{8\pi\eta}\frac{(2l+2l'-3)!!}{R_{ij}^{l+l'-1}}\boldsymbol{G}_1^{(l,l')}(\hat{\boldsymbol{R}}_{ij}),$$

$$\boldsymbol{G}_{l0,l'1}(ij) = (-1)^{l'-1}\frac{(-1)^{l+l'-2}}{4\pi\eta}\frac{(2l+2l'-3)!!}{R_{ij}^{l+l'}}\boldsymbol{G}_2^{(l,l')}(\hat{\boldsymbol{R}}_{ij}), \qquad (C.5)$$

$$\boldsymbol{G}_{l0,l'2}(ij) = (-1)^{l'}\frac{(-1)^{l+l'-2}}{4\pi\eta}\frac{(2l+2l'-1)!!}{R_{ij}^{l+l'+1}}\boldsymbol{G}_2^{(l,l')}(\hat{\boldsymbol{R}}_{ij}),$$

with

$$\boldsymbol{G}_{1;\mu_1...\mu_l,\mu'_1...\mu'_{l'}}^{(l,l')}(\boldsymbol{r}) = \overline{r_{\mu_1}\cdots r_{\mu_l}r_{\mu'_1}\cdots r_{\mu'_l}} + \frac{2(2l+2l'-ll'-1)}{(2l+2l'-3)(2l+2l'-1)},$$

$$\times \overline{\overline{\delta_{\mu_1\mu'_1}\overline{r_{\mu_2}\cdots r_{\mu_l}r_{\mu'_2}\cdots r_{\mu'_l}}}}^{\mu'\mu},$$

$$\boldsymbol{G}_{2;\mu_1...\mu_l,\mu'_1...\mu'_{l'}}^{(l,l')}(\boldsymbol{r}) = \overline{\overline{\varepsilon_{\mu_1\mu'_1\nu}\overline{r_\nu r_{\mu_2}\cdots r_{\mu_l}r_{\mu'_2}\cdots r_{\mu'_l}}}}^{\mu'\mu},$$

$$\boldsymbol{G}_{3;\mu_1...\mu_l,\mu'_1...\mu'_{l'}}^{(l,l')}(\boldsymbol{r}) = \overline{r_{\mu_1}\cdots r_{\mu_l}r_{\mu'_1}\cdots r_{\mu'_l}}.$$

Appendix D

Proof that the second virial coefficient d_2 in the expansion of $\tilde{\Delta}$ vanishes

By solving the problem of two particles ("1" and "2") moving in an incompressible fluid one can show that the two-body mobility matrix $\boldsymbol{\mu}(\boldsymbol{R}_1, \boldsymbol{R}_2)$ has the following form [13, 67, 109]

$$\boldsymbol{\mu}_{12,\alpha\beta} = \boldsymbol{\mu}_{21,\alpha\beta} = a_{12}(R)\hat{\boldsymbol{R}}_\alpha\hat{\boldsymbol{R}}_\mu + b_{12}(R)(\delta_{\alpha\mu} - \hat{\boldsymbol{R}}_\alpha\hat{\boldsymbol{R}}_\mu),$$
$$\boldsymbol{\mu}_{11,\alpha\beta} = \boldsymbol{\mu}_{22,\alpha\beta} = a_{11}(R)\hat{\boldsymbol{R}}_\alpha\hat{\boldsymbol{R}}_\mu + b_{11}(R)(\delta_{\alpha\mu} - \hat{\boldsymbol{R}}_\alpha\hat{\boldsymbol{R}}_\mu), \tag{D.1}$$
$$\boldsymbol{R} = \boldsymbol{R}_1 - \boldsymbol{R}_2$$

with α and β denoting the Cartesian indexes and a_{11}, a_{12}, b_{11} and b_{12} - the scalar functions of the interparticle distance R_{12}.

The symmetries of the above form of the mobility matrix are the reason why the second virial coefficient in the expansion of $\tilde{\Delta}$ (7.54) in section 7.9 vanishes. The above-mentioned coefficient reads (7.56)

$$d_2 = \frac{k_B T}{6N\mu_o\phi^2} \int_0^\infty \mathrm{d}t < T(1,2;t) >^{irr} \tag{D.2}$$

with

$$T(1,2;t) = \Big(\sum_{i,j,k=1}^2 \big[\nabla_i + \beta\boldsymbol{F}_{ji}\big] \cdot \boldsymbol{\mu}_{ik}\Big)\cdot\Big(\sum_{l,m,p=1}^2 \big[\nabla_l + \beta\boldsymbol{F}_{pl}\big] \cdot \boldsymbol{\mu}_{lp}(t)\Big), \tag{D.3}$$

However, from (D.1) one gets

$$\nabla_1 \cdot \boldsymbol{\mu}_{12} = -\nabla_2 \cdot \boldsymbol{\mu}_{12} = -\nabla_2 \cdot \boldsymbol{\mu}_{21},$$
$$\nabla_1 \cdot \boldsymbol{\mu}_{11} = -\nabla_2 \cdot \boldsymbol{\mu}_{11} = -\nabla_2 \cdot \boldsymbol{\mu}_{22},$$

so that

$$\sum_{i,k=1}^{2} \nabla_i \cdot \boldsymbol{\mu}_{ik} = 0 \tag{D.4}$$

Moreover, the sum of interparticle forces in a system vanishes, what in our case boils down to

$$\boldsymbol{F}_{12} + \boldsymbol{F}_{21} = 0. \tag{D.5}$$

This, together with (D.1), guarantees that

$$\sum_{i,j,k=1}^{2} \boldsymbol{F}_{ji} \cdot \boldsymbol{\mu}_{ik} = 0. \tag{D.6}$$

The relations (D.4) and (D.6) give us

$$T(1, 2; t) = 0 \tag{D.7}$$

which in turn results in vanishing of the virial coefficient d_2.

Bibliography

[1] A. Einstein. On the movement of small particles suspended in a stationary liquid demanded by the molecular-kinetic theory of heat. *Ann. d. Phys.*, 17:549, 1905 (republished in 1926 in [138], Chap. 1).

[2] A. Einstein. On the theory of the Brownian movement. *Ann. d. Phys.*, 19:371–381, 1905 (republished in 1926 in [138], Chap. 2).

[3] M. Smoluchowski. Zur kinetischen Theorie der Brownschen Molekularbewegung und der Suspensionen. *Ann. Phys.*, 21:755–780, 1906.

[4] G. G. Stokes. On the effect of the internal friction of fluids on the motion of pendulums. *Trans. Cambridge Philos. Soc.*, 9:8, 1851.

[5] N.G. van Kampen. *Stochastic processes in physics and chemistry*. North-Holland, 1981.

[6] B.J Berne and R. Pecora. *Dynamic Light Scattering*. Wiley, New York, 1976.

[7] P.N. Pusey and R.J.A. Tough. In R. Pecora, editor, *Dynamic Light Scattering: Application of Photon Correlation Spectroscopy*. Plenum, New York, 1985.

[8] P. N. Pusey. Colloidal suspensions. In J. P. Hansen, D. Levesque, and J. Zinn-Justin, editors, *Liquids, Freezing and Glass Transition*, pages 763–942. Elsevier, Amsterdam, 1991.

[9] G. Nägele. On the dynamics and structure of charge-stabilized suspensions. *Phys. Rep.*, 272:215–372, 1996.

[10] W.B. Russel, D.A. Saville, and W.R. Schowalter. *Colloidal Dispersions*. Cambridge University Press, 1989.

[11] Alice P. Gast and William B. Russel. Simple ordering in complex fluids. colloidal particles suspended in solution provide intriguing models for studying phase transitions. *Physics Today*, pages 24–30, December 1998.

[12] J. Happel and H. Brenner. *Low Reynolds Number Hydrodynamics*. Noordhoff, Leyden, 1973.

[13] S. Kim and S.J. Karilla. *Microhydrodynamics*. Butterworth-Heinemann, Boston, 1991.

[14] T. J. Murphy and J. L. Aguirre. Brownian motion of N interacting particles. i. extension of the Einstein diffusion relation to the N-particle case. *J. Chem. Phys.*, 57(5):2098–2104, 1972.

[15] R. Zwanzig. In W. Brittin, editor, *Lectures in Theoretical Physics*, volume 3, pages 106–141. Interscience, New York, 1961.

[16] Hazime Mori. Transport, collective motion, and Brownian motion. *Prog. Theor. Phys.*, 33(3):423–455, 1965.

[17] W. Hess and R. Klein. Generalized hydrodynamics of systems of Brownian particles. *Adv. Phys.*, 32(2):173–283, 1983.

[18] L. Onsager. *Phys. Rev.*, 37:405, 1931.

[19] L. Onsager. *Phys. Rev.*, 38:2265, 1931.

[20] D. Forster. *Hydrodynamic Fluctuations, Broken Symmetry and Correlation Functions*. W.A. Benjamin, Inc., New York, 1975.

[21] C. W. J. Beenaker and P. Mazur. Self-diffusion of spheres in a concentrated suspension. *Physica*, 120A:388–410, 1983.

[22] C. W. J. Beenaker. The effective viscosity of a concentrated suspension of spheres (and its relation to diffusion). *Physica*, 128A:48–81, 1984.

[23] B. Noetinger. Two fluid model for sedimentation phenomena. *Physica*, 157A:1139–1179, 1989.

[24] H. J. H. Clercx and P. P. J. M. Schram. Three-particle hydrodynamic interactions in suspensions. *J. Chem. Phys.*, 96(4):3137–3151, 1992.

[25] A. Einstein. The elementary theory of the Brownian motion. *Zeit. für Elektrochemie*, 14:235–239, 1908 (republished in 1926 in [138], Chap. 5).

[26] G. K. Batchelor. Diffusion in a dilute polydisperse system of interacting spheres. *J. Fluid Mech.*, 131:155–175, 1983.

[27] J.G. Kirkwood. *J. Chem. Phys.*, 4:592, 1936.

[28] J. D. Ramshaw. Existence of the dielectric constant in nonpolar fluids. *Physica*, 62:1–16, 1972.

[29] Rolf Landauer. Electrical conductivity in inhomogeneous media. In J.C. Garland and D.B. Tanner, editors, *Electrical Transport and Optical Properties of Inhomogeneous Media, AIP Conf. Proc. No. 40*, pages 2–43. AIP New York, 1978.

[30] W. C. Saslaw. *Gravitational Physics of Stellar and Galactic Systems*, chapter 30. Cambridge University Press, Cambridge, 1985.

[31] M. E. Fisher and D. Ruelle. The stability of many-particle systems. *J. Math. Phys.*, 7(2):260–271, 1966.

[32] B. J. Hiley and G. S. Joyce. The Ising model with long-range interactions. *Proc. Phys. Soc.*, 85:493–507, 1965.

[33] Sergio A. Cannas. One-dimensional Ising model with long-range interactions: A renormalization-group treatment. *Phys. Rev. B*, 52(1):3034–3037, 1995.

[34] T. Padmanabhan. Statistical mechanics of gravitating systems. *Phys. Rep.*, 188(5):285–362, 1990.

[35] Constantino Tsallis. Non-extensive thermostatistics: brief review and comments. *Physica A*, 221:277–290, 1995.

[36] Fernando D. Nobre and Constantino Tsallis. Infinite-range Ising ferromagnet: thermodynamic limit within Generalized Statistical Mechanics. *Physica A*, 213:337–356, 1995.

[37] Constantino Tsallis. Entropic nonextensivity: a possible measure of complexity. *Chaos, Fractals and Solitions*, (submitted), 2001.

[38] Benjamin P. Vollmayr-Lee and Erik Luijten. A Kac-potential treatment of nonintegrable interactions, 2000.

[39] B. U. Felderhof, G. W. Ford, and E. G. D. Cohen. Cluster expansion for the dielectric constant of a polarizable suspension. *J. Stat. Phys.*, 28(1):135–164, 1982.

[40] V. M. Finkel'berg. Virial expansion of the electrostatic polarizability of many-body system. *Doklady*, 8:907, 1964.

[41] M. Smoluchowski. On the practical applicability of Stokes' law of resistance and its modifications required in certain cases. In *Proc. 5th Intern. Cong. Math.*, volume 2, pages 195–208. 1912.

[42] P. Nozières. A local coupling between sedimentation and convection: application to the Beenaker-Mazur effect. *Physica*, 147A:219–237, 1987.

[43] B. U. Felderhof. Sedimentation and convective flow in suspensions of spherical particles. *Physica*, 153A:217–233, 1988.

[44] J. M. Burgers. On the influence of the concentration of a suspension upon sedimentation velocity I. *Proc. Kon. Nederl. Akad. Wet.*, 44:1045, 1942.

[45] J. M. Burgers. *ibid.*, 44:1177, 1942.

[46] J. M. Burgers. *ibid.*, 45:9, 1942.

[47] J. M. Burgers. *ibid.*, 45:126, 1942.

[48] G. K. Batchelor. Sedimentation in a dilute dispersion of spheres. *J. Fluid Mech.*, 52:245–268, 1972.

[49] G. K. Batchelor. Brownian diffusion of particles with hydrodynamic interaction. *J. Fluid Mech.*, 74:1–29, 1976.

[50] Bruce J. Ackerson. Correlations for interacting Brownian particles. *J. Chem. Phys.*, 64(1):242–246, 1975.

[51] Bruce J. Ackerson. Correlations for interacting Brownian particles. ii. *J. Chem. Phys.*, 69(2):684–690, 1978.

[52] G. Nägele and P. Baur. Long-time dynamics of charged colloidal suspensions: hydrodynamic interaction effects. *Physica*, 245A:297–336, 1996.

[53] Gerhard Nägele, Peter Baur, and Rudolf Klein. Non-exponential relaxation of density fluctuations in strongly interacting colloidal suspensions. *Physica A*, 231:49–61, 1996.

[54] Adolfo J. Banchio, Gerhard Nägele, and Johan Bergenholtz. Collective diffussion and freezing criteria of colloidal suspensions. *J. Chem. Phys.*, 113(8):3381–3396, 2000.

[55] R. Verberg, I.M. de Schepper, and E.G.D. Cohen. Theory of long-time wave number dependent diffusion coefficients in concentrated neutral colloidal suspensions. *Europhys. Lett.*, 48(4):397, 1999.

[56] R. Verberg. Transport properties in concentrated colloidal suspensions (phd thesis), 1998.

[57] B. U. Felderhof and J. Vogel. Long-time collective diffusion coefficient of semidilute suspensions of spherical Brownian particles. *J. Chem. Phys.*, 96(9):6978–6983, 1992.

[58] P. Mazur and D. Bedeaux. Generalization of Faxen's theorem to nonsteady motion of a sphere through an incompressible fluid in arbitrary flow. *Physica*, 76:235–246, 1974.

[59] P. Mazur and W. van Saarlos. Many-sphere hydrodynamic interactions and mobilities in a suspension. *Physica*, 115A:21–57, 1982.

[60] B. U. Felderhof. Force density induced on a sphere in linear hydrodynamics I. Fixed sphere, stick boundary conditions. *Physica*, 84A:557–568, 1976.

[61] B. U. Felderhof. Force density induced on a sphere in linear hydrodynamics II. moving sphere, mixed boundary conditions. *Physica*, 84A:569–576, 1976.

[62] B. U. Felderhof. Hydrodynamic interactions between two spheres. *Physica*, 89A:373–384, 1977.

[63] R. Schmitz and B. U. Felderhof. Creeping flow about a sphere. *Physica*, 92A:423–437, 1978.

[64] R. Schmitz and B. U. Felderhof. Mobility matrix for two spherical particles with hydrodynamic interaction. *Physica*, 116A:163–177, 1982.

[65] R. Schmitz and B. U. Felderhof. Creeping flow about a spherical particle. *Physica*, 113A:90–102, 1982.

[66] R. Schmitz and B. U. Felderhof. Friction matrix for two spherical particles with hydrodynamic interactions. *Physica*, 113A:103–116, 1982.

[67] B. Cichocki, B. U. Felderhof, and R. Schmitz. Hydrodynamic interactions between two spherical particles. *PhysicoChemical Hydrodynamics*, 10(3):383–403, 1988.

[68] B. U. Felderhof. Many-body hydrodynamic interactions in suspensions. *Physica*, 151A:1–16, 1988.

[69] B. U. Felderhof. Hydrodynamic interactions in suspensions with periodic boundary conditions. *Physica*, 159A:1–18, 1989.

[70] B. Cichocki, B. U. Felderhof, K. Hinsen, E. Wajnryb, and J. Blawzdziewicz. Friction and mobility of many spheres in Stokes flow. *J. Chem. Phys.*, 100(5):3780–3790, 1994.

[71] B. Cichocki and K. Hinsen. Stokes drag on conglomerates of spheres. *Phys. Fluids*, 7(2):285–291, 1995.

[72] R. Schmitz. Force multipole moments for a spherically symmetric particle in solution. *Physica*, 102A:161–178, 1980.

[73] D. J. Jeffrey and Y. Onishi. Calculation of the resistance and mobility function for two unequal rigid spheres in low-Reynolds-number flow. *J. Fluid Mech.*, 139:261–290, 1984.

[74] L. Durlofsky, J. F. Brady, and G. Bossis. Dynamic simulation of hydrodynamically interacting particles. *J. Fluid Mech.*, 180:21–49, 1987.

[75] B. Cichocki, M. L. Ekiel-Jeżewska, and E. Wajnryb. Lubrication corrections for three-particle contribution to short-time self-diffusion coefficients in colloidal dispersions. *J. Chem. Phys.*, 111:3265–3274, 1999.

[76] A. J. C. Ladd. Hydrodynamic interactions in a suspension of spherical particles. *J. Chem. Phys.*, 88:5051, 1988.

[77] Anthony J. C. Ladd. Hydrodynamic interactions and the viscosity of suspensions of freely moving spheres. *J. Chem. Phys.*, 90(2):1149–1157, 1989.

[78] A. J. C. Ladd. Hydrodynamic transport coefficients of random dispersions of hard spheres. *J. Chem. Phys.*, 93(5):3484–3494, 1990.

[79] John F. Brady, Ronald J. Phillips, Julia C. Lester, and Georges Bossis. Dynamic simulation of hydrodynamically interacting suspensions. *J. Fluid Mech.*, 195:257–280, 1988.

[80] R. J. Phillips, J. F. Brady, and G. Bossis. Hydrodynamic transport properties of hard-sphere dispersions. I. suspensions of freely mobile particles. *Phys. Fluids*, 31(12):3462–3472, 1988.

[81] R. J. Phillips, J. F. Brady, and G. Bossis. Hydrodynamic transport properties of hard-sphere dispersions. II. porous media. *Phys. Fluids*, 31(12):3473–3479, 1988.

[82] J. Piasecki, L. Bocquet, and J.-P. Hansen. Multiple time scale derivation of the Fokker-Planck equation for two Brownian spheres suspended in a hard sphere fluid. *Physica A*, 218:125–144, 1995.

[83] L. Bocquet and J. Piasecki. Microscopic derivation of non-Markovian thermalization of a Brownian particle. *J. Stat. Phys.*, 87(5/6):1005–1035, 1997.

[84] L. Bocquet and J.-P. Hansen. Dynamics of colloidal systems: beyond the stochatic approach. In J. Karkheck, editor, *Dynamics: Models ans Kinetic Methods for Non-equilibrium Many Body Sytems*, pages 1–16. Kluwer Academic Publishers, 2000.

[85] J.N. Roux. *Physica*, A 188:526, 1992.

[86] L. Bocquet. High friction limit of the kramers equation: the multiple time scale approach. *Am. J. Phys.*, 65:140–144, 1997.

[87] B. Cichocki. The Generalized Smoluchowski Equation for interacting Brownian particles with hard cores. *Z. Phys. B*, 66:537–540, 1987.

[88] Walter T. Grady. *Foundations of Statistical Mechanics*. D. Reidel Publishing Company, Dordrecht, 1987.

[89] P. Mazur and de Groot. *Nonequilibrium thermodynamics*. North-Holland, 1981.

[90] M. M. Kops-Werkhoven, A. Vrij, and H. N. W. Lekkerkerker. On the relation between diffusion, sedimentation, and friction. *J. Chem. Phys.*, 78(5):2760–2763, 1983.

[91] B. U. Felderhof. Brownian motion and creeping flow on the Smoluchowski time scale. *Physica*, 147A:203–218, 1987.

[92] B. U. Felderhof and R. B. Jones. Linear response theory of the viscosity of suspensions of spherical Brownian particles. *Physica*, 146A:417–432, 1987.

[93] B. U. Felderhof and R. B. Jones. Linear response theory of sedimentation and diffusion in a suspension of spherical particles. *Physica*, 119A:591–608, 1983.

[94] E. R. Smith, I. K. Snook, and W. van Megen. Hydrodynamic interactions in Brownian dynamics. I. Periodic boundary conditions for computer simulations. *Physica*, 143A:441–467, 1987.

[95] R. Balescu. *Equilibrium and nonequilibrium statistical mechanics*. John Wiley and Sons, New York, 1975.

[96] M.A.J. Michels. The convergence of integral expressions for the effective properties of heterogeneous media. *Physica A*, 157:377–381, 1989.

[97] C. W. J. Beenaker and P. Mazur. Many-sphere hydrodynamic interactions. iv. Wall-effects inside a spherical container. *Physica*, 131A:311–328, 1985.

[98] U. Geigenmüller and P. Mazur. Intrinsic convection near a meniscus. *Physica*, 171A:475–485, 1991.

[99] D. Bruneau, F. Feuillebois, R. Anthore, and E. J. Hinch. Intrinsic convection in a setting suspension. *Phys. Fluids*, 8(8):2236–2238, 1996.

[100] B. U. Felderhof. Hydrodynamics of suspensions. In H. van Beijeren, editor, *Fundamental Problems in Statistical Mechanics VII*, pages 225–254. Elsevier Science Publishers B.V., 1990.

[101] B. Cichocki and B. U. Felderhof. Renormalized cluster expansion for multiple scattering in disordered systems. *J. Stat. Phys.*, 51:57, 1988.

[102] C. W. J. Beenaker and P. Mazur. Diffusion of spheres in a concentrated suspension II. *Physica*, 126A:349–370, 1984.

[103] R. Diestel. *Graph Theory*. Springer, 1997.

[104] B. U. Felderhof. Diffusion of interacting Brownian particles. *J. Phys. A*, 11(5):–, 1978.

[105] B. Cichocki and B. U. Felderhof. Short-time diffusion coefficients and high frequency viscosity of dilute suspensions of spherical Brownian particles. *J. Chem. Phys.*, 89(2):1049–1054, 1988.

[106] J.C. van der Werff, C. G. de Kruif, C. Blom, and J. Mellema. Linear viscoelastic behavior of dense hard-sphere dispersions. *Phys. Rev.*, A 39:795–807, 1989.

[107] W. H. Press, S.A.Teukolsky, W.T. Vetterling, and B.P. Flannery. *Numerical Recipes in Fortran*. Cambridge University Press, 1992.

[108] B. U. Felderhof and R. B. Jones. Displacement theorems for spherical solutions of the linear Navier-Stokes equations. *J. Math. Phys.*, 30(2):339–342, 1989.

[109] R. B. Jones and R. Schmitz. Mobility matrix for arbitrary spherical particles in solution. *Physica*, 149A:373–394, 1988.

[110] H. Hasimoto. On the periodic fundamental solutions of the Stokes equations and their application to viscous flow past a cubic array of spheres. *J. Fluid. Mech.*, 5:317–328, 1959.

[111] W. G. Hoover and F. H. Ree. Melting transition and communal entropy for hard spheres. *J. Chem. Phys.*, 49(8):3609–3617, 1968.

[112] B. J. Alder and T.E. Wainwright. Studies in molecular dynamics. II. Behaviour of a small number of elastic spheres. *J. Chem. Phys.*, 33:1439–1451, 1960.

[113] M. Medina-Noyola. Long-time self-diffusion in concentrated colloidal dispersions. *Phys. Rev. Lett.*, 60:2705–2708, 1988.

[114] I.M. de Schepper, E.G.D. Cohen, P.N. Pusey, and H. N. W. Lekkerkerker. *J. Phys.: Condens. Matter*, 1:6503, 1989.

[115] P.N. Pusey, H. N. W. Lekkerkerker, E.G.D. Cohen, and I.M. de Schepper. *Physica A*, 164:12, 1990.

[116] D. L. Ermak and J. A. McCammon. Brownian dynamics with hydrodynamic interactions. *J. Chem. Phys.*, 69(4):1352–1360, 1978.

[117] E. Dickinson. Brownian dynamics with hydrodynamics interactions: the application to protein diffusional problems. *Chem. Soc. Rev.*, 14:421–455, 1985.

[118] E. Dickinson, S. A. Allison, and J. A. McCammon. Brownian dynamics with rotation-translation coupling. *J. Chem. Soc. Faraday Trans. 2*, 81:591–601, 1985.

[119] G. C. Ansell, E. Dickinson, and M. Ludvigson. Brownian dynamics of colloidal-aggregate rotation and dissociation in shear flow. *J. Chem. Soc. Faraday Trans. 2*, 81:1269–1284, 1985.

[120] G. C. Ansell and E. Dickinson. Brownian dynamics simulation of the fragmentation of a large colloidal floc in simple shear flow. *J. Colloid Interface Sci.*, 110:73–81, 1986.

[121] G. C. Ansell and E. Dickinson. Sediment formation by Brownian dynamics simulation: Effect of colloidal and hydrodynamic interactions on the sediment structure. *J. Chem. Phys.*, 85:4079–4086, 1986.

[122] W. van Megen and I. K. Snook. Brownian dynamics simulation of concentrated charge stabilized dispersions. Self diffusion. *J. Chem. Soc. Farad. Trans.*, 80(2):383–394, 1984.

[123] K. Gaylor, I. Snook, and W. van Meygen. Comparison of Brownian dynamics with photon correlation spectroscopy of strongly interacting colloidal particles. *J. Chem. Phys.*, 75:1682–1689, 1981.

[124] John F. Brady and Georges Bossis. Stokesian dynamics. *Ann. Rev. Fluid Mech.*, 20:111–157, 1988.

[125] D. R. Foss and J. F. Brady. Structure, diffusion and rheology of Brownian suspensions by Stokesian dynamics simulation. *J. Fluid Mech.*, 407:167–200, 2000.

[126] T. N. Phung, J. F. Brady, and G. Bossis. Stokesian dynamic simulation of Brownian suspensions. *J. Fluid Mech.*, 313:181–207, 1996.

[127] B. J. Alder and T.E. Wainwright. Studies in molecular dynamics. I. General method. *J. Chem. Phys.*, 31:459–466, 1959.

[128] M. P. Allen and D. J. Tildesley. *Computer Simulation of Liquids.* Clarendon Press, Oxford, 1987.

[129] D. Frenkel and B. Smit. *Understanding Molecular Simulation. From Algorithms to Applications.* Academic Press, San Diego, 1996.

[130] B. J. Ackerson and L. Fleishmann. Correlations for dilute hard core suspensions. *J. Chem. Phys.*, 76:2675–2679, 1982.

[131] B. Cichocki and B. U. Felderhof. Time-dependent self-diffusion coefficient of interacting Brownian particles. *Phys. Rev. A*, 44:6551–6558, 1991.

[132] B. Cichocki and B. U. Felderhof. Slow dynamics of linear relaxation systems. *Physica*, 211A:165–192, 1994.

[133] R. Zwanzig and N. K. Ailawadi. Statistical error due to finite time averaging in computer experiments. *Phys. Rev.*, 182(1):280–283, 1969.

[134] D. Frenkel. Intermolecular spectroscopy and computer simulations. In J. van Kranendonk, editor, *Intermolecular spectroscopy and dynamical properties of dense systems. Proceedings of the International School of Physics Enrico Fermi Varenna 1978*, pages 156–201. North-Holland, Amsterdam, 1980.

[135] M. M. Kops-Werkhoven and H. M. Fijnaut. Dynamic behavior of silica dispersions studied near the optical matching point. *J, Chem. Phys.*, 77(5):2242–2253, 1982.

[136] W. van Megen, R. H. Ottewill, S. M. Owens, and P. N. Pusey. Measurement of the wave-vector dependent diffusion coefficient in concentrated particle dispersions. *J. Chem. Phys.*, 82(1):508–515, 1985.

[137] W. van Megen. private communication.

[138] A. Einstein. *Investigations on the theory of the Brownian movement.* Methuen & co., London, 1926.